Universität Zürich[UZH]

Department of Geography

The mystery of the enhanced NDVI signal on Mt. Etna. Dendrochronological analysis of pine trees growing near the 2002/2003 eruptive fissure.

GEO 511 Master's Thesis

Author: Valentino Känzig, 19-742-527

Supervised by: Prof. Dr. Paolo Cherubini (paolo.cherubini@wsl.ch)

Faculty representative: Prof. Dr. Markus Egli

25.04.2025

The mystery of the enhanced NDVI signal on Mt. Etna

Dendrochronological analysis of pine trees growing near the 2002/2003 eruptive fissure

Valentino Känzig

19-742-527

Master's Thesis

Supervisor: Prof. Dr. Paolo Cherubini, WSL
Faculty representative: Prof. Dr. Markus Egli, University of Zurich
Department of Geography, University of Zurich
April 2025

Abstract

This study investigates the potential for trees to perceive and react to volcanic activity prior to an eruption. Previous research found an unusual increase in the Normalized Difference Vegetation Index (NDVI) in the two years preceding the 2002/2003 eruption near Piano Provenzana on Mt. Etna. This finding suggests that trees were more photosynthetically active during this time. While prior studies were unable to ascertain the precise cause, one hypothesis suggests that extra soil moisture from condensed volcanic vapor may have contributed to the elevated NDVI signal. The sampling location of this thesis is located closer to the eruptive fissure, compared to previously analyzed trees.

In this thesis, tree-ring analysis revealed that some trees near the eruption site exhibited missing rings, suggesting potential disruptions to their growth patterns. Statistical analysis indicated that their growth patterns were not primarily influenced by precipitation or temperature, suggesting the presence of other environmental factors. To further explore this phenomenon, a series of chemical analyses were conducted, including stable isotope analysis (of oxygen, hydrogen, and carbon), radiocarbon dating, and trace element measurements. The results suggest that stomatal activity may have undergone changes prior to the eruption, possibly due to the influence of deep-origin CO_2 influencing the trees. Lower $\delta^{18}O$ values suggest that the trees accessed a different water source during and after the eruption. Stem-water analysis further confirmed that trees in proximity to the eruption site absorbed water with distinct isotopic signatures compared to trees in a control area. These findings provide evidence for potential changes in groundwater chemistry. Furthermore, the presence of certain trace elements found in the tree rings during and following the eruption suggest an increased availability of nutrients. This augmented nutrient availability is likely due to volcanic activity. Despite these findings, a single factor does not clearly explain the pre-eruptive NDVI increase, rendering it an ongoing mystery. Subsequent research efforts will be key to uncovering the full picture.

Acknowledgments

I would like to express my profound gratitude to my supervisor Prof. Dr. Paolo Cherubini of the Swiss Federal Research Institute for Forest, Snow and Landscape (WSL) in Birmensdorf, who proposed this research topic, assisted during fieldwork and provided support during the analyses as well as the literature review.
Additionally, I would like to thank Prof. Dr. Markus Egli from the Department of Geography at the University of Zurich, who served as a faculty member during this research and provided assistance with the organizational part of this thesis.
Further, I want to thank the people at WSL, especially the Dendroscience group within the Forest Dynamics research unit. The laboratory work was facilitated by Daniel Nievergelt, Anne Verstege, Nadja-Tamara Studer and LoÏc Schneider. Their assistance included the field work, the analysis of the tree-ring cores and the preparation before the chemical analysis. Additionally, Dr. Marco Lehmann from the biogeochemistry department supported me in extracting the stem water from the samples.
Furthermore, Dr. Irka Hajdas from the Ion Beam Physics Laboratory at the Eidgenössische Technische Hochschule Zürich (ETH Zurich) helped me with the preparation and analysis of the radiocarbon in the tree samples, for which I am profoundly thankful. The research was further enriched by the contributions of Prof. Dr. Olivier Bachmann and Dr. Marcel Guillong from the Institute of Geochemistry and Petrology at ETH Zurich. Their support regarding volcanic trace elements and laser ablation trace element analysis was greatly appreciated.
Additionally, gratitude is extended to Enzo Crimi and Antonino Ruffino from the Corpo Forestale della Regione Siciliana (Distaccamento di Linguaglossa) for their authorization to collect samples on Mt. Etna. They also helped us find the way through the woods of the Ragabo forest and getting to the designated sampling spots.
On a more personal note, I am grateful for the support provided by Svenja Poik during this project, and her consistent efforts to uplift my spirits. In addition, I would like to thank Micaela Dassié and Simona Staub for their assistance and the pleasant experiences I had during my lunch breaks at the WSL.

Contents

List of Figures

List of Tables

Chapter 1

Introduction

Detecting volcanic activity and anticipating possible eruptions are crucial for mitigating hazards and protecting human life, particularly in regions surrounding active volcanoes. Monitoring of volcanic activity is typically accomplished through the implementation of a combination of geophysical, geodetic, and geochemical methods. These include tracking ground deformation, analyzing variations in seismic signals, and measuring changes in the emission of key volcanic gases such as H_2O, CO_2, and SO_2 (Seiler et al. 2021) (Aiuppa et al. 2008). Advancements in remote sensing technology have enabled the assessment of numerous parameters through satellite observations. Remote sensing techniques allow for continuous monitoring of surface deformation linked to the ascent of magma, in addition to the detection of gas emissions indicative of subsurface magmatic processes (Lagios et al. 2013). However, difficulties in the detection of volcanic volatile emissions still exist, thereby posing challenges in the identification of volcanic unrest (Bogue et al. 2023). Furthermore, forest surveys were facilitated due to advances in remote sensing technology. As scientific knowledge expanded, combining older data with less temporal resolution, with more recent methods, contributed to the establishment of remote sensing in forest surveys. The Normalized Difference Vegetation Index (NDVI) holds special importance as it has been correlated to green leaf biomass and to the green leaf area index (Sader & Winne 1992). The NDVI is calculated using the following equation:

$$NDVI = \frac{NIR - RED}{NIR + RED} \tag{1.1}$$

This equation is a well-established tool for quantifying the greenness of vegetation. It does so by combining spectral bands that exhibit distinct reflective patterns. Green vegetation shows a high reflectance in the near infrared (NIR) range and a low degree of reflectance in the red range. NDVI values can range from -1 to +1. However, values close to zero are associated with soil and rock, whereas values closer to +1 correspond to green vegetation. Intense photosynthetic activity in green vegetation leads to higher NDVI values (Houlié et al. 2006).

It is noteworthy that remote sensing techniques have also revealed changes in the photosynthetic activity of vegetation, which may be linked to volcanic activity. During the summers of 2001 and 2002, enhanced NDVI signals were detected on the northern flank of Mt. Etna in Sicily, Italy. These anomalies appeared as a distinct linear feature, which matched the location of a flank eruption that occurred in October 2002. A comparable signal was observed on Mt. Nyiragongo in 2001 (Houlié et al. 2006). The eruption on Mt. Etna started on the night of the 26^{th} to the 27^{th} of October 2002 on both the northern, as well as the southern flank. The eruptions in the northern part lasted until 5^{th} of November, whereas on the southern flank, they continued until 28^{th} of January (Spilliaert et al. 2006). The spatial correlation between the

NDVI anomaly and the subsequent eruption suggests that pre-eruptive volcanic activity may have influenced vegetation, possibly by altering local environmental conditions and enhancing photosynthetic activity. To further investigate this phenomenon, dendrochronological analyses were carried out to determine the potential causes of the increased NDVI signal (Seiler et al. 2017a).

According to Schweingruber (1996), dendrochronology is defined as a combined concept of all study areas that utilize tree rings. Annual tree rings can be used to study environmental change. Ring width and ring density are employed as proxies for past environmental conditions and other events of interest that have affected the physiology of the tree. Possible applications are the dating of geomorphological events such as earthquakes or landslides (Cook & Kairiukstis 2013). Dendrochronological studies make use of reference chronologies from the study site to crossdate samples. This is a critical step in properly referencing sampled rings to calendar years and reference-chronologies, as ring anomalies may be present. So-called false or missing rings can appear in wood, as the trees are directly influenced by environmental processes (Gärtner & Heinrich 2013).

In contemporary dendrochronology, the available methods extend beyond the analysis of ring width and density. Advances in technology led to the introduction of tree-ring chemistry. Successful applications included investigating past pollution events and the introduction of new possibilities in tree physiology through the analysis of cell wall chemistry. Polluting events include volcanic activity, as well as anthropogenic pollution. However, the accumulation or translocation of chemicals within the tree present a challenge to scientists, as signals might be blurred (Binda et al. 2021).

Seiler et al. (2017b) investigated multiple hypotheses concerning the drivers of the enhanced vegetation response on Mt. Etna through dendrochronology. Their findings indicate that neither an increased availability of water from volcanic degassing nor elevated temperatures were responsible for the observed boost in photosynthetic activity. This was concluded since the trees in this region are not limited in growth by climatic factors: the trees in this area grow at elevations that are too high to suffer from summer drought and too low be subject to temperature limitations. Despite this, additional research suggested that volcanic degassing could still play a role. Subsequent findings indicate that condensed volcanic water in the soil may have contributed to increased carbon fixation and photosynthesis. Gathered data showed reduced tree-ring stable carbon isotope ($\delta^{13}C$) values in the years before the eruption. Ambiguous results of radiocarbon (^{14}C) analysis led to no definitive determination of whether the trees had also absorbed fossil carbon dioxide (CO_2) prior to the eruption (Seiler et al. 2021).
Despite these insights, the precise mechanisms and contributing factors behind the enhanced NDVI signal remain incompletely understood. Further analysis of trees located in closer proximity to the eruptive fissure is expected to provide more precise insights. By analyzing stable isotopes and conducting ^{14}C measurements, it is possible to gain a deeper understanding of atmospheric conditions that were present during the study period and tree physiological responses to the 2002/2003 flank eruption. A demonstrated by Skelton et al. (2014), a transition in the stable oxygen isotope ($\delta^{18}O$) values of groundwater was identified before an eruption. This finding suggests that magmatic water was injected into the groundwater due to lasting seismic activity. A more comprehensive understanding of these interactions could provide new perspectives on the use of vegetation monitoring as a complementary approach for detecting pre-eruptive volcanic activity. In addition, Seiler (2017c) noted the presence of several open aspects that could be studied in the future. These included inconsistent ^{14}C results and possible fertilization by elements like phosphorus during pre-eruptive activity.

1.1 Research questions and hypotheses

The central objective of this thesis is to get a more profound insight into the responses of the trees, situated on the slopes of Mt. Etna near Piano Provenzana, before the 2002/2003 eruption that led to an increased NDVI signal. As the original trees were destroyed during the eruption, a new sampling location closer to the original eruptive fissure should help provide more closely related proxy trees. In addition to the proposed methods from Seiler et al. (2021), techniques such as laser ablation inductively coupled plasma mass spectrometry (LA-ICP-MS) and stem-water stable isotope analysis are carried out to better comprehend the tree's responses. This thesis tries to answer these research questions:

1. Do stable isotope measurements and radiocarbon analysis reveal that the trees took up fossil CO_2 before the 2002/2003 eruption?
2. Are trace elements found in the wood an explanation for increased nutrient availability in the years with the elevated NDVI signal?
3. Is there evidence that the trees took up water from a different source in 2001/2002?

For these research questions, some hypotheses, based on existing literature, are presented:

1. (a) If more CO_2 was available due to volcanic degassing, low ^{14}C values should indicate the uptake of fossil CO_2 (Seiler et al. 2021).
   (b) Differences in stable carbon isotopes could also indicate a separate CO_2 source (Seiler et al. 2021).
2. Higher concentrations of nutrient trace elements before the eruption can indicate faster growing trees (Scharnweber et al. 2016).
3. Differences in $\delta^{18}O$ values in the tree rings can indicate a change in the water source of the trees before the eruption (Skelton et al. 2014).

To address these research questions and verify the hypotheses, a series of analyses and measurements were conducted. A thorough description is given in the following chapter.

Chapter 2

Material and Methods

Due to the ambiguity surrounding the cause of the elevated NDVI signal exhibited by the trees, various analytical methods were used to cover a broad range of possible causes. They consisted of methods used in previous studies by Seiler et al. (2021) and some further analyses proposed by lab staff and supervisors.

2.1 Study area

Mt. Etna is in the northeastern part of Sicily in Italy. The mountain's height of 3,300 meters above sea level (m.a.s.l.) makes it the largest active volcano in Europe. The regular activity makes Mt. Etna a great site for scientific research. Most of the time, the activity is characterized by degassing and effusive releases (Varrica et al. 2000). These activities are visible in the morphology of Mt. Etna. A study by Marchese and Grillo (2000) revealed the presence of over 2000 secondary craters dispersed across the volcano's surface, with various aged lava flows covering its flanks.

Mount Etna's proximity to the Mediterranean Sea on its eastern slope results in the strong influence of the maritime climate. The western side, however, is characterized by drier climatic conditions. These distinct conditions lead to differences in vegetation. The study area is situated on the northern slope of Mt. Etna (Seiler et al. 2021). Versace et al. (2022) characterize the area of Piano Provenzana by an average annual precipitation of 766 to 881 millimeters and a mean temperature of 6.4 to 7.9°C. The lower areas of the volcano feature small villages and agriculture, while the areas higher up the slope are covered by forests that are occasionally disturbed by lava flows (Seiler et al. 2021). At medium elevations between 1000 and 1600 m.a.s.l., the predominant tree species is the European beech (*Fagus sylvatica L.*). In higher elevations, ranging from 1600 to 1900 m.a.s.l., the forests are dominated by Corsican black pine (*Pinus nigra J.F. Arnold*). Higher altitudes are then more heavily influenced by eruptions. These disturbances by the volcano lead to a lower tree line than the altitude would suggest (Seiler et al. 2017b). Figure 2.1 depicts a drone shot from the sampling site next to the lava flow, representing the forests at the altitude of 1600 to 1900 m.a.s.l., and the scarce landscape observed at higher elevations.

Figure 2.1 Drone shot of the landscape near Piano Provenzana on Mt. Etna Sicily (source: own picture with permission of the Corpo Forestale della Regione Siciliana)

The study location of this thesis is located near the Piano Provenzana ski station situated within the Linguaglossa district, on the northeastern slope of Mt. Etna. The tourist area of Piano Provenzana experienced significant impacts from the 2002/2003 eruption. Until today the consequences are visible all over the area (Clocchiatti et al. 2004). These forests around Piano Provenzana are dominated by *P. nigra* and *F. sylvatica* (Seiler et al. 2017b). The location of the trees that qualified for sampling was decided in advance. The original spectral satellite images were retrieved from the MADAS (METI AIST Data Archive System) run by the National Institute of Advanced Industrial Science and Technology (AIST). The spatial resolution of the pictures is 15-,30-, and 90-m per pixel in the visible, NIR, short infrared, and thermal wavelengths, respectively. Subsequently, the band layers were imported into the ArcGIS Pro software from Esri. The NDVI for the scene was calculated with the corresponding band images (Houlié et al. 2006). The resulting image for the year 2002 is displayed in figure 2.2. The picture that was used is represented by the picture ID:*AST_L1T_00307072002100113_20150423045548_56446*. A zoomed-in version of this exact picture is available in the appendix.(figure 5.1)

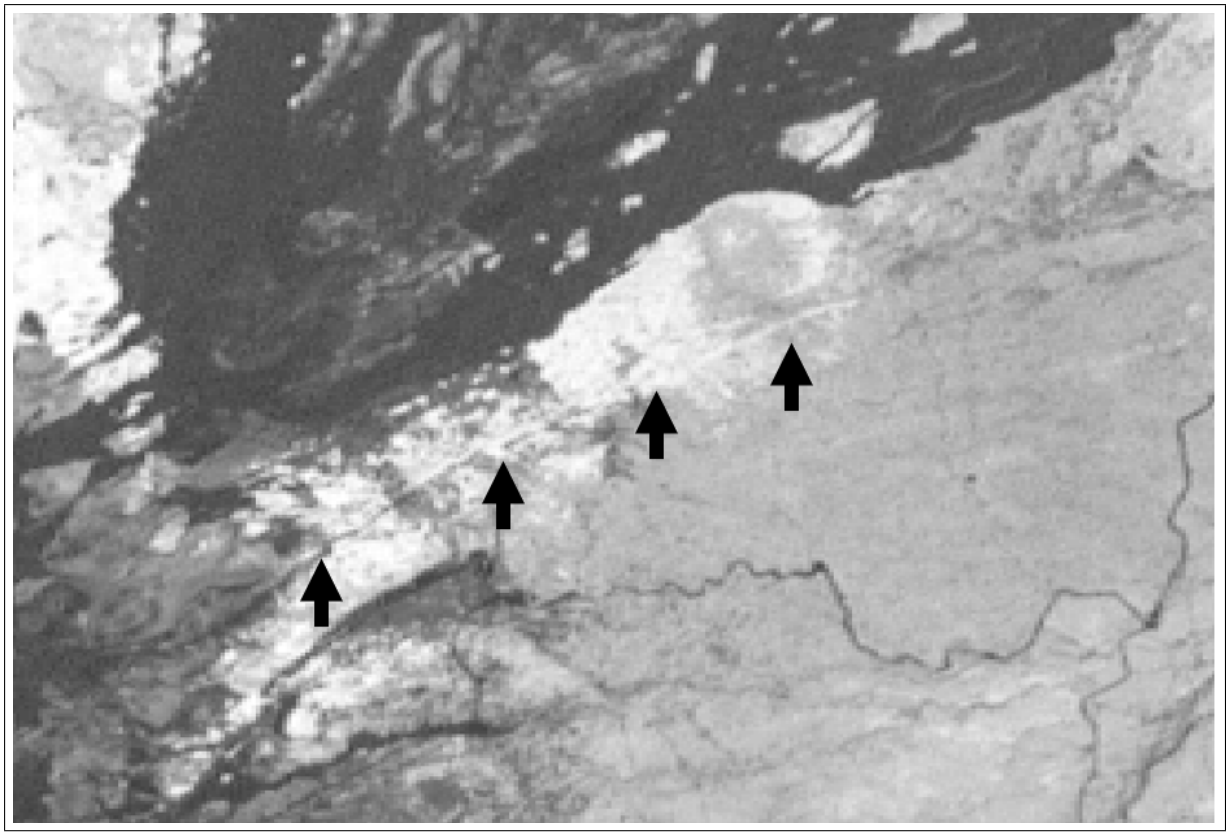

Figure 2.2 2002 NDVI picture from Piano Provenzana composed in ArcGIS Pro with the band images from MADAS.

The monochrome image was then geolocated in ArcGIS Pro. The selection of a sampling location along the lava flow was based on information about the exact location of the elevated NDVI line in both the 2001 and 2002 images. This location was closer to the NDVI line than the original sampling location from Seiler (2017c), yet it also featured enough living trees for sampling. The sampled trees are only proxy trees, as the trees that showed the elevated NDVI signals were destroyed during the eruption. The sampling locations were situated at an altitude range of 1700-1800 m.a.s.l.

Figure 2.3 illustrates a schematic representation of the sampled *P. nigra* trees in the sampling location. It is noteworthy that one tree sample was taken near the original sampling location by Seiler (2017c) for the purpose of comparison.

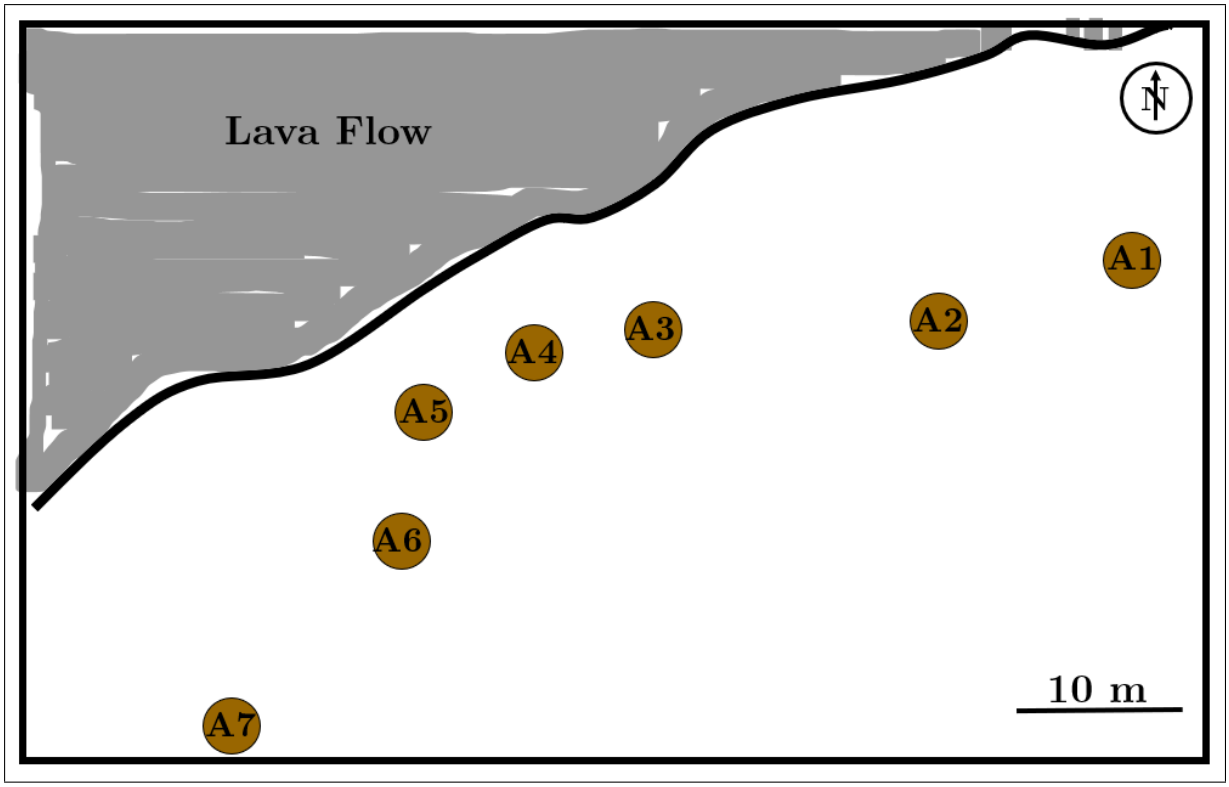

Figure 2.3 Sketch of the sampled *P. nigra* trees at the sampling location near the lava flow (source own sketch).

The location for the control group of *P. nigra* was also chosen ahead, based on the control group of Seiler (2017c). The area near Monti Sartorius is located at a comparable elevation to the sampling location close to the eruptive fissure. Those trees are 3 kilometers away from the sampling trees, however, grow in no vicinity to modern lava flows. This ensures that the trees are not disturbed by close lava flows since the 2002/2003 eruption. In figure 2.4 it is also visible that the sampled control trees are far away from any recent lava flows. For the sampling of the *F. sylvatica*, a closer control location was chosen, due to sparse tree distribution in the location of the *P. nigra* control group.

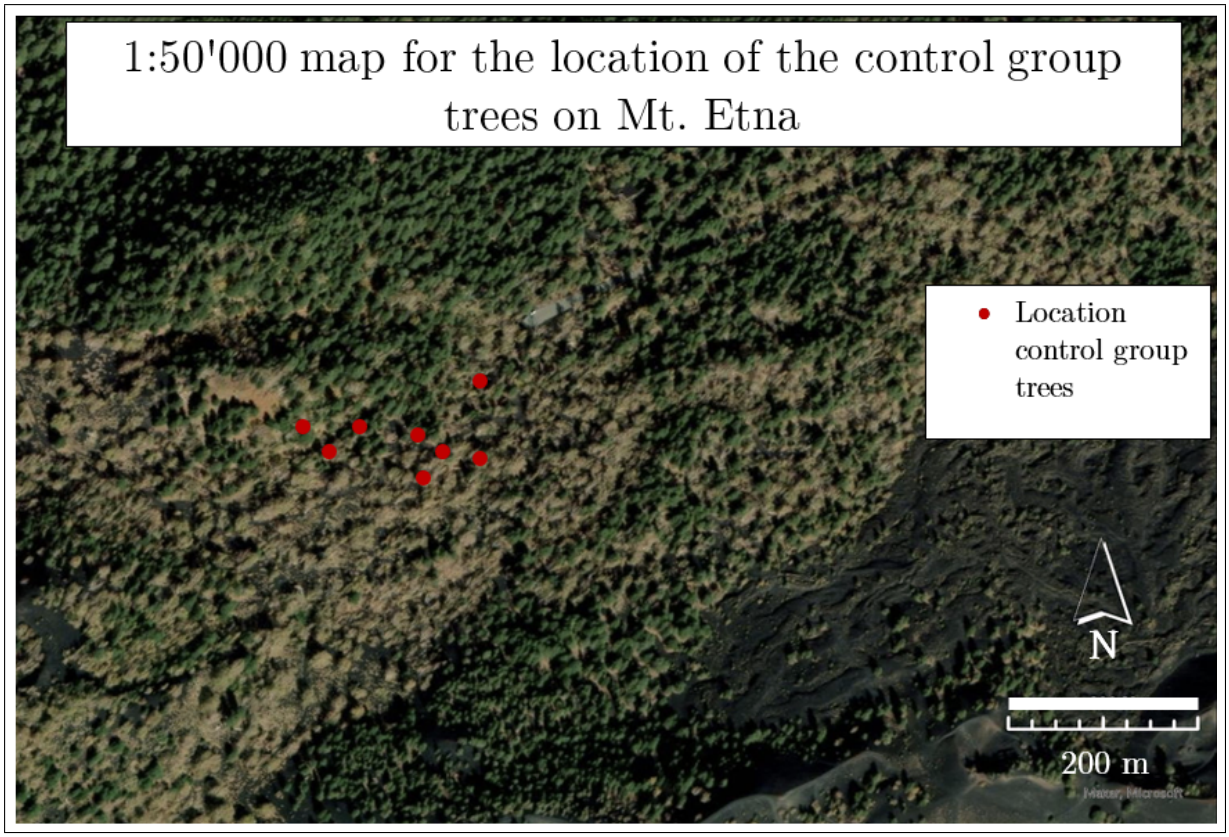

Figure 2.4 Map with the location of the control group trees (source: own map made with ArcGIS Pro).

2.2 Sampling methodology

The sampling occurred in late May 2024. In the field, the previously designated location was identified by map. On-site, the largest living trees that were closest to the lava flow were selected for the sampling location. The geographical coordinates of each tree were recorded using a GARMIN GPSMAP 64st device. It recorded the position as well as the altitude of each tree. Figure 2.5 presents a map of all the sampled *P. nigra* trees along the lava flow plus the NDVI line of 2001. It has been determined that certain trees have been damaged by human activity. Those trees were not sampled. In the control group site, similar trees in height and diameter were chosen. As the forest consisted primarily of *P. nigra*, the sampling was concentrated on this species. From each *P. nigra* tree of the sampling site and the control site, five samples were taken, as a lot of material was needed for the analysis. For dendrochronological and chemical analysis, four samples were taken that reached the tree core. One sample per tree was used to get stem-water samples and therefore not drilled to the core. A total of 14 *P. nigra* trees were sampled: seven from the sampling site and seven from the control site, in addition to one from a higher elevation. The sample from the higher elevation did not include a stem-water sample. The *F. sylvatica* trees were each drilled one time. Five trees from the sampling site and five from the control site, plus two extra trees were sampled. A total of 90 samples were taken on Mt. Etna. 72 samples were identified as *P. nigra*, 12 as *F. sylvatica*, and 6 samples from dead trees as the species being non-identifiable. Table 5.1, located in the appendix, contains information about all the samples collected during the field trip. All samples followed the same procedure. The trees were sampled using a 0.5 cm-diameter corer with a three-threaded auger by Haglof (Haglof Inc., Sweden). The cores were extracted at a tree height of 1.3 meters. After sampling the wood was placed in paper and stored in a plastic tube for transport to the laboratory. Only the stem-water samples were directly put into a glass container to preserve the moisture inside

the wood. These glass containers were stored, except during transportation, in a fridge. The samples in the glass containers were later only used for water extraction and did not follow the same dendrochronological analysis as the other samples.

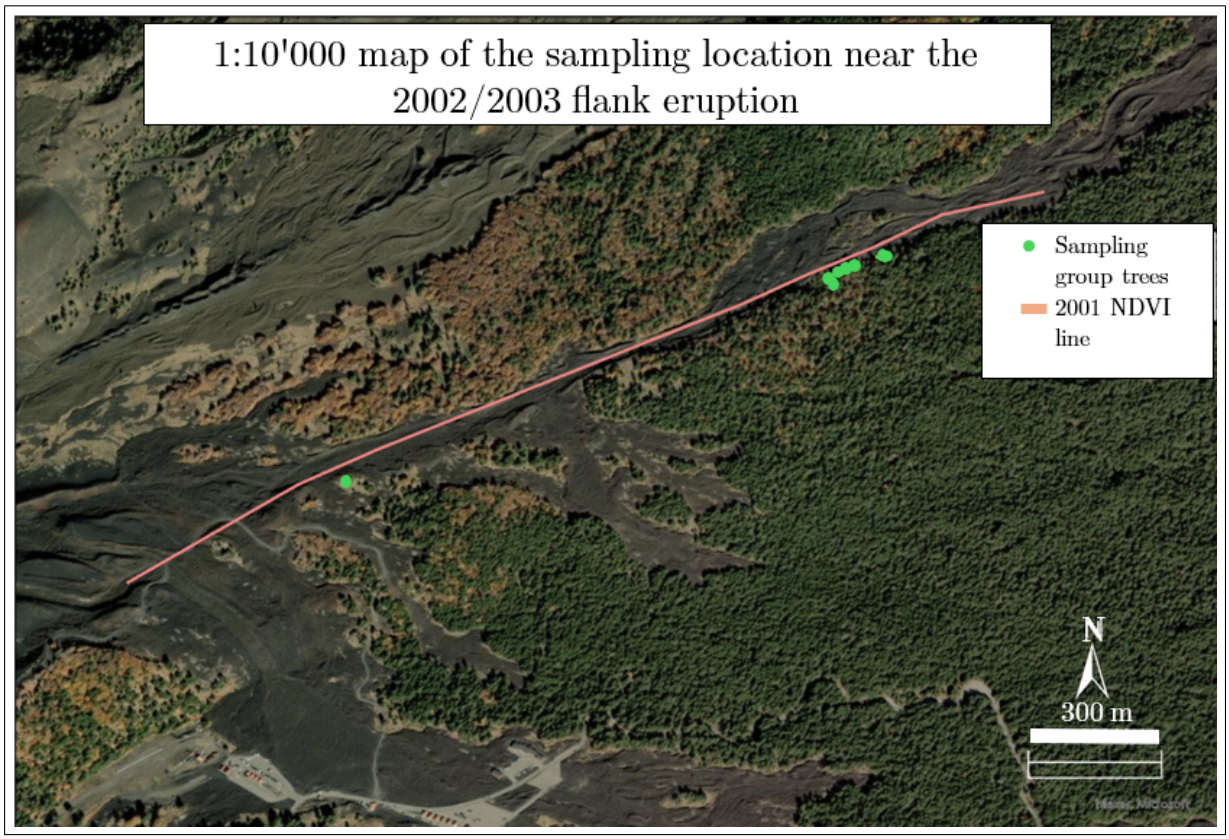

Figure 2.5 Map with the location of the sampling group trees and the 2001 NDVI line (source: own map made with ArcGIS Pro).

2.3 Dendrochronological analyses

All the samples were transported to the laboratory at the WSL in Birmensdorf. There, the samples in the paper straws were dried. This prevents the wood from rotting. For a better overview, the cores were later put into plastic holders and labeled on the plastic. No core was directly labeled and the surface was not prepared with sanding paper. This was done to avoid the influence on chemical analyses by these standard procedures. The surface of each sample was carefully cut with the core-microtome to reveal its ring structure. The core microtome is a device, developed by the WSL in Birmensdorf. With this specialized microtome, the entire core can be cut to a plane surface. This is accomplished by gradually lowering the blade after each cut. Therefore, only thin layers of the wood are removed. It mainly consists of a core holder and an attached sled with a movable blade holder. Figure 2.6 shows the microtome with its components (Gärtner & Nievergelt 2010). To preserve enough material for later analysis, a minimal part was removed to generate a plane surface. In an effort to eliminate possible cross-contamination, the blade and the microtome were wiped down with ethanol after every sample. Additionally, the work area was cleaned regularly with a brush.

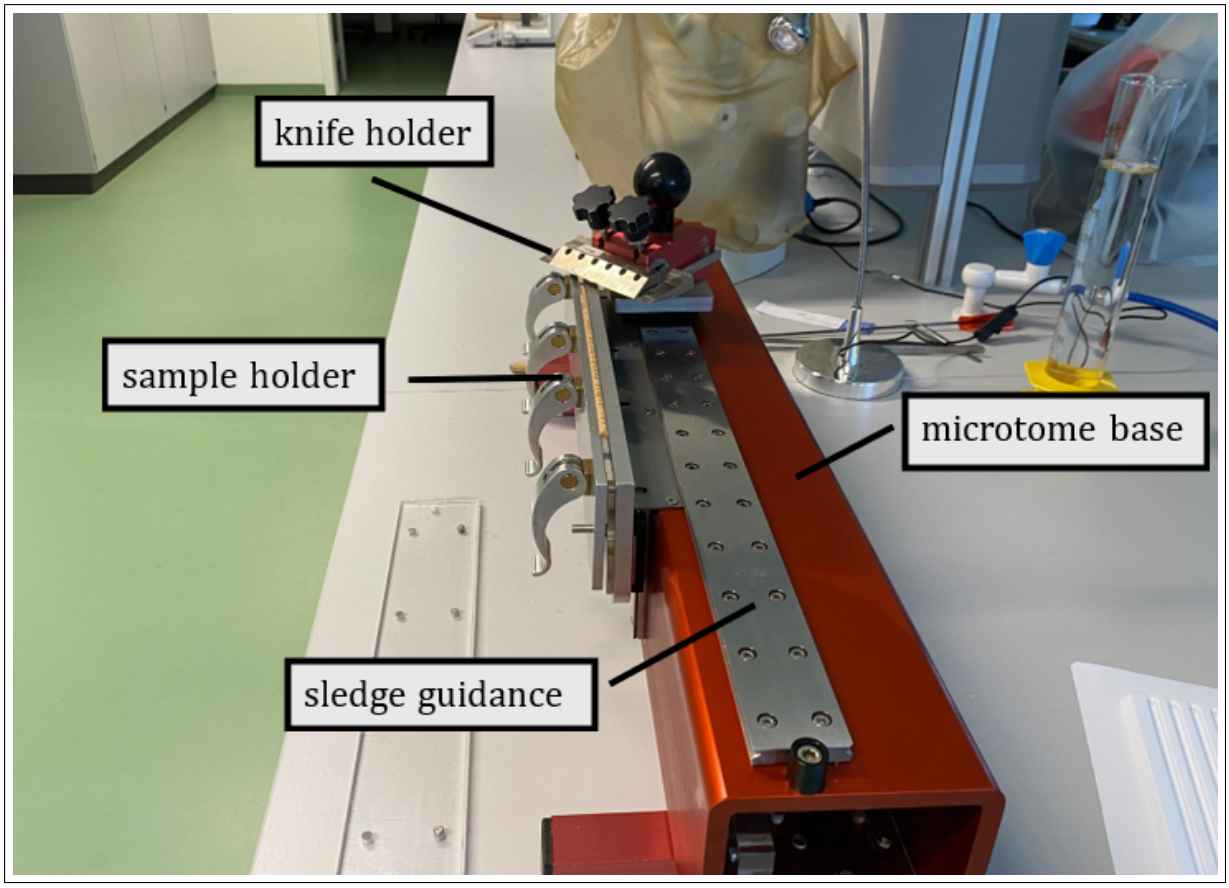

Figure 2.6 Microtome with a sample (source: own picture).

2.3.1 Ring width

Previously explained preparation is needed for the analysis of the ring widths. The ring-width measurements are used for crossdating and the accurate assignment of the years to the rings. It is also used to digitalize wood samples and store them for later analysis.

Skippy

The device, called Skippy, is a Canon 5DSR equipped with a 100 mm Canon Macro lens affixed to a movable table. Other versions include various types of cameras and lenses. Figure 2.7 shows the used Skippy device. This technology was developed at the WSL by LoÏc Schneider and Holger Gärtner. Skippy produces multiple pictures along a sample by automatically moving a table after every image taken. In this thesis, cores were placed on the moving table and the length of the core was put into the program (Skippy, WSL). In addition to the cores, a calibration sheet was placed on the table. The resulting pictures were then stitched together with the program PTGui (Graphical User Interface for Panorama Tools). The stitching was always manually reviewed to erase possible errors by the software.

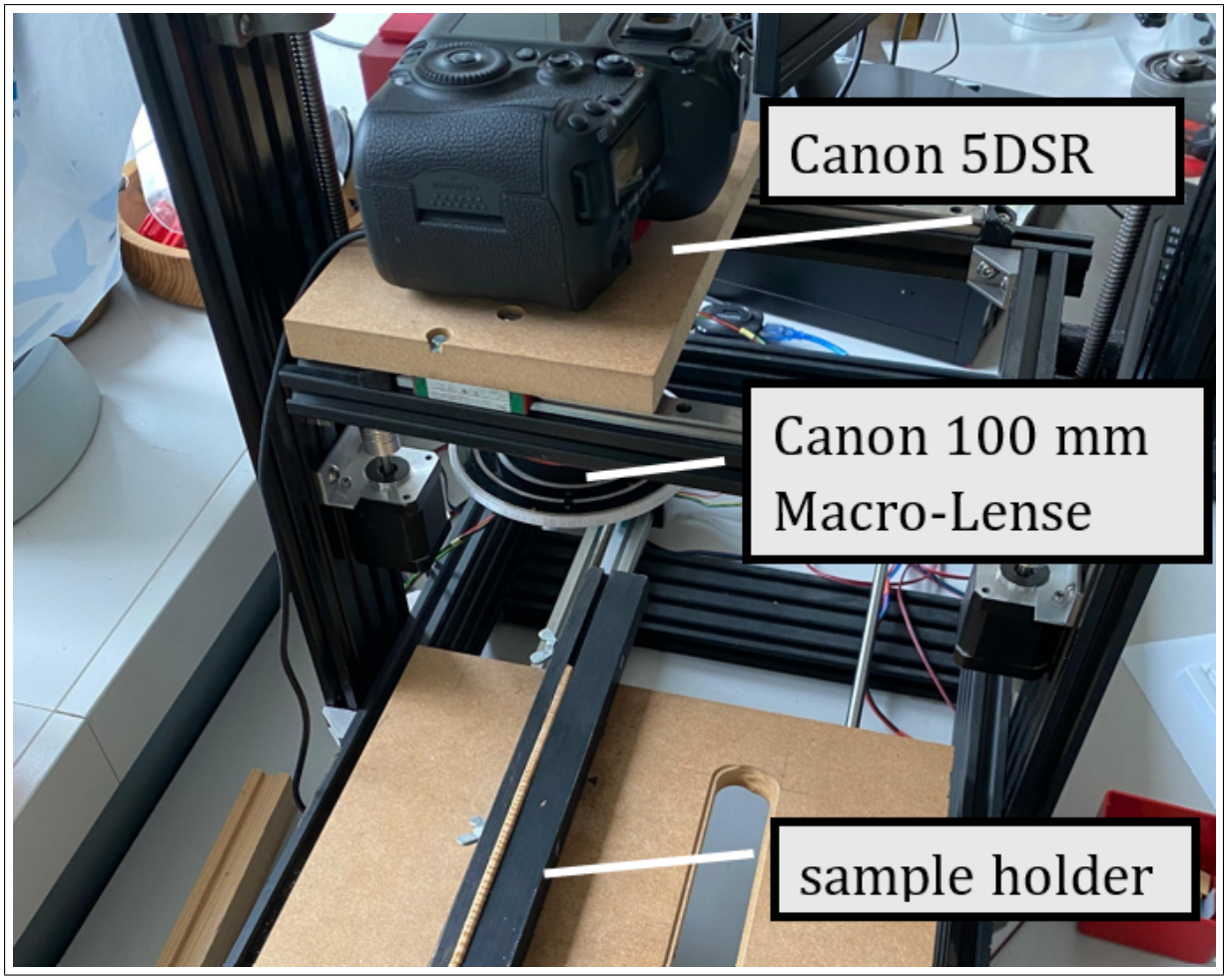

Figure 2.7 Skippy with Canon 5DSR camera (source: own picture).

The resulting panorama image was then exported in TIFF format. An example of such a panorama file is visible in figure 2.8. With this method, a more exact image with a higher pixel count can be made compared to a single image. This is particularly useful when the samples extend to a certain length.

Figure 2.8 Panorama image produced by merging the pictures from Skippy in PTGui.

CooRecorder

Subsequently, the panorama files were loaded into CooRecorder to facilitate the ring-width measurements. CooRecorder, a software developed by Cybis Elektronik & Data AB, is widely used in tree-ring studies. Given that tree-ring measurements form the basis of the resulting analysis, the accuracy of this step is of particular importance. Initially, the image resolution was calibrated using the prepared calibration sheets. In CooRecorder, the ring boundaries can be easily marked by a simple mouse click. Furthermore, missing rings and injuries can be marked in the software. By assigning a known year to a ring boundary, the program automatically allocates the resulting years to the ring boundaries (Maxwell & Larsson 2021).

Due to the challenges associated with accurately delineating ring boundaries in the *F. sylvatica* samples, it was decided that sanding would enhance the visibility of the rings. However, following a second review of the newly prepared samples, it was determined that they would be set aside. The focus would instead be directed towards the *P. nigra* samples. After marking all boundaries in the *P. nigra* samples, the resulting ring-width curves could then be loaded into the software TSAP WIN^{TM} by Rinntech for crossdating. Given that the accurate allocation of years to the tree rings constitutes the basis for further analyses, it was done extra carefully, and subsequent statistical examination was conducted.

Crossdating

Normally, trees from the same species should react likewise in a similar environment. The crossdating technique relies on this thesis and was developed by Andrew Ellicott Douglass for tree-ring research (Gärtner & Heinrich 2013).

In this thesis, the tree ring curves were evaluated in TSAP WIN^{TM} and crossdated within the samples to remove potential ring anomalies. A comparative analysis was conducted of the curves in TSAP WIN^{TM}, with the statistical indices being considered. When a problem was identified, the images of the two trees were visually checked in CooRecorder for evidence of ring anomalies (Gärtner & Heinrich 2013). It started by comparing the four curves within a tree, followed by their alignment with each other. In certain instances, missing rings had to be added, or interannual density fluctuations, that were falsely classified as ring borders, were eliminated. After this step, the tree chronologies, which were constructed using the four individual tree-ring curves, could be compared to each other. This seven-tree chronology formed the master chronology of the sampling site. This master chronology was then put against the existing chronology from Seiler (2017c). Two major inconsistencies were spotted. One was around the year 2000 when the two master chronologies differed around one year. The other one was in the earliest years. The second inconsistency was dismissed for the moment, as only a few trees were that old, and single trees from Seiler (2017c) were also inconsistent in those early years. The divergence around the year 2000 was of major importance, as it was chronologically proximate to the 2002/2003 eruption. An erroneous dating of this event could result in subsequent inaccuracies.

Consequently, microscope images of the trees with the inconsistencies were obtained. The research was conducted using a Leica DVM 6 microscope. The resulting images were then compared to the images in CooRecorder. This comparison revealed that some sampled trees were missing one or two years of growth after the eruption. When incorporated into the individual chronologies of the trees, the resulting master chronology corresponded to the master chronology previously established by Seiler (2017c). As only with proper crossdating of the samples, further analyses are possible.

2.4 Chemical analyses

This section describes all chemical analyses that were conducted in addition to the standard dendrochronology methods. This thesis incorporates the following analytical techniques: stable isotope measurements, laser ablation analysis, radiocarbon measurements and water-content stable isotope analysis. All preparations were carried out while wearing gloves to prevent contamination of the wood.

Given the significance of differentiating between pre-eruptive and post-eruptive years in the research context, it was decided to use individual rings for the analysis. A temporal span of 10 years seemed appropriate for the extent of the work, with the eruption period in the middle. This resulted in the years 1998 to 2007 being taken as studied years. The years from 1998 to 2000 are used as a reference before the NDVI signal. The years 2001 and 2002 as a reference for the elevated NDVI signal years, and 2003 to 2007 for the post-eruption years.

2.4.1 Stable isotopes

This thesis focuses on the stable oxygen and carbon isotopes archived in the tree-ring cellulose.

Sample preparation

Each year-ring is being analyzed individually. This step involved five cores from the sampling site and an equivalent number from the control site. The individual ring removal was performed using a sterile carbon steel surgical blade. The single rings were then cut into small pieces. This work was performed under a binocular with a 25X magnification. After each ring, the material was deposited in an Eppendorf tube. To prevent cross-contamination, the instruments and workspace were cleaned with a brush and wiped down with ethanol-impregnated tissue. Furthermore, the blade was replaced after four cores, to ensure a clean cut. As previously mentioned, not all cores had all the years present in the investigated period. When faced with a missing ring, or a ring too narrow to examine, each side was cut off, to prevent contaminating the attached rings. Figure 2.9 depicts the work environment with the tools used for the ring separation.

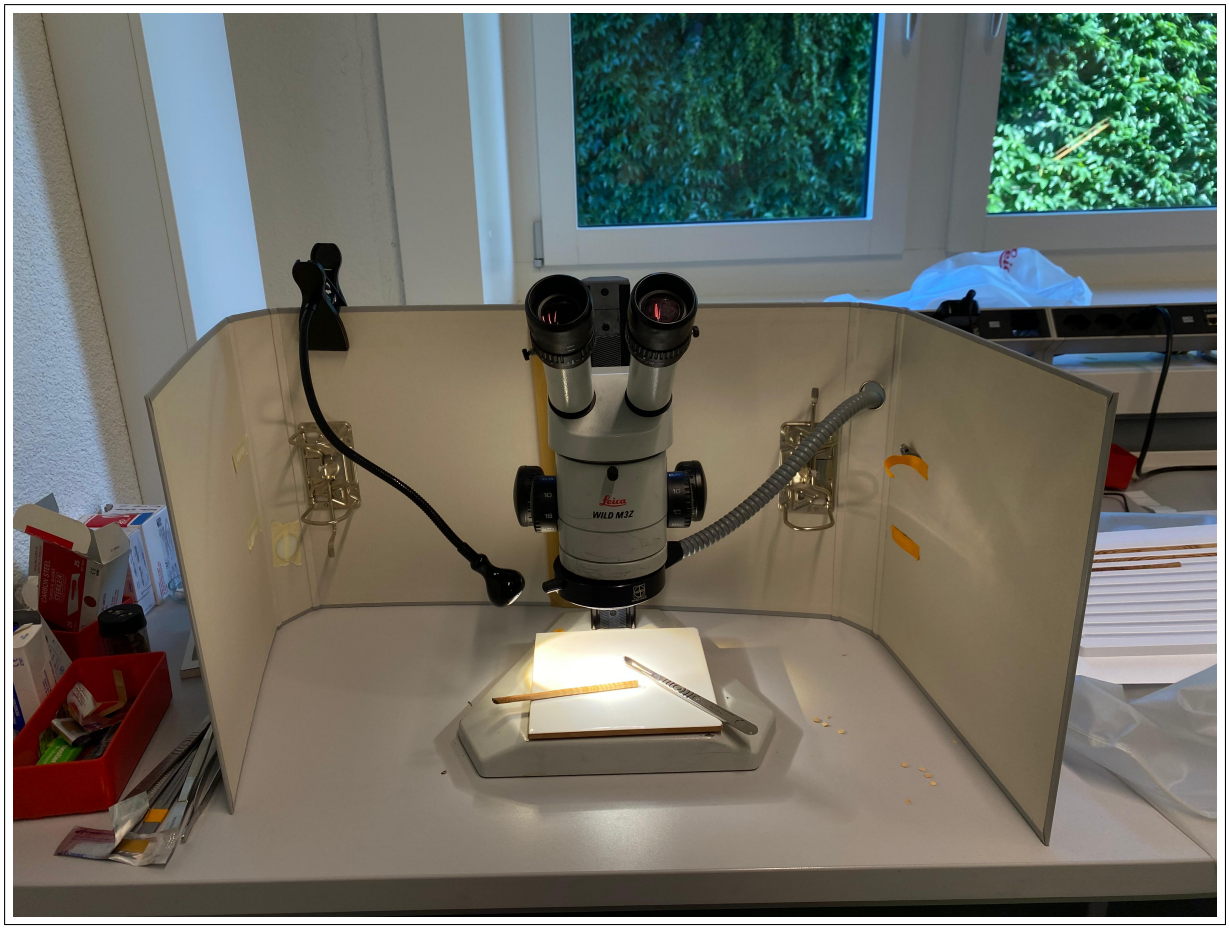

Figure 2.9 Working environment during sample preparation (source: own picture).

The next step involved the extraction of cellulose. The method used was proposed by the lab technicians at the WSL and is based on the method of Boettger et al. (2007). The collected material was initially weighted, placed into Teflon bags, and registered with a binary code to ensure clear identification after washing. The Teflon bags were assembled into an Erlenmeyer flask. Each Erlenmeyer flask had a capacity of 50 bags. Firstly, a solution of 5% sodium hydroxide (NaOH) was introduced into each Erlenmeyer flask. This solution removes fats, resins, oils, tannins, and some hemicelluloses from the sample (Boettger et al. 2007). For the water bath, deionized water was heated up to 60° Celsius. The flasks then sat in the water bath at 60°C for a duration of two hours. The setup of the water bath is visible in figure 2.10. After two hours, the solution was poured into a recycling canister, and the step was repeated once again. After the second round, the samples were rinsed three times with boiling deionized water. The next step was to prepare a solution of 7% sodium chlorite ($NaClO_2$). The pH was fixed between 4 and 5 by adding Glacial acetic acid (100%) and tested with pH indicator strips. This solution was added to the samples and the Erlenmeyer flasks were put into the 60°C water bath. As the solution is only active for 10 hours, it is necessary to change the solution after 10 hours to achieve a total reaction time of 30 hours. In this thesis, the solution was changed three times after 8 hours, resulting in a total of 32 hours. Subsequent to this step, the samples were rinsed again with boiling deionized water and put into a drying oven at 60°C overnight. Afterward, the Teflon bags were opened, the material was weighed and put into Eppendorf tubes.

Figure 2.10 Teflon bags in the Erlenmeyer flask in the 60°Celcius water bath (source: own picture).

The final step was to homogenize the samples, as differences between the early and late wood can appear. A total of one milliliter of deionized water was added to each tube, and the samples were soaked for a period of three hours. An Ultrasonic transducer was used for mixing. After each sample, it was whipped down and rinsed with deionized water. Afterward, the tubes were stored overnight in the freezer with the lid open. The samples were then put into a -80°C freezer in preparation for the following freeze-drying process. After drying in the freeze-dryer for one day, they were ready to weigh in. For this analysis, 3.3 x 5 mm silver capsules for solids from Säntis analysis were utilized. The mass of all samples ranged from 0.9 to 1.1 milligrams. Following the preparation, all samples were analyzed using the elemental analysis-pyrolysis (EA-py) method coupled with an isotope ratio mass spectrometry system (IRMS). This analytica approach has been successfully applied to $^{18}O/^{16}O$ and $^{13}C/^{12}C$ analysis. During the pyrolysis process, carbon monoxide (CO) gas is generated and then transported via a carrier gas to the mass spectrometer, where the isotope ratios are measured (Fourel et al. 2011). The resulting data were then plotted individually against the date of the ring. Further, mean chronologies of the $\delta^{18}O$ and $\delta^{13}C$ values were obtained.

2.4.2 Radiocarbon

As previous studies showed non-conclusive results in ^{14}C measurements of the tree-ring samples, this work again analyzes radiocarbon in the tree rings around the 2002/2003 eruption.

Sample preparation

The tree rings were separated individually and cut into narrow disks. These samples were transferred into Eppendorf tubes and transported to the Laboratory of Ion Beam Physics at ETH Zurich. For this analysis, two distinct cellulose extraction methods for the samples were used. One of these techniques was analogous to the technique used for isotope samples. This method was added as previous studies from Seiler (2017c) saw inconsistent results in different cellulose extraction techniques. The second method was proposed by the lab technicians at ETH Zurich. It is similarly used in various papers (Cercatillo et al 2021) (Němec et al. 2010). The BABAB method involves a sequence of sample cleaning with base, acid, base, acid, and base. Cercatillo et al. (2021) write, that this method, although rather aggressive, produces the most trustworthy results compared to others. They added that ^{14}C-dead samples are preferably prepared with this method. In this thesis, samples can be expected to have rather low ^{14}C content because of potential uptake of fossil CO_2. The cellulose extraction follows the protocol established by the laboratory technicians at the ETH Zurich. It is based on the method proposed by Němec et al. (2010).

The procedure was initiated by leaving the samples sitting in 1mol NaOH solution at 60°C for a duration of two hours. This should dissolve lignin to make the cellulose more reagent-friendly, in addition to the breakdown of humic acid. Afterward, the solution was drained, and the samples were washed three times with deionized water. Subsequently, 1mol of hydrochloric acid (HCl) solution was added to the samples, and they were left on a hot plate at 65°C for one hour. This step is intended to remove contaminating carbonates. After washing again three times, the samples were once again put into a solution of 1mol NaOH and left at 65°C for two hours on the hot plate. Washing the samples three times led to a bath in 1 mol HCl solution for 15 minutes at 65°C. These two procedures are done to remove absorbed atmospheric CO_2. After this step, the samples were not washed, only the solution was removed. The final step involved the samples resting for two hours in a bath of 5% $NaClO_2$ and 0.5 mol HCl at 70°C, helping to remove lignin and other contaminants. Following the drying process in the oven overnight, the samples were weighed into aluminum capsules. The weight of the samples ranged between 2.6 and 3 mg per capsule according to protocol. The weighing took place on a stable base equipped with a sensitive scale, as shown in figure 2.11. The working area was carefully whipped down with ethanol after each sample. Afterward, the samples were combusted, and the resulting graphite was pressed into an aluminum container.

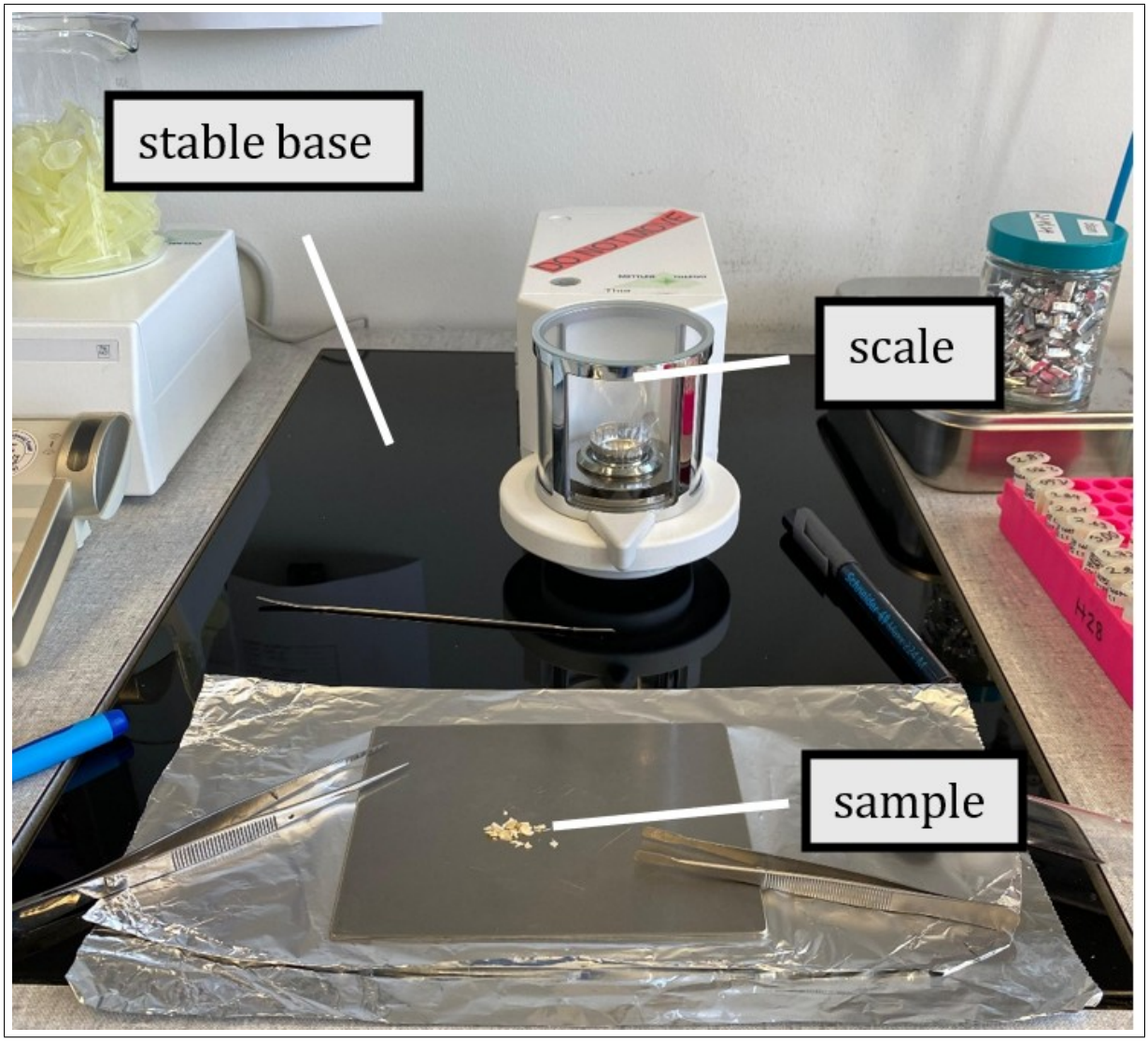

Figure 2.11 Working environment during radiocarbon sample weighing (source: own picture).

The prepared samples were subsequently measured using accelerator mass spectrometry (AMS). To optimize time management, the analyses were carried out using a MICADAS (Mini Carbon Dating System) and an LEA (Low Energy Accelerator) system. Both are types of AMS that are used to precisely measure ^{14}C and their performance is entirely comparable. The main difference lies in the voltage that accelerates particles. As the name implies, the LEA system uses less energy, lowering the acceleration voltage to about a fourth used by the MICADAS system (Ramsperger et al. 2024).

All samples intended for the radiocarbon analysis were also analyzed for the stable isotope $\delta^{13}C$. Some samples followed the preparation from the stable isotope analysis, while others were prepared according to the method described in the radiocarbon analysis chapter. These results for the $\delta^{13}C$ are presented in the stable isotope part.

Data preparation

The raw data was prepared by the lab staff and provided in a Microsoft Excel datasheet. The results are expressed in $F^{14}C$ values. This symbology, called Fraction Modern, was advocated

by Reimer et al. (2004) to prevent confusion with Fm, a symbology previously used in ^{14}C studies. The new symbology is used in reporting post-bomb ^{14}C measurements that were fraction-corrected (Reimer et al. 2004). Stenström et al. (2011) also recommend the use of this unit in post-bomb samples as it follows a clear definition.

2.4.3 LA-ICP-MS

Laser ablation measurements were conducted at the laboratory of the Institute for Geochemistry and Petrology at ETH Zurich. As laser ablation is considered a non-destructive measurement method, no sample processing was required (Loader et al. 2017). Prior to mounting the selected samples onto the support, a small perforation was made in the years 1997 and 2008 for later identification of the period of interest, between 1998 and 2007. The mounting positions on the sample rig are visible in figure 2.12. During the mounting of the samples, gloves were worn all the time to minimize potential contamination.

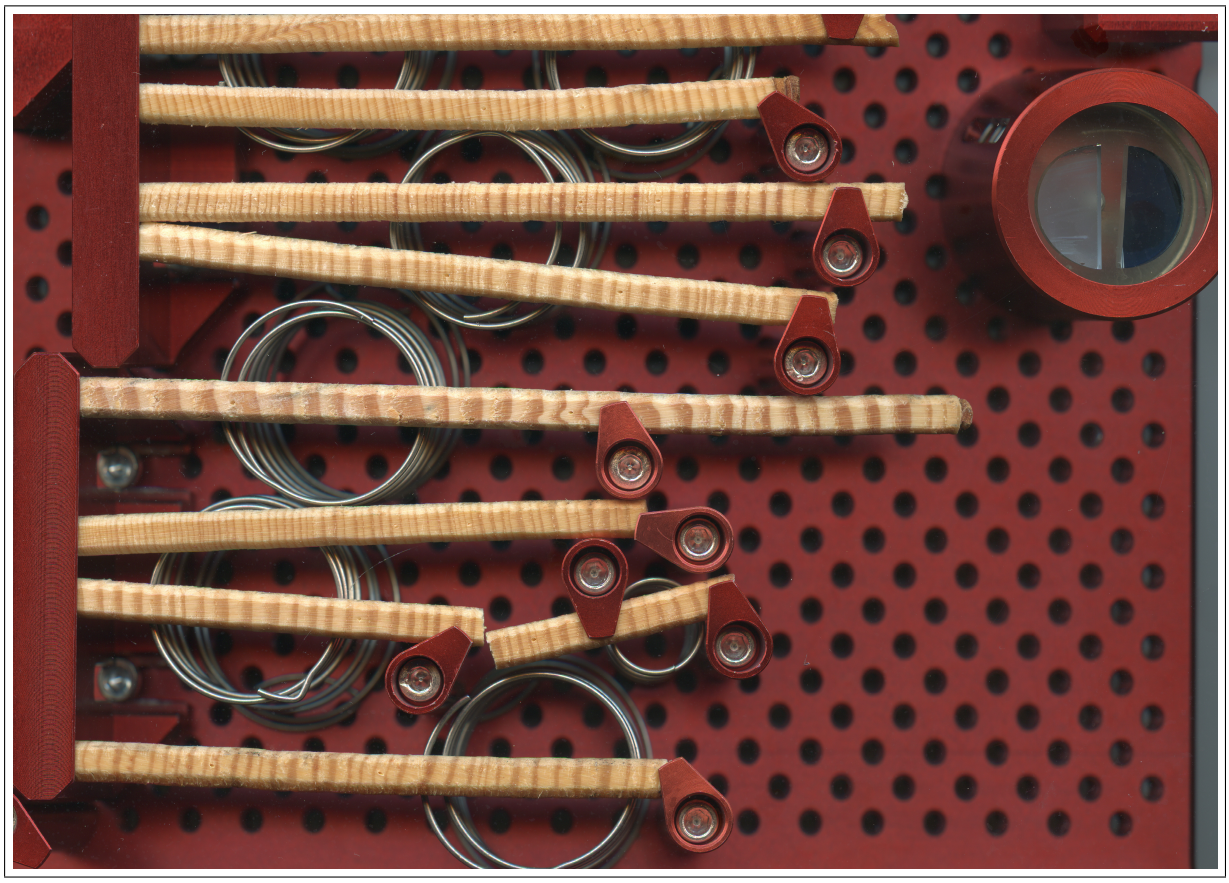

Figure 2.12 Mounted samples on the sample rig before laser-ablation measurements (source: own picture).

This thesis used LA-ICP-MS to identify trace elements in wood. This method utilizes a laser to ablate small portions of material. Subsequently, a carrier gas transports the ablated material to the IRMS where elemental contents are determined. In this work, two different techniques were used. One was the spot ablation, where each tree ring was measured three times on a small spot. With this technique, each ring can be associated with a value, and differences between the years are uncovered. The second technique is the single-line ablation. One straight line across ring borders is ablated to obtain a continuous measurement along the

period of interest. Although showcasing the results, and interpretation, are more difficult, conclusions about changes during the growing period can be drawn. The dimensions of the spot and the line are decided together with laboratory staff based on the tree species (Perone et al. 2018).

Data preparation

The raw data was processed by laboratory staff according to the methodology outlined by Paton et al. (2011). The processed data was then shared in a Microsoft Excel document. The visualization of the point-measurement data and the line-measurement data followed two different paths.

The point measurements were prepared differently, with each ring had assigned measurement points. The processed data was visualized using the same method previously employed by Perone et al. (2018). Previously, the three points in one ring were averaged by calculating the mean. Then, with the method of Perone et al. (2018), the data from four trees per location were averaged using a normalization procedure. This technique makes the data of two different sites comparable. First, the elemental values of the four trees of the site are normalized using the formula:

$$X_{Normalized} = \frac{X - X_{min}}{X_{max} - X_{min}} \tag{2.1}$$

,where X is the mean elemental value of each year.

Subsequently, the normalized values per site were averaged. Afterward, the two resulting series were plotted against the years.

For the line measurements, the data of the three lines was compacted by calculating the mean values. For each measured element, a mean line was then visualized using a line chart in Microsoft Excel. This line was then matched with the picture of the measured line on the core sample, to obtain a visual combination of the rings and the measured elements. With this technique proposed by laboratory staff, possible elemental peaks are visible on the measurement location on the wood. As the lines are adjusted on the individual cores and their ring widths, comparison and other visualization methods are not feasible. A single tree core from Piano Provenzana was measured two times, as it was the only core showing the year 2003.

Element selection

Together with laboratory staff, the decision was made to analyze 32 different trace elements in the samples. This approach should maximize the chances of finding a signal before the 2002/2003 eruption. Following the data preparation, signals within the data were identified and potential nutrients, based on literature, were closely inspected. Not all elements demonstrated peaks and only a subset of elements could act as nutrients for the trees. Accordingly, only a portion of the data will be displayed in this work. For the possible peaks, mean data was plotted over the period and the sampling site at Piano Provenzana was compared to the control site. Especially trace elements connected to volcanic activity were closely inspected. For example, Potassium (K), Calcium (Ca), Sulfur (S), Copper (Cu), Iron (Fe), Aluminum (Al), Magnesium (Mg), Lead (Pb), and Zinc (Zn) (Aiuppa et al. 2007) (Calabrese et al. 2011) (Calabrese et al. 2015).

Scharnweber et al. (2016) identified Ca, Mn, and K as the nutrients most suitable for dendrochemical analyses in pine trees, as they tend to be less mobile between tree rings. These possible nutrients also fit with the findings of Calabrese et al. (2011), which demonstrated that K and Ca belong to the most abundant metals in volcanic aerosols.

2.4.4 Stem-water stable isotopes

From each *P. nigra* tree, one sample for stem-water analysis was taken. In this part, the water extraction method is described. Stable isotopes of the water molecule, such as (δ^2H and δ^{18}O), are used to estimate water flow pathways, the residence time of water, and water storage. (Zuecco et al. 2022). A better understanding of the water source of these trees could help to identify if a change in the water source led to the elevated NDVI signal.

Sample preparation

The glass containers of the samples were stored in a refrigerator prior to the preparation. The preparation in this step was restricted to water extraction. For this purpose, cryogenic vacuum distillation (CVD) was used. The method was proposed by the laboratory technicians and is similar to the method described by Zuecco et al. (2022). A bath containing deionized water was heated to 80°C. The water extraction setup is visible in figure 2.13. The whole system is attached to a vacuum pump. First, the whole system was flushed with N_2 gas. Subsequently, the samples in the glass containers were attached. Buckets containing liquid N_2 are positioned beneath the U tubes. After this step, the sample containers together with the U-tubes were lowered into the water bath and the liquid N_2, respectively. The vacuum was connected, and the resulting flow then sucked the water vapor from the samples into the line. In the U-tubes, the water trap of this setup, the vapor condensates instantly and becomes ice. Following a two-hour extraction period, all the water is extracted. The ice-filled U-tubes were closed and left at room temperature until the ice melted. The water was then filtered using a 13 mm Yeti High-Performance Liquid Chromatography (HPLC) filter with a nylon membrane from Infochroma ag. The pore size measured 0.45 μm. The filtered water was transferred into gas chromatography (GC) vials. The prepared vials were then stored in a freezer until the analysis.

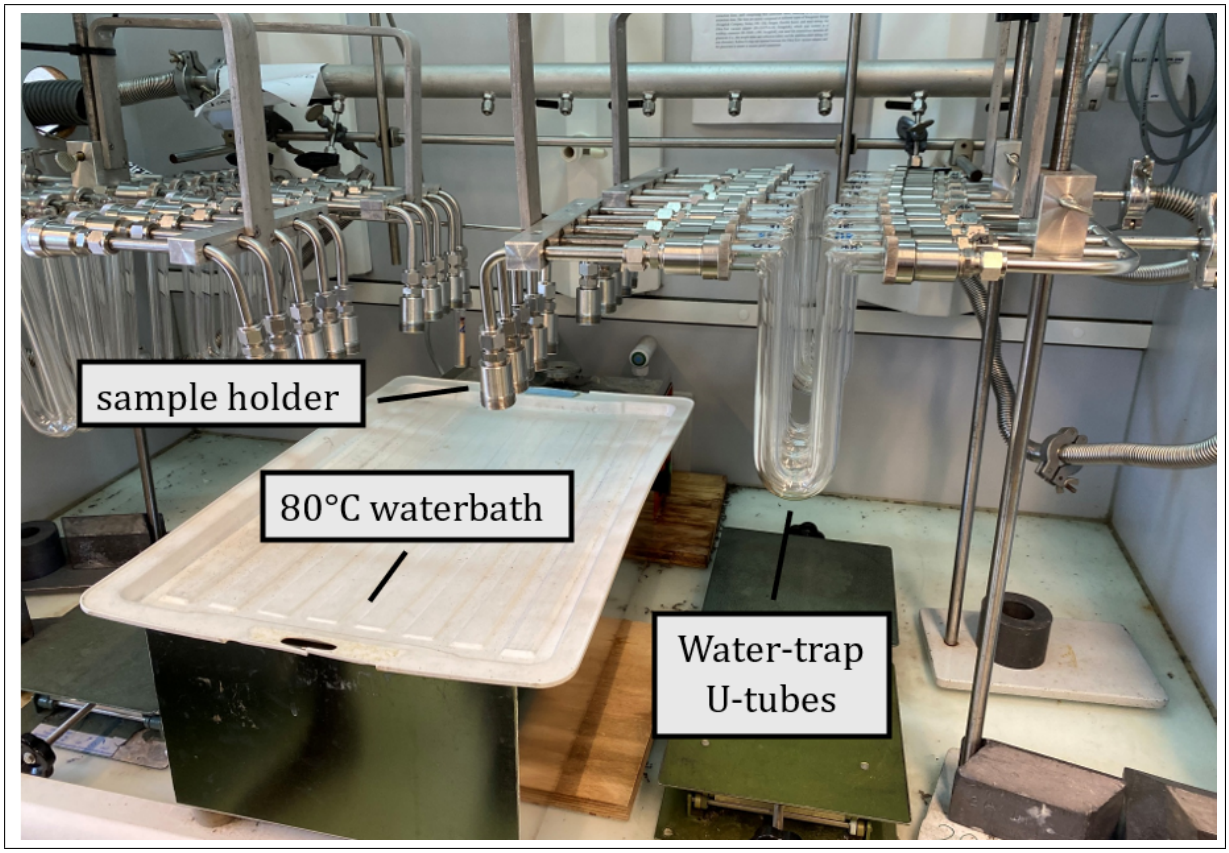

Figure 2.13 Setup of Cryogenic Vacuum Distillation in the lab (source: own picture).

The prepared stem-water samples were analyzed by pyrolysis isotope-ratio mass spectrometry. The pyrolysis technique offers a rapid and precise method for water analysis. This technique utilizes pyrolysis, a qualitative high-temperature conversion, to transform oxygen into CO and hydrogen into ^{2}H. This process occurs in a reducing environment at high temperatures of 1420°C. The resulting gases are separated by a gas chromatography column, prior to being transferred to the isotope-ratio mass spectrometer. This technique is widely used for natural abundance of δ^{2}H and δ^{18}O and tracer studies of liquid samples (Begley & Scrimgeour 1997).

Subsequently, the results were plotted in a δ^{2}H -δ^{18}O -diagram, in which the Global Meteoric Water Line (GMWL) and several Local Meteoric Water Lines (LMWLs), found in the literature, were added.

2.4.5 Meteorological data

In this thesis, meteorological data is used to compare the ring widths with the climatic settings. This helps to see if the ring-width variation is correlated to the local climate or if disturbances have influenced the growth. The monthly interpolated precipitation dataset of the Mt.Etna region, with its center at 37.75 N and 15.25 E, ranged from 1901 to 2023. It was obtained from Durre et al. (2008) and Lawrimore et al. (2011). Mean temperature, minimum temperature, and maximum temperature datasets were found at the "Deutscher Wetterdienst". The data was collected from three stations around Mt. Etna: Messina (38.20 N 15.55 E, timespan: 1999-2022), Enna (37.57 N 14.28 E, timespan: 1999-2022), and Catania (37.41 N 14.92 E, timespan: 1999-2022).

To detect droughts, different indices such as the Palmer Drought Severity Index (PDSI), the Standardized Precipitation Index (SPI), or the Standardized Precipitation Evapotranspiration Index (SPEI) can be used. In this work, the SPI and SPEI are used to detect differences in the water availability of the trees. Other studies, including the one from Aschale et al. (2024), used the SPI and SPEI in the region of Mt. Etna. The SPI and the SPEI are easy to calculate, as they require minimal input data. Whereas the SPI only uses precipitation as a single input value, the SPEI is derived from a combination of precipitation and temperature values. In this thesis, the SPI was calculated for the years 1901 to 2023 and the SPEI between 1999 and 2022, due to the availability of the meteorological data. A significant distinction can be made by selecting the time scale of the indices. The varying timescales represent different droughts and are differentiated by the number of months within the rolling window. A one-month window (SPEI1) represents meteorological, a three-to-six-month window (SPEI3-6) is an agricultural, and a 12-month window (SPEI12) means a hydrological drought (Tirivarombo et al. 2018). Vicente-Serrano et al. (2014) concluded that forests that respond to short-term droughts are often located at humid sites and medium-to long-term droughts at subhumid conditions. As the climate on Mt. Etna is very diverse, the classification of the local climate at the sampling site in Piano Provenzana is difficult. Additionally, the water availability in the soil is miscellaneous, as younger and less developed soils may have a lower water-holding capacity (Seiler et al. 2017b). With the meteorological characteristics given by Seiler (2017c) and Versace et al. (2022), it was decided to primarily concentrate on SPI6 and SPEI6 for this thesis. However, results for SPI1 (figures 5.2 and 5.3), SPEI1 (figures 5.4 and 5.5), SPI12 (figures 5.6 and 5.7), and SPEI12 (figures 5.8 and 5.9) were added to the appendix. Overall, their patterns showed similarities to the SPI6.

2.5 Statistics

A variety of statistical analyses were done to the data gathered in this thesis. They are listed in this chapter. All statistical analyses were carried out with RStudio (Version: 4.4.2, Posit Software PBC).

2.5.1 Crossdating

The process of crossdating commences with the comparison of individual trees to each other. Consequently, the chronology established in this thesis should be tested. The series intercorrelation is an established measure of crossdating to see if the individual trees in a series show a common growth signal and that the assigned calendar years match (Seiler et al. 2021).

As previously stated, crossdating involves not only a visual comparison of curves but also a statistical analysis. The TSAP WIN^{TM} software has different statistical calculations that are run on the curves. Used in various tree-ring studies, the Gleichläufigkeitskoeffizient (GLK) expresses the synchrony of two curves. It tests whether the curves behave the same on an annual basis (Trouet et al. 2006). This thesis calculated the Gleichläufigkeit between the series used by Seiler (2017c) and the series built up in this work. The Gleichläufigkeit is calculated according to the formula from Eckstein & Bauch (1969):

$$\Delta_i = (x_{i+1} - x_i), when \quad \begin{array}{c} \Delta_i > 0 : G_{ix} = +\frac{1}{2} \\ \Delta_i = 0 : G_{ix} = 0 \\ \Delta_i < 0 : G_{ix} = -\frac{1}{2} \end{array} \tag{2.2}$$

for two curves x and y, the value of $G_{(x,y)}$ is given by:

$$G_{(x,y)} = \frac{100}{n-1} \sum_{i=1}^{n-1} |G_{ix} + G_{iy}| \tag{2.3}$$

,where G is the Gleichläufigkeit, n is the number of values and Δ_i is the difference in tree-ring width between two successive years.

2.5.2 Climate

For the climate statistics, different correlations were calculated between either the SPI or the SPEI and the tree-ring series from Piano Provenzana. Initially, the individual tree-ring widths from the sampling location near Piano Provenzana were detrended. Then, the individual tree-ring widths were merged. The resulting mean tree-ring curve was then correlated to the different SPI and SPEI indices, each representing a different drought type. The SPI was calculated between 1901 and 2023, and the SPEI between 1999 and 2022. Different correlation values were calculated, including Pearson's correlation coefficient, a measure of linear dependence between two variables (Ly et al. 2018), and a running Pearson's correlation, which is commonly used to investigate the temporal differences of correlations between two series (Zhao et al. 2018). These tests should help to find possible periods where the tree-ring widths were not predominantly influenced by climatic factors.

2.5.3 Stable isotopes

In this thesis, a Spearman's rank correlation is calculated between the δ^{13}C and the δ^{18}O values to investigate their synchronicity in the measurement period. Spearman's rank correlation is a simple statistical tool to detect trends in chemical concentrations over time. The primary function of this statistical tool is to assess the correlation between two independent variables. Each value is ranked separately and the difference in the rank between pairs is registered (Gauthier 2001). It is calculated as follows:

$$rs = \frac{1 - 6\sum_{i=1}^{1} d_i^2}{n^3 - n} \tag{2.4}$$

,where Δ_i is the difference between ranks for each pair and n being the number of pairs (Gaulthier 2001). It was not possible to carry out a running Spearman's rank correlation, due to the short period of only 10 years.

Chapter 3

Results

As previously stated in the methods part, some trees of the sampling group at Piano Provenzana had missing rings in the year 2003, with some even missing in the year 2004. Consequently, some of the results have been missing data in these years. Most of the data was plotted with RStudio (Version: 4.4.2, Posit Software, PBC).

3.1 Crossdating

A notable increase in the weight of detached rings was observed in many trees during the years 2001 and 2002. In figure 3.1 the weights of some of the sampled trees are presented against the year in two plots. One for the sampling site trees and one for the control site trees. Unfortunately, only one sample of the sampling site shows all the rings between 1998 and 2007. In the first plot, the other samples have one or two missing rings. Nevertheless, the ring weights of all samples increase between 2001 and 2002. Most of the samples also increase between 2000 and 2002. Later, A3b, which shows all the rings, has a steep decrease in the year 2003, demonstrating a small ring in this year. The second plot of the control group demonstrates a similar trend, exhibiting an increase in 2002. However, most of these samples show a relatively flat path between 2000 and 2001, with a pronounced increase in 2002. All of them then again decreased in 2003 and again increased in 2004. The two plots show increased values in 2002; however, the samples from the sampling site near the eruption show lower values in the years after the eruption. In general, they also show lower weights in comparison to the trees from the control site.

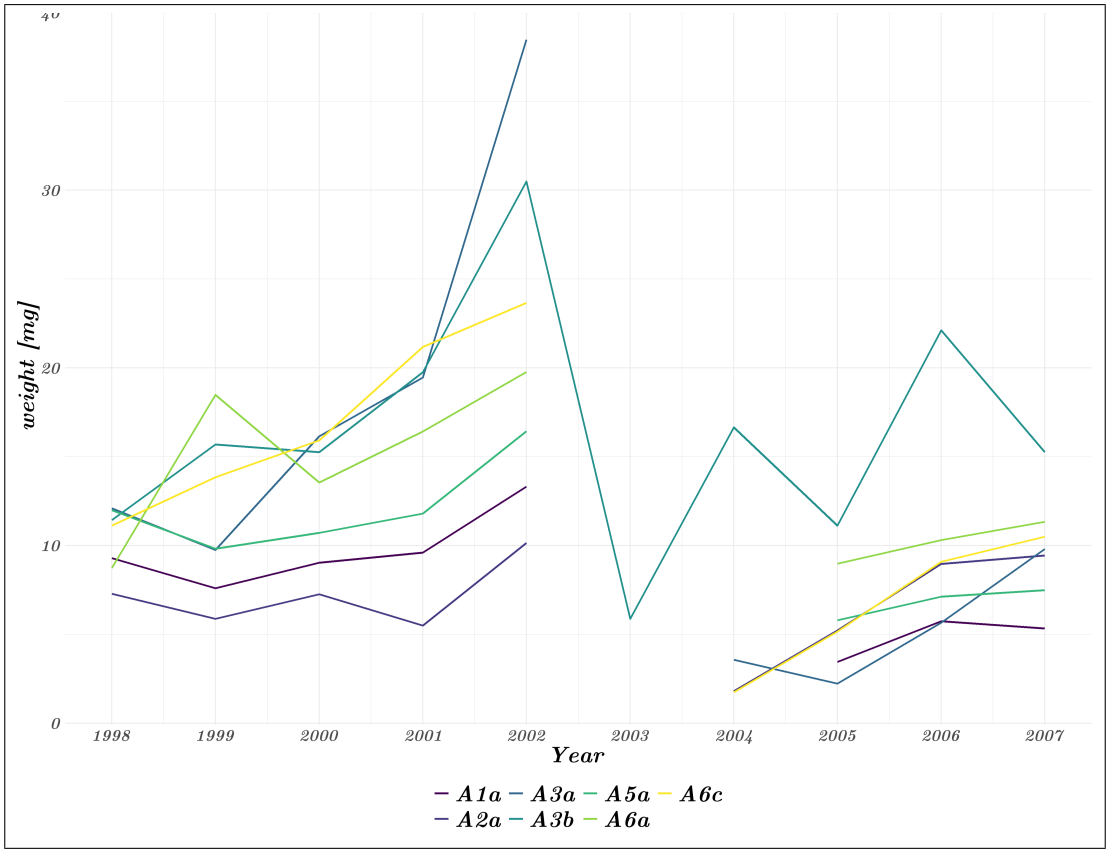

(a) Sampling Site weights

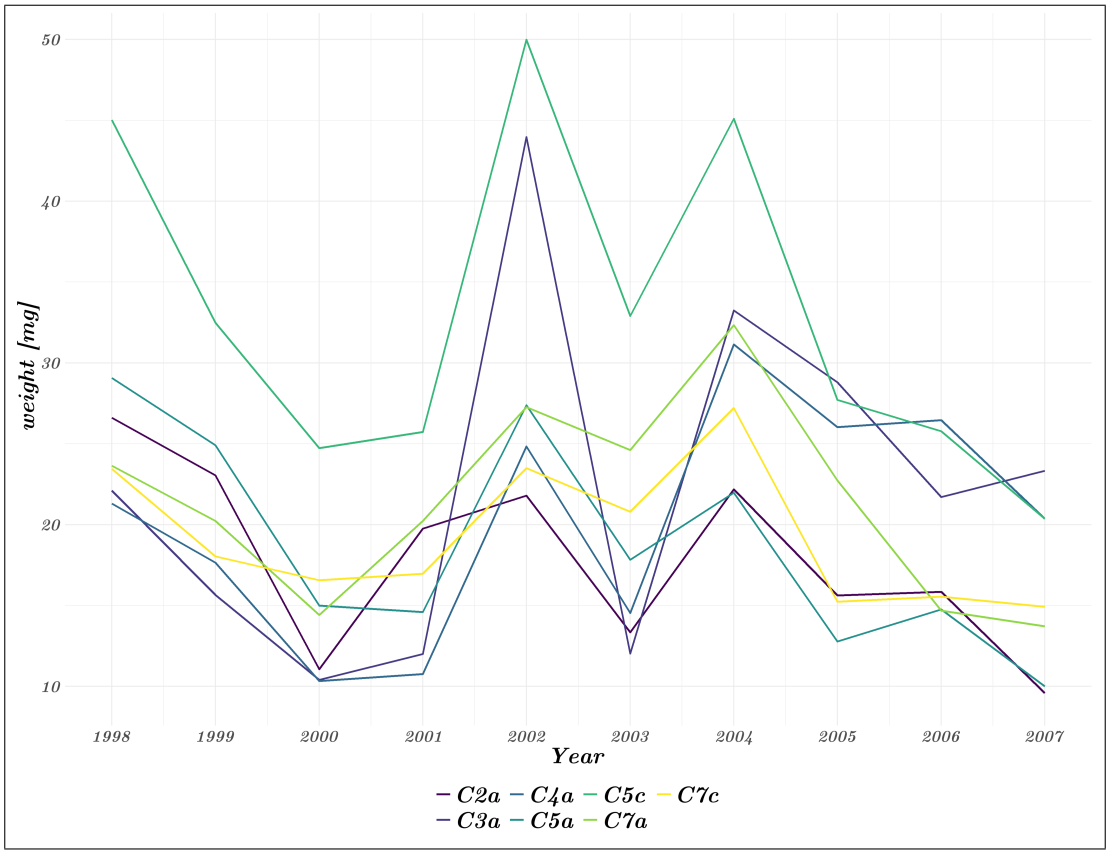

(b) Control Site weights

Figure 3.1 Plots of weights per detached tree ring of sampled trees plotted against the year.

The increase in 2002 is also evident in the ring-width curve. Figure 3.2 illustrates the ring-width chronology that was built with tree samples from the sampling site. The individual trees are depicted in white, while the mean curve is displayed in yellow. The whole chronology ranges from 1792 to 2023, with a mean tree age of 204 years.

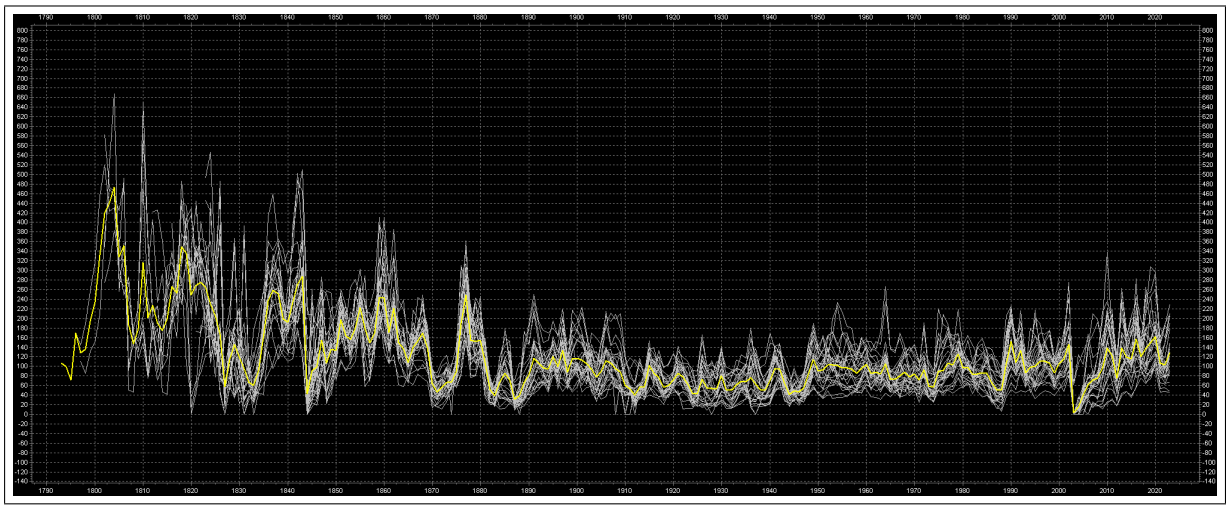

Figure 3.2 Ring-width chronology from all sampled trees at the sampling site near Piano Provenzana together with individual tree ring curves. Made with TSAP WIN^{TM}.

The individual curves were statistically tested against the mean curve. These values are presented in table 3.1. This table shows the length of the individual tree curves and the GLK to the mean curve from all trees of the sampling site. The GLK ranges from 66 to 81.4 in this sampling group.

Table 3.1 Table with the lengths of the individual samples from the sampling site plus the GLK to the master chronology.

Sample ID	A1a	A1b	A1c	A1d	A2a	A2b	A2c	A2d	A3a	A3b	A3c	A3d	A4a	A4b
length	185	202	207	208	186	167	190	179	214	198	212	222	222	231
GLK	76.4	74.6	78.6	79.5	74.3	69.9	71.2	66	74.6	72.3	73.7	72.2	80.1	77.8

Sample ID	A4c	A4d	A5a	A5b	A5c	A5d	A6a	A6b	A6c	A6d	A7a	A7b	A7c	A7d
Length	220	220	204	203	183	185	222	227	215	203	201	204	201	201
GLK	76.5	76.7	77.8	81.4	77.2	78.3	78.3	75.9	76.6	78	69.8	71.2	71.8	70.8

The same statistical analysis was also conducted for the trees from the control group and their mean curve. There, the GLK ranges from 62.8 to 87.2. Yet, this mean curve only shows a duration of 162 years with a mean tree age of 97 years.

In figure 3.3, the mean curve from this thesis (in yellow) for the sampling location near Piano Provenzana is plotted against the mean curve from Group 1 of Seiler (2017c) (in red). The two curves do not cover the same period, as the chronology from Seiler (2017c) extends roughly 10 years further back. However, given that the trees were sampled in 2014, the chronology extends only as far as 2013. The GLK was calculated for these two mean curves, yielding a GLK of 61 between the mean curve from the sampling site and Group 1 of Seiler (2017c), with an overlap of 221 years.

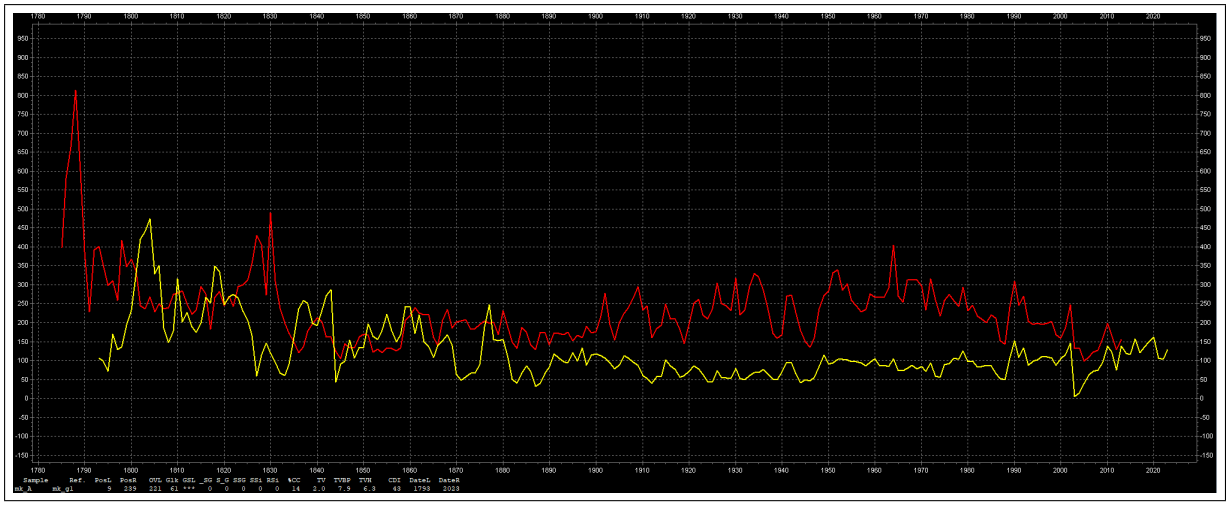

Figure 3.3 Tree ring-width chronology of this thesis vs. the mean curve of group 1 of Seiler (2017c). Made with TSAP WIN^{TM}.

3.2 Meteorological influence

Figure 3.4 displays the SPI6 for the study area over the available years. The plot consists of two parts: the upper plot shows all available years from 1901 to 2023, while the lower plot shows the years from 1999 to 2023. SPI6 demonstrates variability over time, with more pronounced fluctuations observed before 1975. It is also evident that the SPI6 values decrease after 2010 and remain below or close to 0. In the years before and during the eruption, 2000 and 2002 show negative values, whereas 2001 and 2003 exhibit positive values.

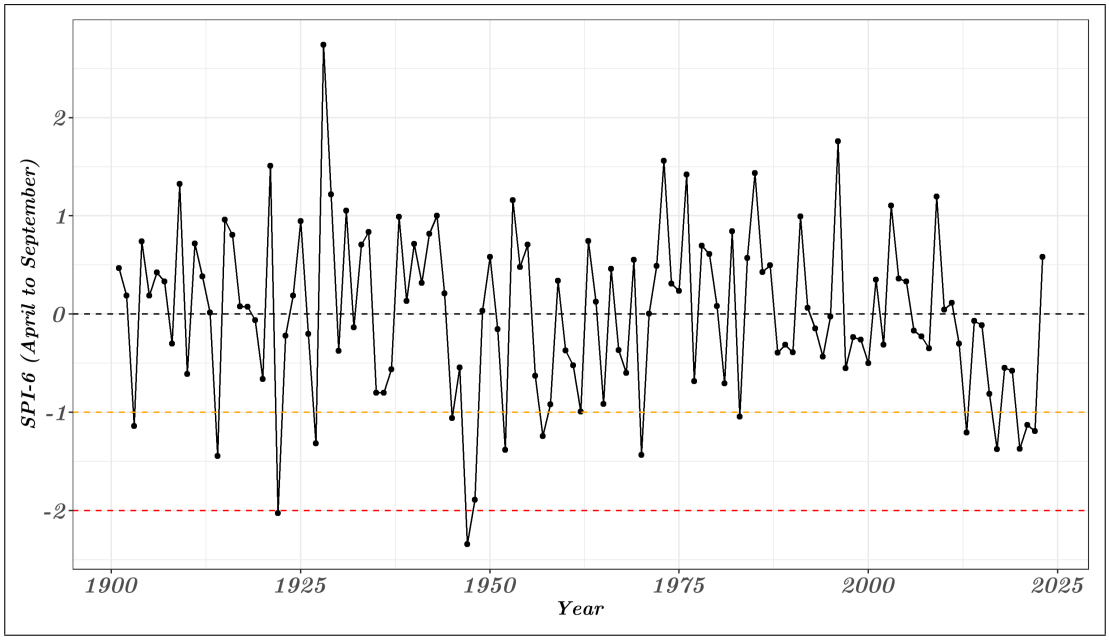

(a) SPI6 of the whole period (1901-2023)

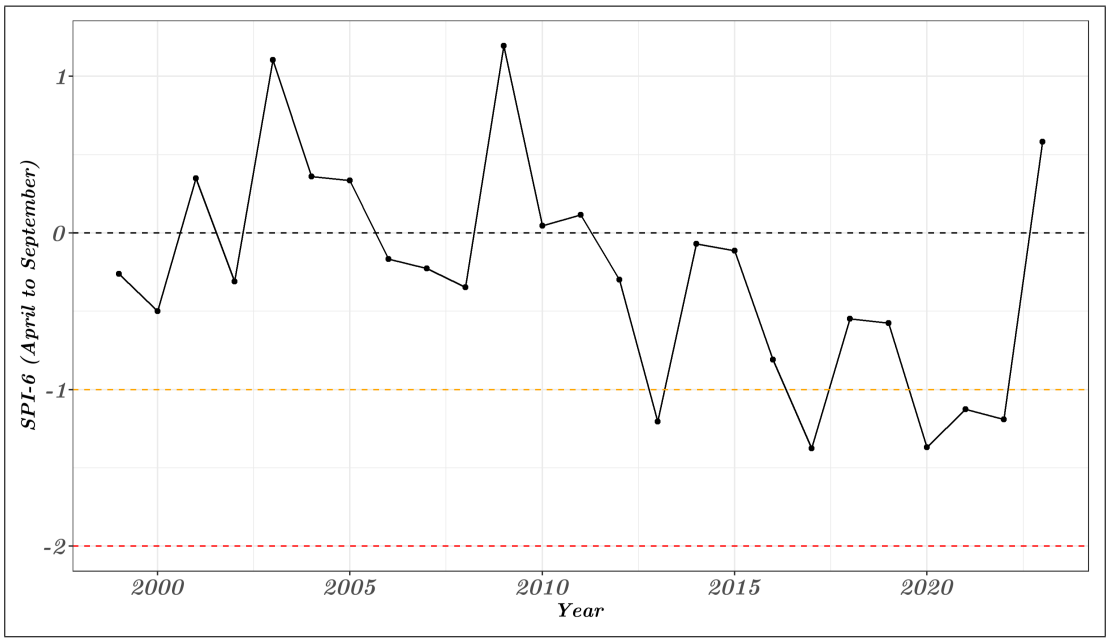

(b) SPI6 of the period (1999-2023)

Figure 3.4 SPI6 plotted against the years 1901 to 2023 for the study area on Mt.Etna.

Additionally, figure 3.5 shows the SPEI6 values between the years 1999 to 2022. In this plot, the vast majority of values ranging from 2000 to 2003 are above 0, except for 2000, which exhibits a negative value. A notable decrease in values after 2011 is also visible, with eight negative values recorded from 2012 to 2022.

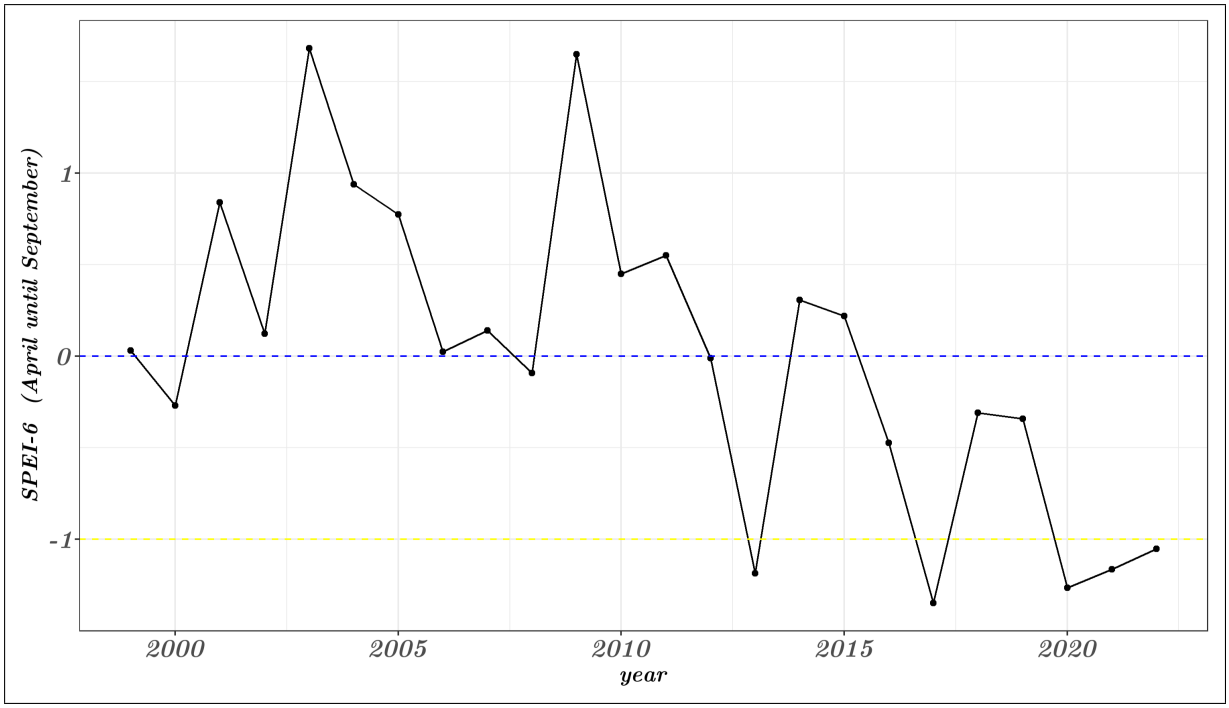

Figure 3.5 SPEI6 plotted against the years 1999 to 2022 for the study area on Mt.Etna.

Statistical analyses should reveal whether the ring widths of the sampled trees near Piano Provenzana correlate with the drought indices. Table 3.2 shows the output data for Pearson's correlation coefficient. Both t-values are negative, with the t-value in the SPEI6 column being more negative. The remaining output values, p-value, degrees of freedom, correlation coefficient and the confidence interval vary between the two indices.

Table 3.2 Table of the statistical output from the Pearson's correlation between SPI6/SPEI6 and the detrended tree ring chronology.

Pearson's correlation	SPI6 vs. detrended tree ring chronology	SPEI6 vs. detrended tree ring chronology
H1: true correlation is not equal to 0		
t-value	-2.0797	-3.0909
p-value	0.0397	0.0053
Degrees of freedom	121	22
Correlation coefficient	-0.1858	-0.5503
95% confidence interval	-0.3513 to -0.0090	-0.7804 to -0.1888

Figure 3.6 demonstrates the results plotted of the running correlation of the tree-ring chronology and the SPI. The upper plot provides a comprehensive view of the entire period between 1901 and 2023, while the lower shows the running correlation only between 1999 and 2023. The running correlation of the SPI6 reveals no clear trend of the correlation. In the beginning, the correlation seems positive until around 1920 when it drops and stays negative until around 1938. After that, it stays positive until a drop in 1970. Until before the year 2000, the correlation varies between slightly negative and positive. However, prior to the year 2000, there is a sudden drop in the correlation value. It is especially low in the year 2001. Until 2010, the correlation value then increases, though always staying in the negative range.

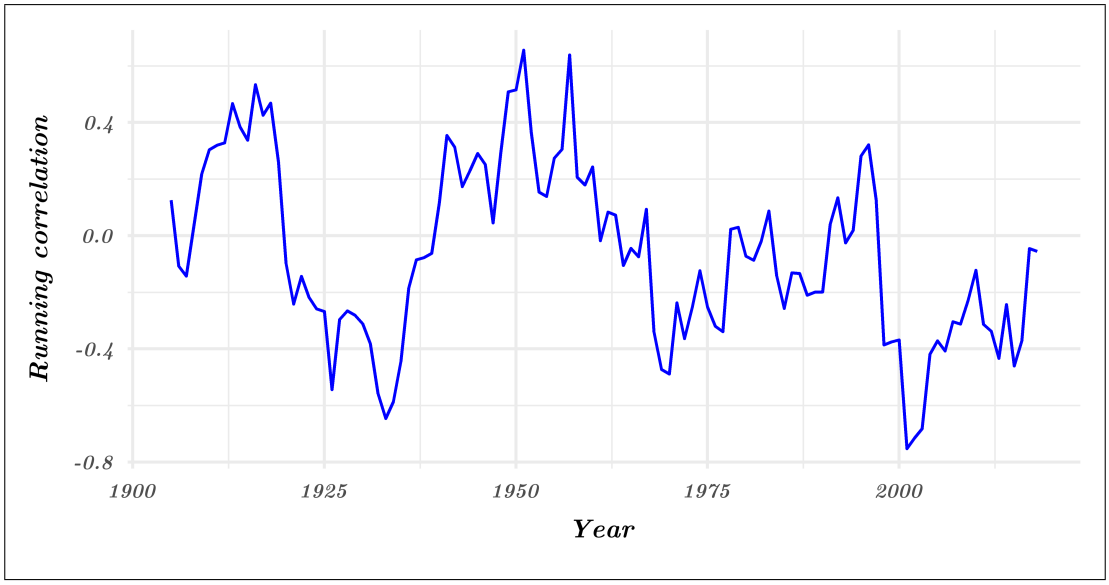

(a) Running correlation of the whole period (1901-2023

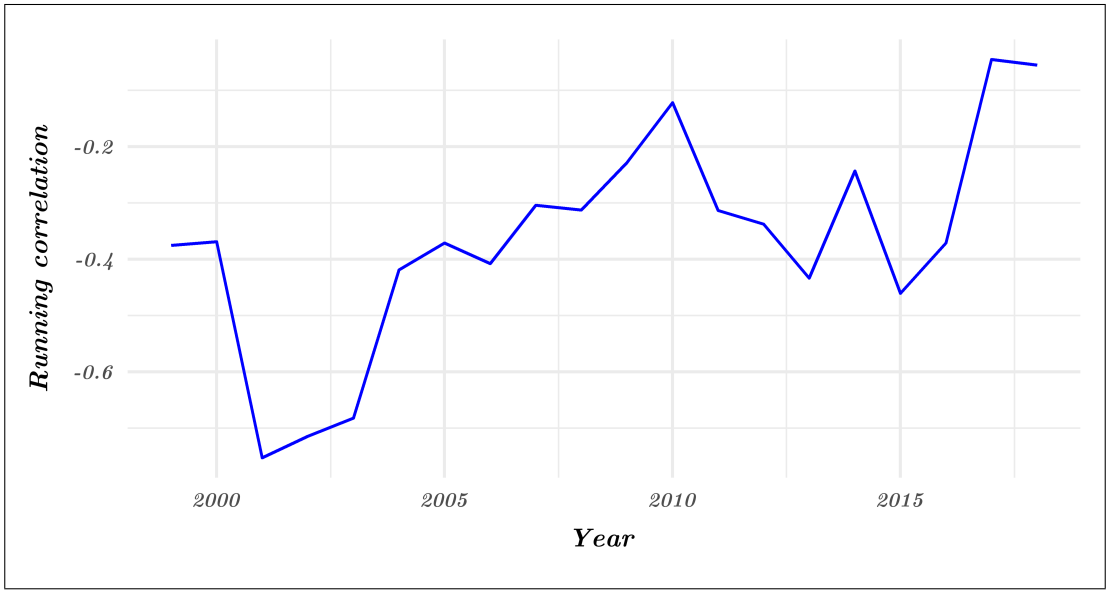

(b) Running correlation of the period (1999-2023

Figure 3.6 Running correlation values of the detrended tree ring chronology vs. SPI6 for the years 1901 to 2023 and 1999 to 2023.

The running correlation of the tree-ring chronology and the SPEI6, displayed in figure 3.7, reveals that all values between 2000 and 2006 are negative. Particularly the years 2001 to 2005 have values of -1. Afterward, the years 2007, 2010, 2016, 2017 and 2019 show high positive values. All other years indicate a negative correlation coefficient.

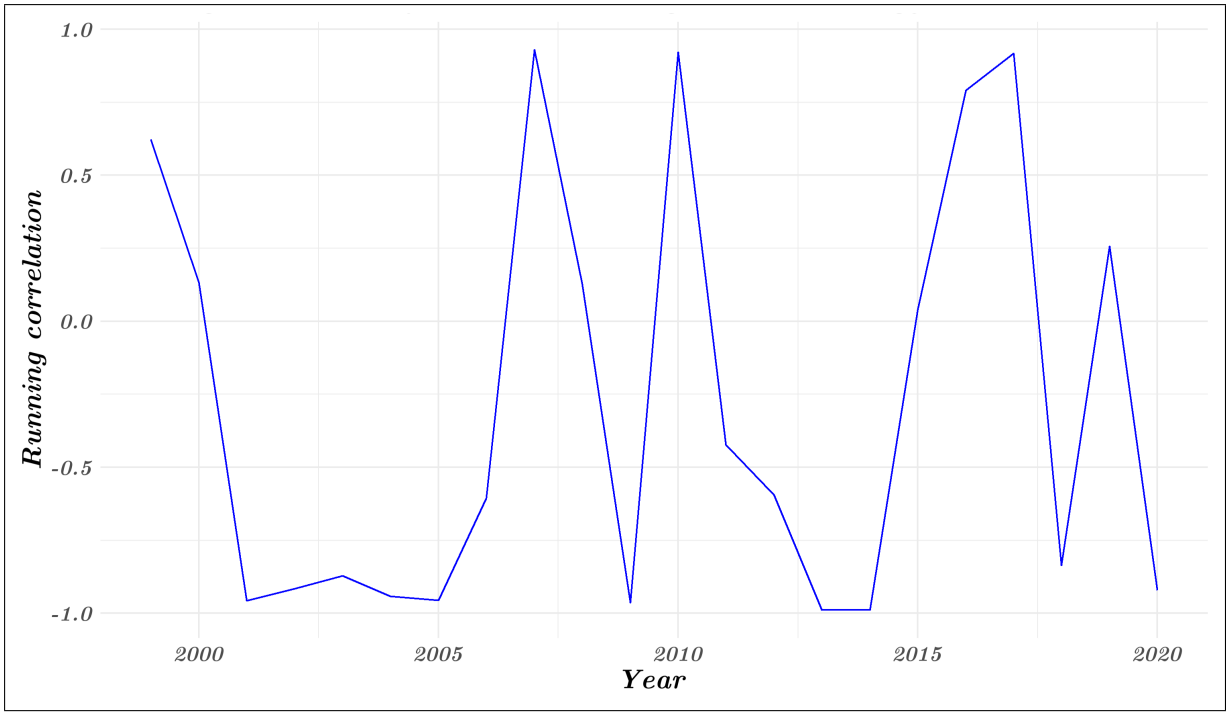

Figure 3.7 Running correlation values of the detrended tree ring chronology vs. SPEI6 for the years 1999 to 2020.

3.3 Stable isotopes

In table 3.3 the δ^{13}C and the δ^{18}O values for the 10 samples from both sampling sites are presented. Annual results for the period investigated between 1998 and 2007 are present. Due to some measurement errors and missing year rings, some values are missing. The δ^{13}C ranges in the sampling site from – 25.37 to -22.04 and in the control group from -24.64 to -22.53. The δ^{18}O results lie between 30.31 and 34.68 in the sampling group and between 31.66 and 34.91 in the control group. The average carbon content was 39.22% for the sampling site samples and 39.61% for the control site samples.

Table 3.3 Table of the stable isotopic values from the analyzed individual samples.

YEAR	A1a δ^{18}O [‰]	A1a δ^{13}C [‰]	A2a δ^{18}O [‰]	A2a δ^{13}C [‰]	A3b δ^{18}O [‰]	A3b δ^{13}C [‰]	A5a δ^{18}O [‰]	A5a δ^{13}C [‰]	A6a δ^{18}O [‰]	A6a δ^{13}C [‰]
1998	32.74	-23.46	33.67	-23.47	33.99	-23.87	32.89	-22.81	33.48	-22.32
1999	31.91	-23.56	32.99	-23.65	32.9	-24.05	33.17	-22.87	32.56	-22.04
2000	32.37	-23.56	32.01	-23.77	33.22	-24.34	32.09	-22.8	32.91	-22.47
2001	32.84	-23.76	33.25	-23.75	34.68	-23.92	32.6	-23.21	33.71	-22.36
2002	32.45	-23.76	32.15	-24.13	33.62	-24.62	32.96	-23.51	33.59	-22.71
2003					31.56	-24.36				
2004			32.65	-25.37	33.44	-24.59				
2005	31.87	-24.58	32.57	-24.93	32.59	-24.27	31.23	-24.07	32.08	-23.82
2006	32.55	-24.48	33.95	-24.39	34.26	-23.77	32.94	-24.18	32.17	-23.89
2007	30.31	-24.55	33.82	-24.19	34.34	-23.91	31.76	-23.98	32.13	-23.48

YEAR	C2a δ^{18}O [‰]	C2a δ^{13}C [‰]	C3a δ^{18}O [‰]	C3a δ^{13}C [‰]	C4a δ^{18}O [‰]	C4a δ^{13}C [‰]	C5a δ^{18}O [‰]	C5a δ^{13}C [‰]	C7a δ^{18}O [‰]	C7a δ^{13}C [‰]
1998	33.23	-23.43	33.48	-23.37	33.02	-24.49	33.26	-22.6		
1999	33.48	-23.53	33.98	-23.75	33.6	-24.06	33.32	-22.6	33.54	-23.77
2000			32.63	-23.63	32.73	-24.31	31.78	-22.82	32.73	-23.99
2001			34.55	-22.46	33.07	-23.03	32.9	-22.53	33.63	-23.51
2002	32.25	-23.71	34.16	-24.23	33.52	-23.86	33.11	-23.13	33.39	-23.88
2003	33.05	-23.71	32.8	-24.64	32.66	-24.21	32.77	-23.65	33.44	-23.68
2004	32.85	-24.03	34.66	-24.18	34.18	-23.92	32.84	-23.81	33.65	-24.03
2005	31.66	-24.14	33.15	-24.63	33.19	-24.19	31.92	-23.36	32.28	-24.06
2006	33.19	-24.06	34.5	-24.19	34.91	-24.07	33.64	-23.17	33.63	-24.31
2007	33.26	-23.87	34.22	-23.84	34.16	-23.85	32.05	-22.74	33.99	-23.91

In figure 3.8 the results of the δ^{13}C analysis are plotted. A total of ten samples are plotted against the years of interest. Samples, A1a, A2a, A5a, and A6a, have incomplete results because of the missing year rings. A3b is the only continuous measurement of the sampling site. A slight depression is evident in all samples between 2001 and 2005. Further, the trees from the control site and sample A3b show a peak in 2001. Especially C3a shows a clear peak of less negative values in 2002 with a difference to the values of 2000 and 2002 of 1.17 and 1.77, respectively.

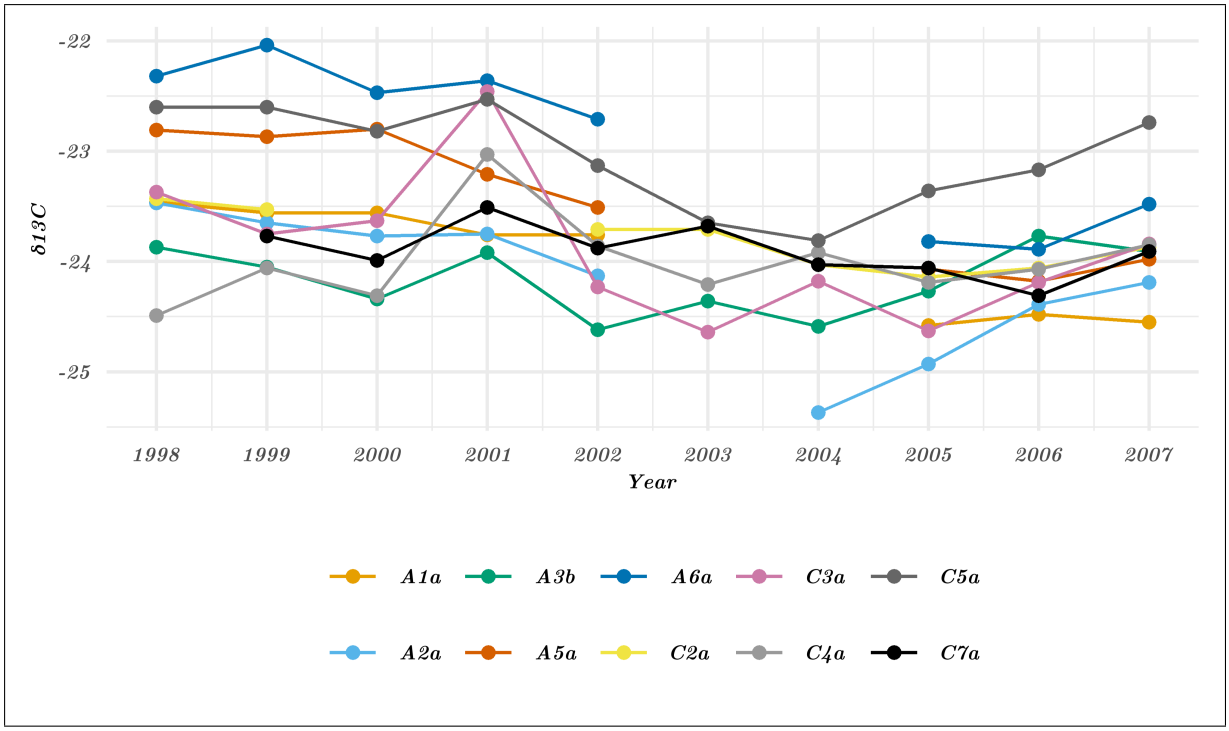

Figure 3.8 δ^{13}C values of all measured samples plotted against the year.

Figure 5.10 located in the appendix exclusively depicts the trees at the sampling site. It is visible that all samples show lower values after the eruption compared to pre-eruptive times. Yet, due to the missing rings, no continuous records are available. The difference between the 2002 and 2004 values is greatest in the A2a sample with a drop of -1.2. The depression is also visible during the years 2002-2004 on the A3b line.
Stable carbon isotopes were also analyzed for samples primarily prepared for radiocarbon analysis. The results are displayed in the plot, seen in figure 3.9. The tree samples from the sampling site are represented by shades of blue and green, while the control site trees are indicated by shades of orange and yellow. The samples A3a and A6c did not show a year ring in 2003 and consequently have no results in δ^{13}C.

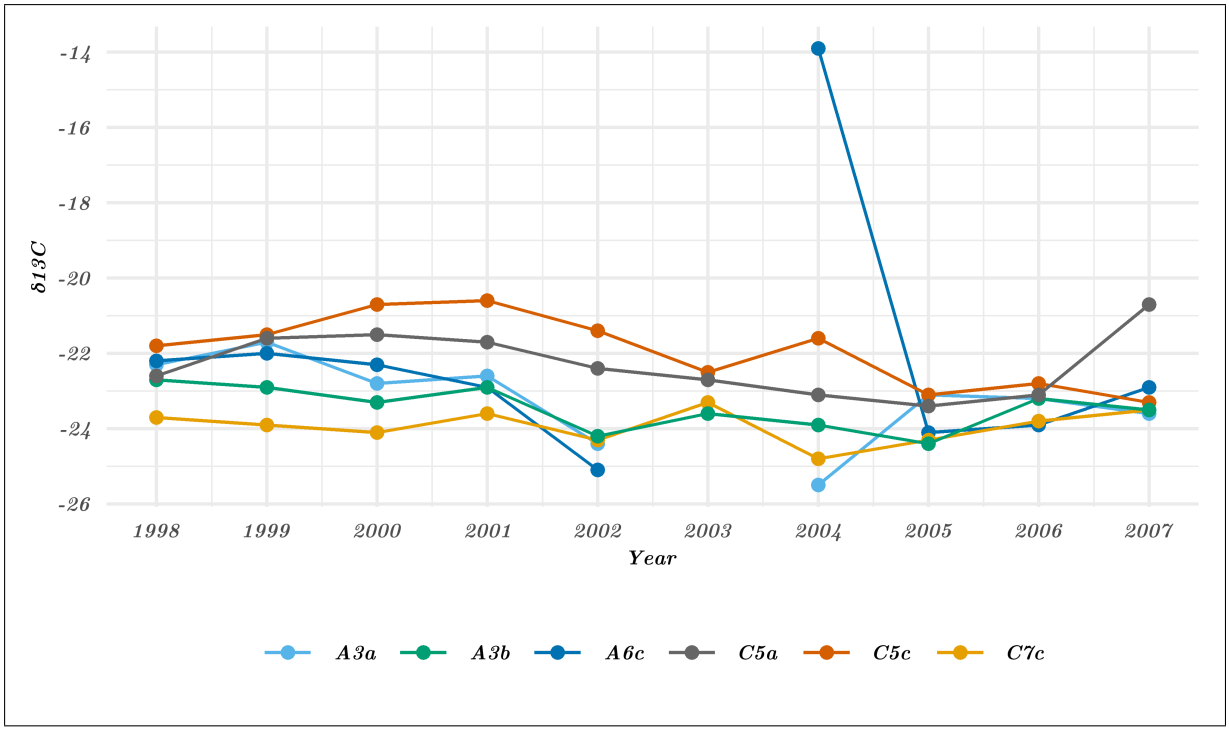

Figure 3.9 δ^{13}C values of individual trees on Mt. Etna, values from the radiocarbon analysis.

This plot demonstrates that all trees seem to follow the same trend with values ranging from -25.5 to -21.7 in the sampling group and –24.8 to -20.6 in the control group. An exception is obseerved in the sample A6c from 2004, with a δ^{13}C value of -13.9. Another noteworthy observation is evident in sample A3a in 2004, which is lower than the 2005, following an opposite trend than the other trees.
In figure 3.10, the δ^{18}O values of all measured samples are presented. Overall, all values are closely grouped, and no clear trend is visible. However, A3b, C3a, and C4a exhibit a negative peak in the year 2003. The other samples from the control group do not show this negative peak. It must be added that most of the samples also display a negative peak in 2005.

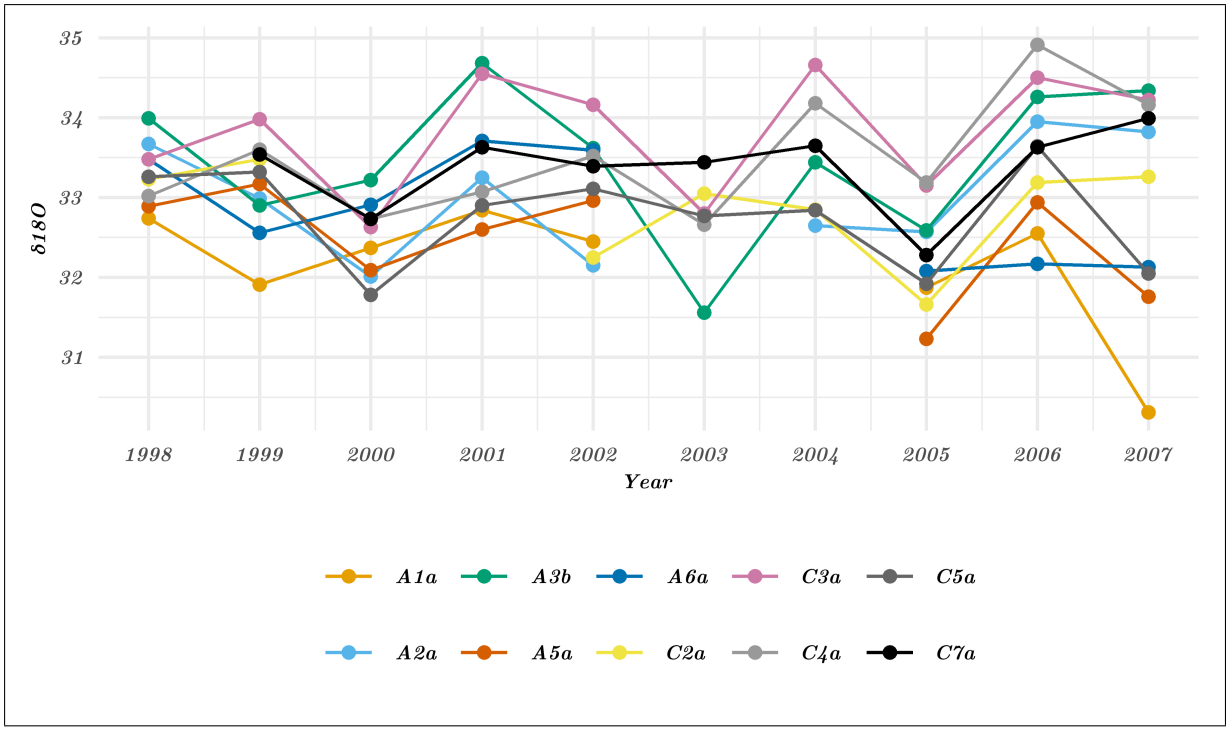

Figure 3.10 δ^{18}O values of all measured samples plotted against the year.

Figure 5.11 in the appendix once again represents only the sampling site values. A3b shows a distinct pattern. The course of this sample's δ^{18}O values shows a peak in 2001, with a drop until 2003 and a rise again in 2004. The other samples with discontinuous data all show lower values after the eruption in comparison to the year 2002.

Figure 3.11, depicts the average δ^{18}O and δ^{13}C chronologies for the sampling site. The δ^{13}C chronologies are divided into the two measurement practices of the stable isotope measurements and the values gathered in the radiocarbon analysis. The two δ^{13}C chronologies exhibit rather distinct patterns. It must be added that the scale here is inverted, with the less negative values occupying the bottom part. However, as only one sample of each chronology had continuous measurements, the averages are rather heavily influenced by these values in the years 2003 and 2004. Nevertheless, the δ^{13}C _radio curve has a peak in 2002 and a strong peak in 2004, whereas the δ^{13}C values of the stable isotope analysis show a clear decrease until 2004 and then an increase afterward.

Figure 3.11 Mean stable isotope chronologies against the years 1998-2007 for the sampling site.

The mean δ^{18}O chronology displays a peak in 2001 and negative peaks in 2003 and 2005. Once more, only A3b exhibits continuous measurements and thus heavily influences the average in the years 2003 and 2004.
The Pearman's rank correlation coefficient of the δ^{18}O chronology against the δ^{13}C of the stable isotope measurements was 0.39 and for the δ^{18}O chronology against the δ^{13}C values from the radiocarbon analysis 0.43.

3.4 Radiocarbon

In this section, the results of radiocarbon analysis are presented. In figure 3.12 the $F^{14}C$ values per analyzed tree sample are plotted against the years of interest. The values from the sampling site are represented by the orange and yellow shades, while the values from the control site are represented by the blue and green shades. The tree samples A3a and A6c are missing values in the year 2003, as no rings were available in these years. In this plot, all years follow the same path, except for sample A3d which is higher in 2003 and 2004. Further, samples A3a and A6c are lower in the year 2002 compared to other sample values. Moreover, they reveal a much lower value in the year 2004, compared to the other tree samples. In 2005, the values of these two samples once again increase to the level of the other samples.

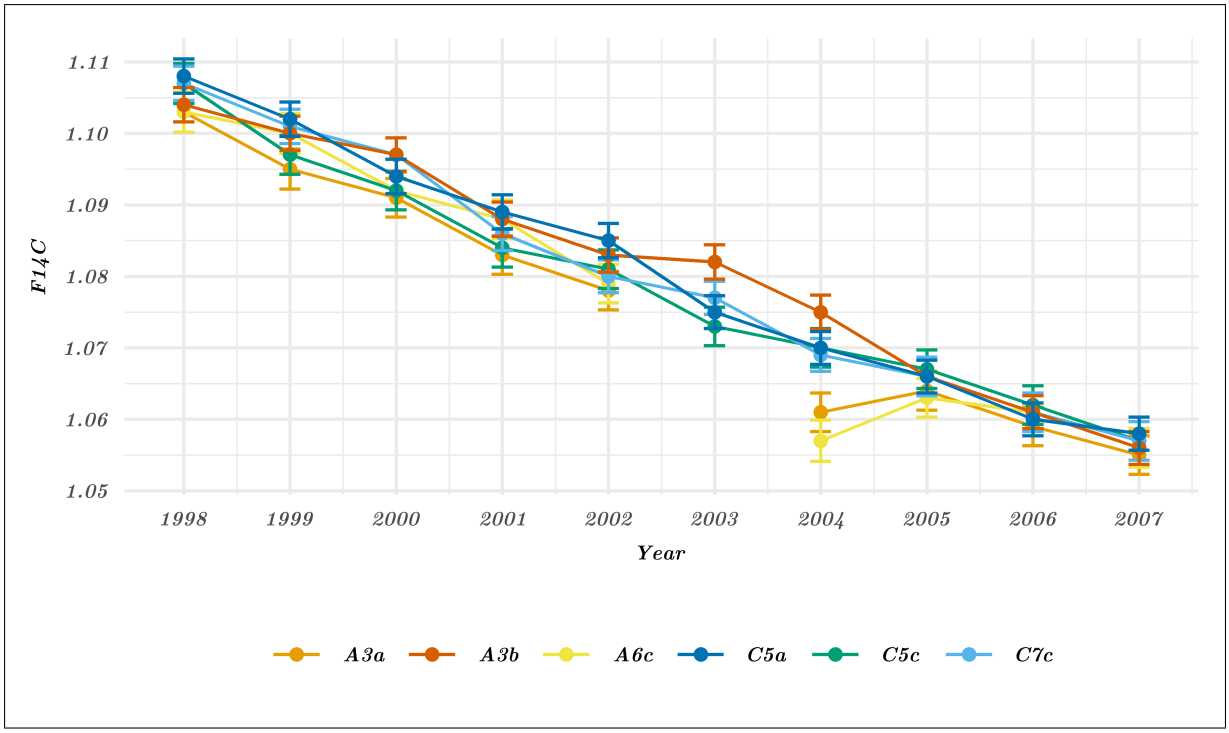

Figure 3.12 Plot of individual $F^{14}C$ values against the years of interest of all analyzed tree samples.

The second plot in this part is displayed in figure 3.13. This plot illustrates the mean $F^{14}C$ values per site for both the sampling site near Piano Provenzana and the control site. The mean values obtained from the sampling site are represented by orange dots, while the values derived from the control site are indicated by blue dots. The sampling site values follow the same path as the control site values until the year 2003 at which point they demonstrated higher values at the sampling site. In the subsequent year, 2004, the values are lower than in the control site. In the following years, the curves follow the same path again.

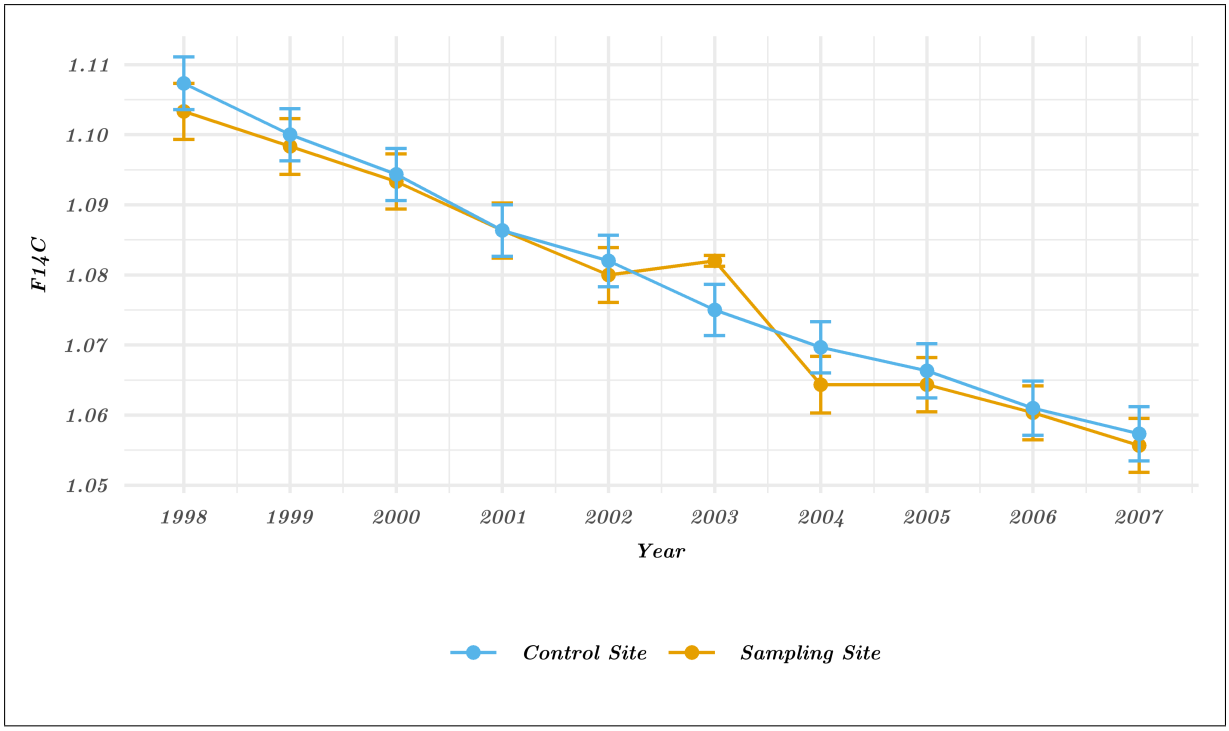

Figure 3.13 Plot of mean $F^{14}C$ values against the years of interest per site.

3.5 LA-ICP-MS

In this section, the results from the laser ablation of trace elements are presented. In the initial phase, the point measurements are visualized, followed by the line measurements. The data from the sampling site in Piano Provenzana is always presented in orange, while the data from the control group is colored blue. The plots of the point measurements once again demonstrate the values from the sampling site, represented here in orange, and the values from the control site, represented here in blue. The individual trace elements in the line measurements do not follow this color code.

3.5.1 Point measurements

Firstly, the point measurement results for the trace elements Ca, K, and Mn are presented. Figure 3.14 shows the plots created in RStudio. The elements Ca and K show an increase in the year 2003 followed by a subsequent decrease to lower values at the sampling site. Interestingly, both plots also show smaller peaks in 1999 and 2001 or a sudden decrease in the year 2000. In contrast, the trees in the control site exhibit slightly higher values in the years 2003 and 2004, with a drop afterward. The clearest peak is visible in the plot of Mn. The values at the sampling site are rather stable until the year 2002, when they are higher, and an even higher value in 2003, with a sudden drop in 2004. The values in the control site also follow a stable line with a small peak in 2002.

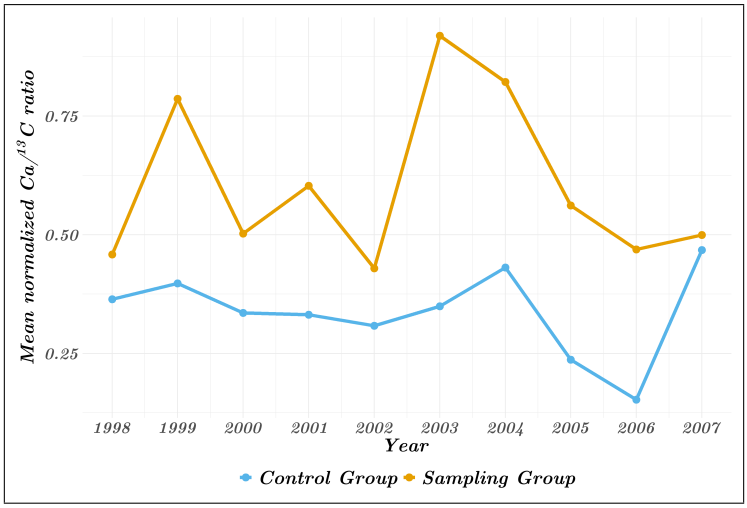

(a) Mean normalized Ca/^{13}C ratio for the two sampling sites.

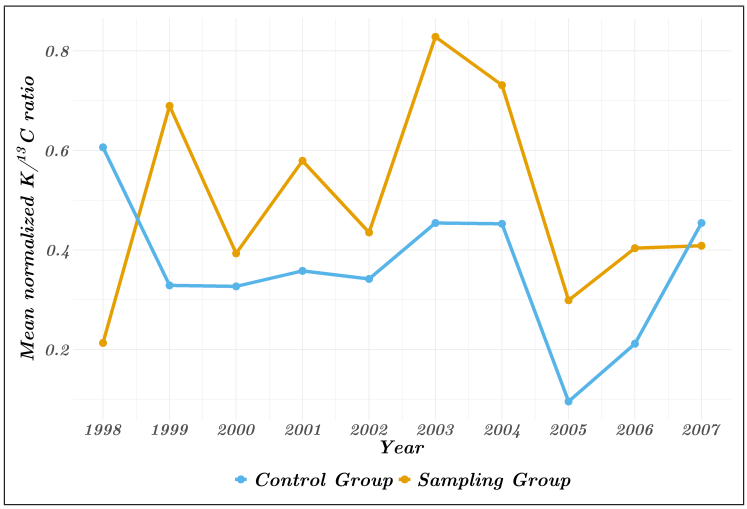

(b) Mean normalized K/^{13}C ratio for the two sampling sites.

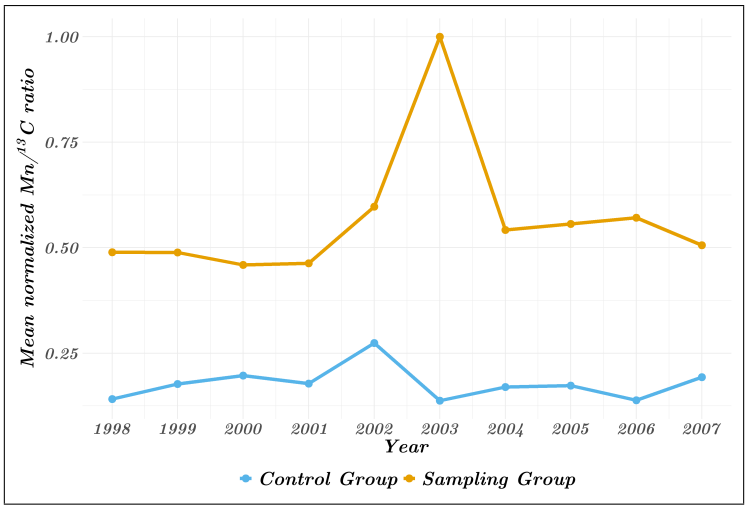

(c) Mean normalized Mn/^{13}C ratio for the two sampling sites.

Figure 3.14 Mean normalized element (Ca, K, Mn) to ^{13}C ratios for the two sampling sites.

Trace elements that showed a peak around the eruption in 2002/2003 in the trees at the sampling site were: Mg, Al, Silicon (Si), S, Titanium (Ti), Chromium (Cr), Mn, Cu, Zn, Arsenic (As), Strontium (Sr), Mercury (Hg), Thallium (Tl) and Fe in the year 2004. Distinct peaks in

the sampling site trees were found especially in Cu, Mg, S, and Zn, as illustrated in figure 3.15. A modest increase in Cu and S elements was observed in 2002, followed by a pronounced peak in 2003 and a notable decline in 2004 for the sampling site. Conversely, the control site values demonstrate no clear trend. The Mg plot exhibits a small drop in 2002 and a big peak in 2003 for the sampling site. It then stays in higher values until 2007, at which point it underwent a subsequent decline. In this instance, the control site shows no trend with a flat curve. The Zn plot demonstrates a strong peak in 2003; nevertheless, the values fluctuate from year to year and do not form a flat curve. A notable observation is the abrupt decline in the values of the control site in 2003.

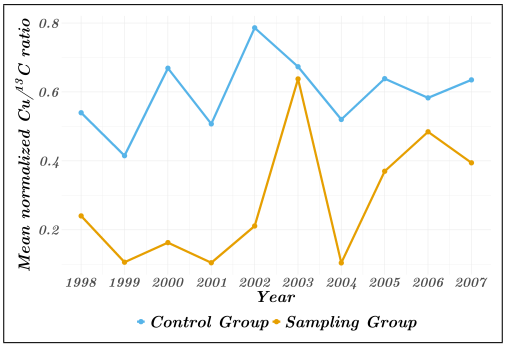

(a) Mean normalized Cu/^{13}C ratio for the two sampling sites.

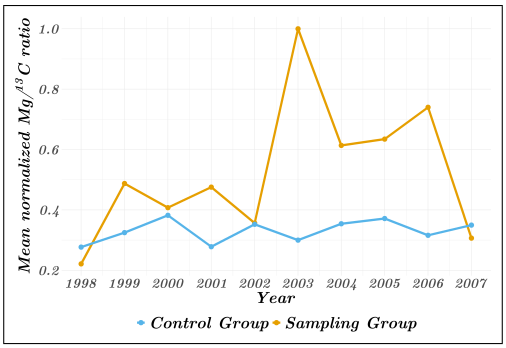

(b) Mean normalized Mg/^{13}C ratio for the two sampling sites.

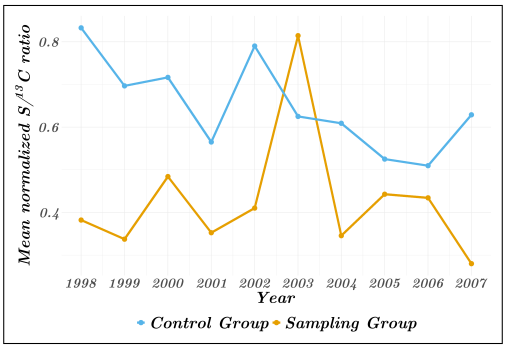

(c) Mean normalized S/^{13}C ratio for the two sampling sites.

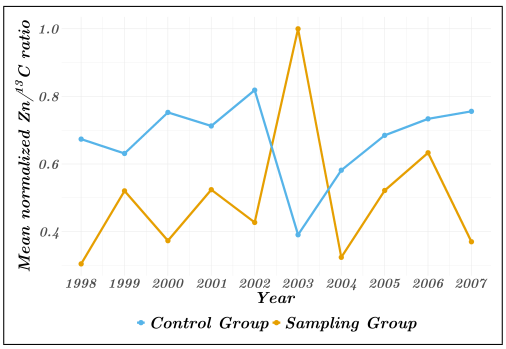

(d) Mean normalized Zn/^{13}C ratio for the two sampling sites.

Figure 3.15 Mean normalized elements (Cu, Mg, S, Zn) to ^{13}C ratios for the two sampling sites.

3.5.2 Line measurements

As A3d displays all years between 1998 and 2007, these results demonstrate a full timeline of trace element measurements. Figure 3.16 shows a plot of the trace elements Pb and Cu plotted against the tree core of A3d. Both trace elements have a distinct peak around the time of late 2002. In the element Cu, this peak is more distinctive. The peak of these two trace elements was also visible in the second measurement of this tree sample.

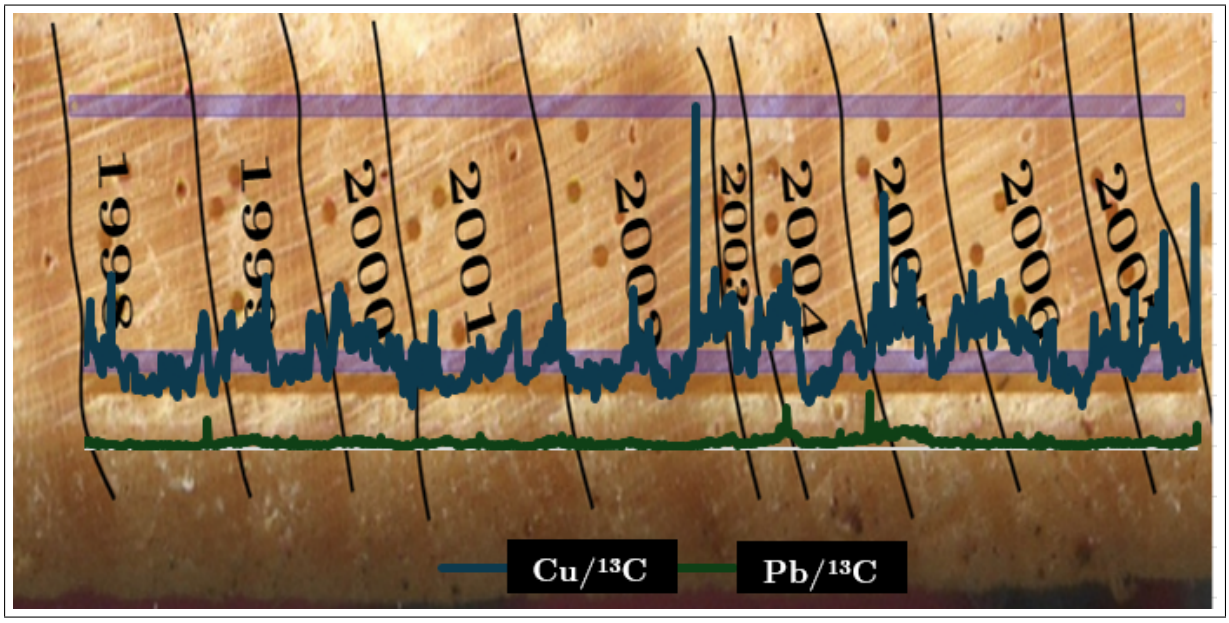

Figure 3.16 Plot of mean element to ^{13}C ratio of the trace elements Pb and Cu along a timeline between 1998 to 2007 for the tree sample A3d.

In figure 3.17, the same tree, A3d, is displayed with the trace element Mn. Here, the year-to-year fluctuations are visible in element concentration. Moreover, the years preceding the eruption in 2002/2003 show a possibly higher amount of Mn and a sudden drop at the end of 2002. This finding could not be reproduced in the second measurement. It must be added that both measurements also showed a minor peak surrounding the eruption in the trace element Fe.

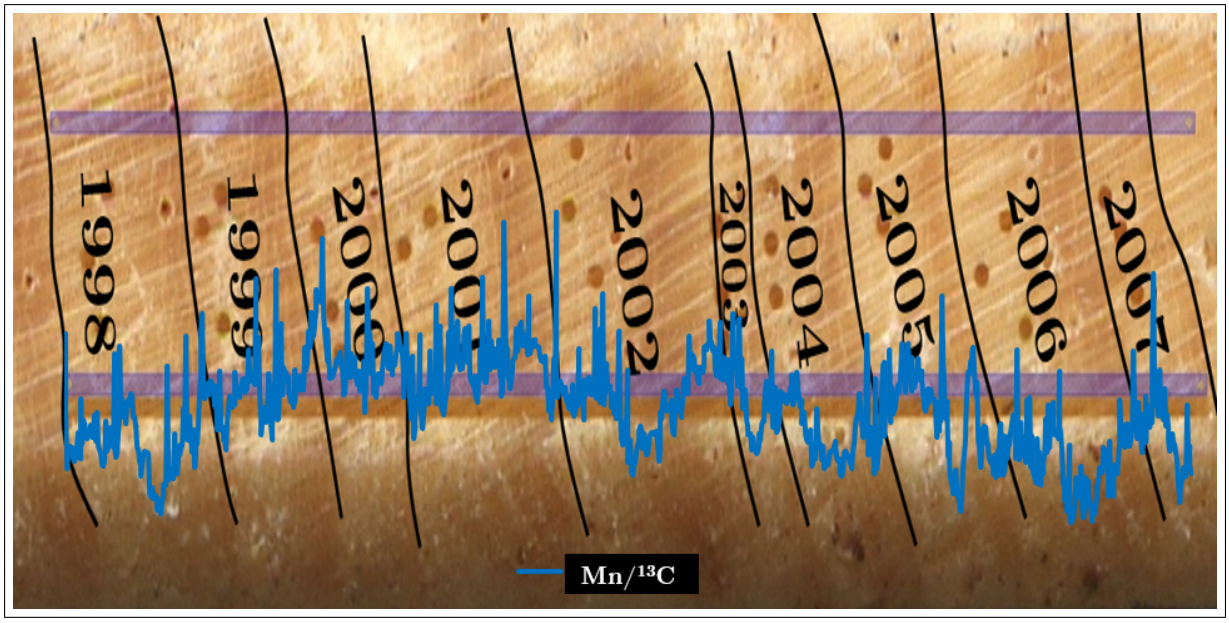

Figure 3.17 Plot of Mn to ^{13}C ratio along a timeline between 1998 to 2007 for the tree sample A3d.

In figure 3.18 a plot of a second tree from the sampling site is presented. Sample tree A5b exhibits distinct peaks in the elements S, Ca, and Fe. These peaks are displayed in the year 2005 and 2006. Other than these years, all three elements show a rather stable path. It must be added that this tree sample does not show the years 2003 and 2004. Furthermore, a decline in the S values appears to occur at the close of 2002, preceding the volcanic eruption.

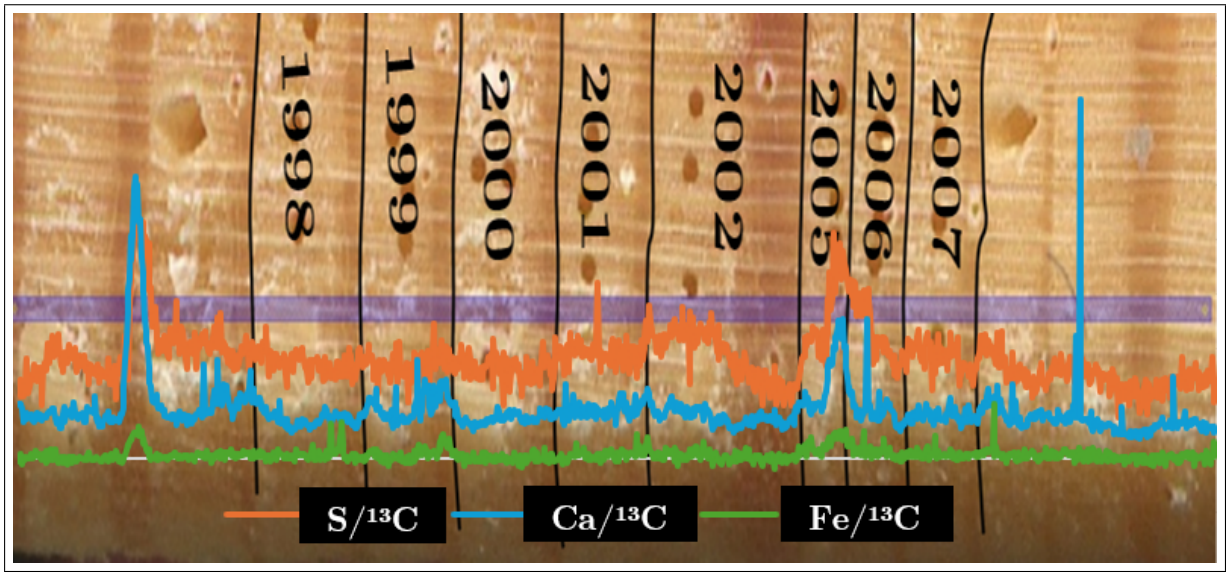

Figure 3.18 Plot of mean element to ^{13}C ratio of the trace elements S, Ca and Fe along a timeline between 1998 to 2007 for the tree sample A5b.

Other tree samples show additional distinct peaks in the trace element K. However, no such peaks or elevated levels of elements were detected before the 2002/2003 eruption.
Tree samples from the control site also show distinct peaks in trace elements around the 2002/2003 eruption. The detected elements were Al, S, K, Pb, Mg, Mn, and Fe. Figure 3.19 shows a plot of the tree sample C7b showing the trace elements Al and Fe. These two trace elements show distinct peaks in late 2003. In a similar manner, Pb exhibits this peak in this

tree sample; the magnitude of the peak was smaller. Prior to the 2002/2003 eruption, no peaks or elevated values were detected in the samples from the control group.

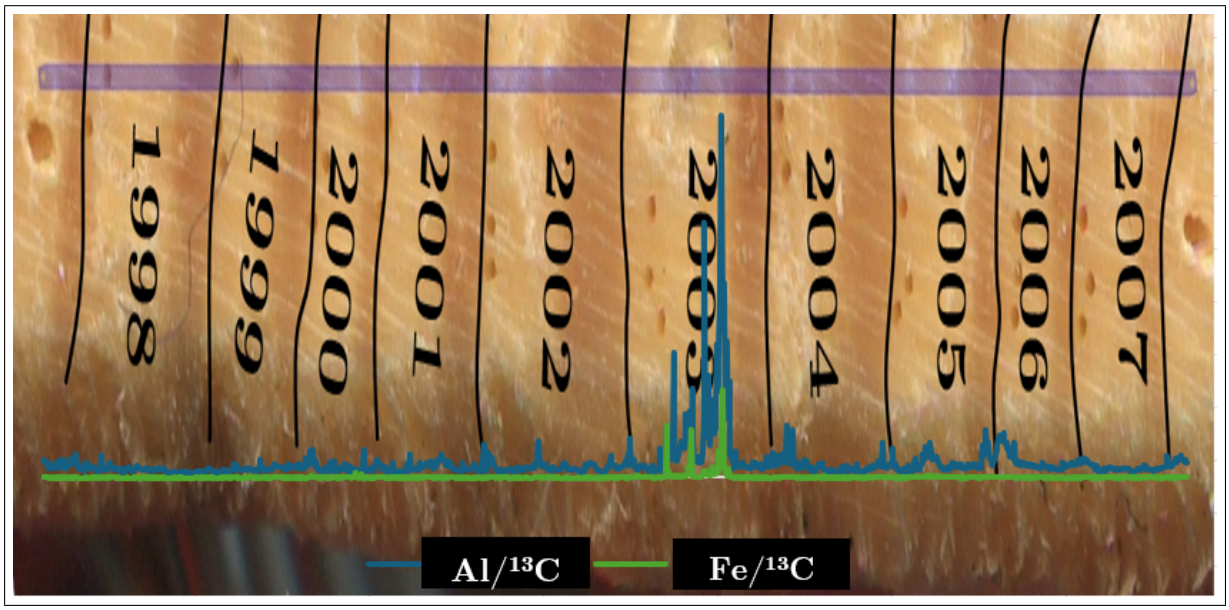

Figure 3.19 Plot of mean element to ^{13}C ratio of the trace elements Al and Fe along a timeline between 1998 to 2007 for the tree sample C7b.

3.6 Stem-water stable isotopes

In figure3.20 the analyzed stem-water samples are plotted together with the GMWL, the LMWL of Southern Italy, the LMWL of the Mediterranean Sea (Pennisi et al. 2000) (Hatvani et al. 2023), the LMWL determined by Parello et al. (2001) and the LMWL proposed by Liotta et al. (2013). In this particular plot in figure 3.20, it is evident that all the samples from both sites are situated beneath all five Meteoric Water Lines (MWL). They all appear closest to the GMWL and furthest to the LMWL of Southern Italy. The values from the sampling site are close together in the δ^{18}O values (range: -8.26 to -6.86), whereas the δ^{2}H values vary between -60.82 and -53.63. The data from the control site, however, appears compactly clustered in the plot. The δ^{18}O values range from -6.36 to -5.69 and the δ^{2}H varies between -57.81 and -49.59. While both sites have a similar range in the δ^{2}H, they notably differ in the δ^{18}O values.

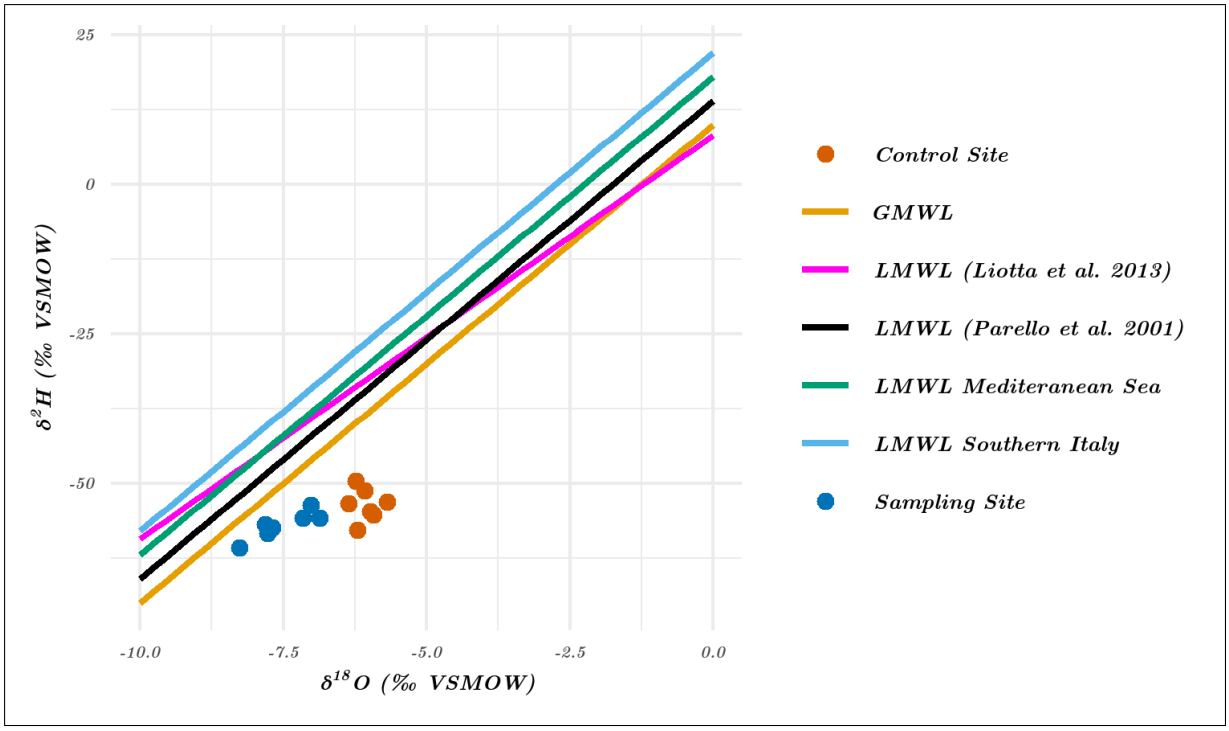

Figure 3.20 δ^2H-δ^{18}O plot of the stem water samples from the trees on the sampling site and the control site near Piano Provenzana on Mt. Etna. Plotted together with the GMWL, the LMWL of Southern Italy, the LMWL of the Mediteranean Sea, the LMWL determined by Parello et al (2001) and the LMWL proposed by Liotta et al (2013)).

Table 3.4 presents a comprehensive listing of all values derived from the stem-water analysis. This includes the sample name, the related sampling group, the δ^2H and δ^{18}O values with the respective group mean, the altitude for each sampled tree plus the group mean, the fresh and dry weight, the differences between fresh and dry weight, as well as the water content of each sample and the group mean. The mean values of δ^2H and δ^{18}O differentiate by 1.5 and 3.3, respectively. The mean elevations of the trees show a difference of around 45 meters. The water content is close together, highlighted by the difference of 0.5% in the mean values and only 0.3% in the median between the groups.

Table 3.4 Table with important information from the water extraction analysis, including Tree ID, site name, atable isotope content , altitude, fresh and dry weight, as well as their difference and the water content of the sample.

Tree ID	Site name	δ^{18}O [‰]	δ^{2}H [‰]	Altitude [m.a.s.l.]	Fresh weight [mg]	Dry weight [mg]	Difference fresh and dry [mg]	Water content [%]
A1	Sampling	-8.26	-60.82	1739	14098.7	13471.4	627.3	4.45
A2	Sampling	-7.78	-58.34	1741	14223.1	13563.2	659.9	4.64
A3	Sampling	-7.69	-57.41	1743	14553.1	13641.4	911.7	6.26
A4	Sampling	-7.02	-53.63	1744	14370	13618.2	751.8	5.23
A5	Sampling	-7.82	-56.83	1748	14415.5	13602.1	813.4	5.64
A6	Sampling	-7.16	-55.82	1749	14072.9	13528.1	544.8	3.87
A7	Sampling	-6.86	-55.87	1757	14376.2	13531.5	844.7	5.88
mean A		-7.51	-56.967	1745.9				5.14
C1	Control	-6.08	-51.30	1700	14297.7	13532.8	764.9	5.35
C2	Control	-6.21	-57.81	1700	14780.5	13880.6	899.9	6.09
C3	Control	-5.93	-55.21	1705	14800.3	13730.5	1069.8	7.23
C4	Control	-6.36	-53.43	1700	14325.9	13531	794.9	5.55
C5	Control	-5.69	-53.12	1710	13976.1	13403.1	573	4.1
C6	Control	-6.23	-49.59	1699	14270	13446.6	823.4	5.77
C7	Control	-5.98	-54.76	1699	14358.8	13563.1	795.7	5.54
mean C		-6.07	-53.6	1701.9				5.66

Chapter 4

Discussion

The following part discusses the results presented in the previous chapter. It is divided into the same subchapters.

4.1 Crossdating

This part discusses the results of the crossdating.

4.1.1 Ring weight

The ring weights depicted in figure 3.1 on page 25 are utilized to underline the difference in the ring sizes encountered during the preparation of the samples. Shen et al. (2022) found in other species that the ring weight is predominantly controlled by the ring width and not its density. This means the weights also highlight differences in ring widths and can be used to assess the growth of a tree in a year. In this thesis, both tree groups show an increase in the year 2002 and then a decrease in weight in the year 2003. However, the increase in weight was manifested in some trees of the sampling group as early as 2001. This finding corresponds temporally with the increased NDVI signal documented in 2000 and 2001 by Houlié et al. (2006). Moreover, the difference between the sites is also visible in the declining trend before the eruption in the control group, while the sampling group near Piano Provenzana seems stable in weight or even increasing. Given the SPI6 data indicating relatively arid conditions prior to 2000, the observed decrease in ring widths within the control group would be more indicative of the observed trend, as tree-ring growth is known to be influenced by environmental factors. A decrease in precipitation and higher temperatures could indicate less growth. (Seiler et al. 2017b).

4.1.2 Missing rings

The plots of figure 3.1 on page 25 also reveal missing values, which are associated with the missing ring in 2003 and 2004 of some trees. The identification of these missing rings was achieved through crossdating of the individual trees to the existing chronology of Seiler (2017c). If not added, the curves visually and statistically differed. This phenomenon of missing rings after a volcanic eruption was already observed on Mt. Etna by Seiler et al. (2017a). In their work, tree samples had one or two consecutive years missing after the 1974 eruption. The underlying cause of this phenomenon is believed to be the result of heat radiation from the nearby lava flow that injured the trees (Seiler et al. 2017a). As trees from Seiler (2017c) do not show missing rings after the 2002/2003 eruption, it can be assumed that the trees sampled for this thesis are

in closer proximity to the lava flow, as the radiation influenced their growth. The high GLKs from table 3.1 on page 26 also indicate that missing rings were correctly added to the individual trees at the sampling site. The same applies to the control group with GLK ranging from 62.8 to 87.2 for the individual trees to the mean curve.

The GLK of 61 between the sampling group trees and group 1 of Seiler et al. (2017b) is not particularly elevated. However, when looking at figure 3.3 on page 27, they visually match from 2013 until approximately 1910. The majority of the peaks are observed within the same years. Afterward, the curves are visually diverse. This could provide a potential explanation for the relatively low GLK. The root of this may lie in the preparation of the samples. As in both researches, the time after 1910 was not of great importance, the focus lays in the years after 1910. This could be the reason that led to a lower standard in ring width measurements. This work concentrates on the years around the 2002/2003 eruption. Yet, all trees were carefully analyzed throughout the entire time series. This should also be visible in figure 3.2 on page 26 where the trees also match after 1910. Another possible explanation is that the few trees further back in the chronology might have too much weight in the mean chronology. Notwithstanding, a GLK of 61 falls within an acceptable range. This conclusion is supported by the findings of Trouet et al. (2006) and other studies, such as that by Bernabei (2018), which utilized comparable values.

4.2 Meteorological influence

In this thesis, both the SPI and the SPEI were calculated for the region of Mt. Etna. Given that the SPI exclusively utilized precipitation as input data, it was feasible to calculate it over an extended period. Because the SPEI had three input parameters and added to the precipitation the possible evapotranspiration through temperature values, it was only calculated for the period around the 2002/2003 eruption. Results revealed a similar trend between 1999 and 2022 for the SPI6 and SPEI6. The SPI6 and SPEI6 results in the appendix also exhibit a similar pattern. The two temporal trends of both SPI6 and SPEI6 are visible in figure 3.4 and figure 3.5. The most obvious seems to be the similarity in the trend paths in both plots. They agree when a year is drier and when it gets wetter. However, they show differences in the degrees of severity. Examples are the years 2014 and 2015 which were categorized as no drought in SPEI6 with a value above 0, whereas values slightly under 0 indicate a light drought event in the SPI6. These differences in the identification of the severity of drought events were also highlighted in the work of Tirivarambo et al. (2018). They revealed that both indices were able to identify temporal variation of drought, however differed in the drought condition. Though, the main purpose of these indices is to find out how the ring width curve compares to them. This helps to find periods where the ring widths are more strongly influenced by other effects than the climate.

Table 3.2 on page 29 examines the Pearson correlation between two drought indices (SPI6 and SPEI6) and a detrended tree-ring chronology. The objective is to identify potential relationships between climatic conditions and tree growth. SPI6 shows a calculated correlation of -0.1858, suggesting a modest negative relationship between the SPI6 index and the tree-ring chronology. Statistical significance is given with a p-value of 0.03967, which is below the conventional 5% threshold. The 95% confidence interval ranges from -0.3512 to -0.0090, indicating that the true correlation value is likely to be negative. The negative value suggests that an increase in SPI6 (wetter conditions) corresponds with reduced tree growth. This is contrary to literature that points out that droughts limit the growth of trees (Seiler et al. 2017a) (Binda et al. 2021) (Trouet et al. 2006). However, Shen et al. (2022) highlight, that trees in higher altitudes demonstrate positive relationships between summer temperatures and ring widths, while trees at lower altitude exhibit a positive relationship between precipitation and ring widths. Nevertheless, as

the SPI is designed to describe droughts and not only precipitation (Tirivarombo et al. 2018), the negative correlation could be related to other factors heavily influencing the ring growth of the trees. The low negative correlation, however, does not show a strong relationship between the years 1901-2023, indicating the influence of other factors. This could indicate a potential weakness of the SPI, given its reliance on precipitation as the sole input data. Tirivarombo et al. (2018) suggest the use of SPI only when temperature data is missing and that its interpretation should be undertaken with caution. Additionally, the running correlation in figure 3.6 on page 30 demonstrates that the relationship between the SPI6 and the ring width chronology is not consistently negative and exhibits a considerable range. Higher positive values are found in two positive periods between 1901 and 1920 and 1938 to 1970. Noteworthy is the drop before the 1974 eruption, which was also described by Seiler et al (2017a). However, this observation might just be coincidental, as this eruption happened on the western flank of Mt. Etna. Nevertheless, a sudden drop before 2000 can be observed. This drop seems especially interesting, as it is before the 2002/2003 eruption and ranges from a positive correlation coefficient of nearly 0.4 before to nearly -0.8 afterward. In the years 2001 and 2002 with the elevated NDVI signal, an especially strong negative correlation is visible. Yet, as mentioned above, the SPI and consequently the correlation with it should be interpreted with caution.

In the column of the SPEI6 value in table 3.2 on page 29, a much stronger negative correlation of -0.5503 is observed, indicating a moderate to strong relationship. The p-value of 0.0053 confirms the substantial significance of this correlation. The 95% confidence interval (-0.7804 to -0.1888) shows greater variability but still confirms the negative association. This suggests that the SPEI6 index exhibits a stronger connection to tree growth compared to the SPI6. Notwithstanding, the negative relationship once again shows contrary results to common literature. This might again indicate that other factors than climate influenced the tree growth of the studied trees. One potential explanation might be the presence of pollution. Perone et al. (2018) for example, found restricted growth near industrial plants, suggesting that pollution is the primary factor limiting tree growth in these areas. This pollution might also occur near volcanic eruptions, as they release high amounts of gases (Aiuppa et al. 2008) and particles into the surrounding area and atmosphere (Calabrese et al. 2015). The running correlation in figure 3.7 on page 31 helps to reveal the trend of the correlation over the period investigated. This is especially useful, as the statistical output in table 3.2 on page 29 shows great variability. The running correlation indicates that the correlation coefficient does not always exhibit a negative relationship; in some cases, it shows higher positive values. Strongly negative values are found in the years before and during the 2003 eruption. Different from the SPI however, the negative correlation remains visible until 2006. The signal around the period of the eruption could be possibly explained by the fact that trees were observed to show different growth patterns in the years before, during, and after volcanic eruptions (Seiler et al. 2021). Nonetheless, the curve demonstrates erratic behavior, indicating an absence of a clear relationship between the drought index SPEI and the ring width curve over the course of the study period. This finding contrasts with the extant literature, which demonstrates robust correlations between tree-ring width and SPEI (Islam et al. 2019) (Bhuyan et al. 2017).

The SPI and SPEI analyses revealed that the growth of the sampled trees near the eruptive fissure of the 2002/2003 eruption can be hardly explained by drought indices, which contradicts existing literature. Possible pollution by the eruption (Calabrese et al. 2015) and other growth-influencing factors before, during, and after the eruption (Seiler et al. 2021) might have contributed to the unclear relationship between the climate and tree growth. However, it must be noted that the meteorological data used in this study comes from stations around Mt. Etna and not the exact sampling site. As also described by Seiler et al. (2021) and Versace et al. (2022), the climatological setting on Mt. Etna is very diverse. Consequently, average meteoro-

logical data from three stations around Mt. Etna might not be best suited for the evaluation of the climatological influence on the trees at the sampling site. Future work could include closer meteorological stations for data collection.

4.3 Stable isotopes

In general, the carbon content of the extracted cellulose is found to be slightly lower than what the literature would suggest. Nevertheless, the values lie only around 5% under the estimations of wood carbon content in Mediterranean species proposed by Thomas & Martin (2012).

Overall, the measured δ^{13}C values in table 3.3 on page 32 match the range with the values obtained on Mt.Etna near Piano Provenzana by Seiler et al. (2021). Additionally, the values of the two measurement methods match. The sample A3b can be utilized to compare the two approaches to measuring δ^{13}C, as it was analyzed in both the stable isotope and the radiocarbon methods. This sample underwent the same preparation, and the only difference is the measurement, which was done by IRMS for stable isotopes and AMS with the radiocarbon samples. The data of the sample A3b reveals that the absolute values do not match. However, a similar curve is found in both measurements. In figure 3.8 and figure 3.9 it is visible that both chronologies follow a similar trend with higher values before the eruption and more negative values after the eruption, with a slight peak in 2001. This indicates, that while the absolute values are not directly comparable between the measurement procedures, the δ^{13}C curves can be compared in terms of general trends and curve shape. This finding aligns with literature, which finds AMS to be less precise than IRMS in δ^{13}C measurements, but both being equally suitable for ^{14}C correction (Prasad et al. 2019) (McIntyre et al. 2017). However, the mean chronologies from the sampling site in figure 3.11 on page36 do not show a similar trend. This is mainly due to the individual outlier of sample A6c in the radiocarbon group, causing an unnaturally high value (less negative). Further, all samples from the radiocarbon group demonstrated more negative values in 2002, leading to the mean curve having a rather low δ^{13}C value in 2002. This differs from the higher δ^{13}C value of the group from the stable isotope measurement.
The slight depression with more negative values found in the years around the eruption in figure 3.8 on page 33 is not visible in the samples measured with the radiocarbon method in figure 3.9 on page 34. However, radiocarbon preparation samples appear to exhibit slightly more negative values during and after the eruption. As Tognetti et al. (2012) write, tissue δ^{13}C provides a record of changes in stomatal activity, as well as photosynthetic rates. More negative δ^{13}C values could indicate stomatal opening and possibly increased photosynthesis (Tognetti et al. 2012). Seiler et al. (2021) highlight the influence of environmental changes on the δ^{13}C in trees. However, one outlier is found in sample A6c in figure 3.9. This sample shows a less negative value in 2004. Higher δ^{13}C values could be indicative to stomatal closure, which can be a result from injury to the tree (Tognetti et al. 2012). The observation of a missing ring in this tree suggests a potential link with the stress experienced by the tree in the aftermath of the eruption. This stress may have led to the closure of the stomata and the absence of the ring.

As illustrated figure 3.8, the samples from both the sampling group and the control group are distributed within the same range of δ^{13}C values. However, it is evident that the sampling group exhibits slightly more negative values. The presence of magmatic CO_2 would result in less negative values, as this deep-origine CO_2 has δ^{13}C values around 0 (Giammanco et al. 2017). However, as they both lie in the same range, the likelihood of such an influence is considered low.
In figure 5.10 in the appendix, all samples with missing rings exhibit a clear drop in values between 2002 and 2004 or 2005, which could indicate higher stomatal conductivity in trees

(Tognetti et al. 2012). The discrepancy is more pronounced than the continuous measurement from A3b suggests. Especially sample A2a reveals a difference of -1.2 between 2002 and 2004. A possible explanation is an increased stomatal opening after the eruptive stress, induced to the trees in 2003. However, this finding contradicts the conclusions of previous studies, which suggest slow recovery decreases stomatal openings after stress (McAdam 2023). Tognetti et al. (2012) emphasize that increased photosynthesis could lead to more negative δ^{13}C. However, Angelopoulos et al. (1996) say that even after stress is released from trees, photosynthesis levels struggle to go back to pre-stress levels. It is therefore unlikely, that increased stomatal openings or elevated levels of photosynthesis resulted in more negative δ^{13}C values after the eruption in the trees from the sampling site. Maybe switches in CO_2 sources (Aiuppa et al. 2007) or other chemical processes linked to volcanic activity (Skelton et al. 2012) led to the lower values. But more negative values in 2002 could be an indication of more stomatal conductivity (Tognetti et al. 2012) prior to the eruption, potentially attributable to more humid conditions in pre-eruptive times (Aiuppa et al. 2008) or a slight influence of deep-origine CO_2 (Giammanco et al. 2017).

The lower δ^{18}O values observed during and after the eruption depicted in figure 3.10 on page 35 can be caused by higher humidity attributed to large amounts of dust in the atmosphere after the eruption (Seiler et al. 2021). This could give an explanation to the lower values in the control group tree samples C3a and C4a, which show a lower δ^{18}O in 2003. However, the presence of atmospheric dust, which may reduce solar radiation and air temperatures (Seiler et al. 2021), was likely not around in 2005, therefore cannot be a sufficient explanation of the reduced δ^{18}O values in the sampling site. However, the sole continuous measurement from A3b also exhibits the decline in 2003 and subsequent rise in 2004, a phenomenon that can be plausibly attributed to a temporal dust cloud. Nonetheless, Seiler et al. (2021) suggest that reduced δ^{18}O in the trees during and after the eruption can be also caused by the uptake of volcanic water through degassing. This could be the cause of the reduced δ^{18}O values found in this study at the sampling site. Skelton et al. (2014) also found δ^{18}O changes in groundwater before, during, and after earthquakes, due to changes in water-rock interaction. This change in the groundwater and the uptake of this water in trees may have also influenced the isotopic composition. Yet, tree-ring δ^{18}O is not a measure of the source water, as the trees δ^{18}O signal is mainly modulated by air humidity (Tognetti et al. 2012). Even though the eruption might have changed the δ^{18}O signal in the trees during and after the eruption, no reduced δ^{18}O was found before the eruption. Moreover, the measured samples near the eruptive fissure show elevated δ^{18}O in the year 2001 in figures X (all A) and figure x (mean von beiden), which is contrary to the results of Seiler et al. (2021). The mean curve of the samples from the sampling site in figure 3.11 on page 36 also demonstrates this trend of elevated δ^{18}O prior to the eruption. The elevated NDVI signal before the eruption cannot be explained by induced volcanic water vapor, according to these results.

The Pearman's rank correlation coefficients in table 3.2 on page 29 between the δ^{18}O series and the two δ^{13}C reveal a modest positive correlation. These values are consistent with the range of correlations demonstrated in Seiler et al. (2021) for the corresponding period. Further, they concluded that the carbon and oxygen isotope ratio variations are more strongly correlated during the period spanning from 1989 to 2006, supporting the values gathered in this thesis. Tognetti et al. (2012) found that positively correlated δ^{18}O and δ^{13}C values indicate that stomatal conductance is the dominant limitation of photosynthesis. If the values are not correlated, the variation in stomatal conductance can be detected by δ^{18}O (Tognetti et al. 2012). The observed positive correlation may, therefore, be indicative of stomatal conductance constituting the limiting factor of photosynthesis. This suggests that open stomata are the main driver of elevated photosynthesis rates in these trees. Therefore, elevated NDVI levels before the 2002/2003 eruption should be accompanied by indicators for increased stomatal conductance. Indicators of higher stomatal conductance would be more negative δ^{13}C, due to changes in supply and de-

mand of CO_2, and lower $\delta^{18}O$ values due to humidity changes (Tognetti et al. 2012). Whereas $\delta^{13}C$ analyses in this work partially showed more negative values before the eruption, possibly showing a change in the CO_2 source, no clear signal was found in $\delta^{18}O$ values.

In summary, the elevated photosynthesis rates, that were observed with the elevated NDVI signal prior to the eruption, could also be visible in the lower $\delta^{13}C$ values in some of the trees before the eruption. Nevertheless, stable isotope analysis could only find indicators for higher stomatal conductance in trees, or a small influence of deep-origine CO_2, but not increased water input through water vapor.

4.4 Radiocarbon

In figure 3.12 on page 37 the plot with the results of the radiocarbon analysis is presented. A thorough examination of the plot reveals that all curves of the six analyzed tree samples share a common path. Except for the years 2003 and 2004, in which the values of the sampling site trees differed from the control site trees. This phenomenon is also visible in figure 3.13 on page 38, which presents the mean values per sampling site. Even though one year of samples A3a and A6c is missing, they show a lower value in the year 2004, whereas sample A3b shows higher values in 2003 and 2004. The presence of missing values also led to the mean curve in the graph in figure 3.13 having a peak in the year 2003. This can be since only one measurement, coming from the A3b sample, was present for the building of the curve. Apart from being extracted from the same sampling location, these samples underwent distinct preparation methods before the analysis, which might have led to these discrepancies. The sample A3b was prepared in accordance with the samples for the stable isotope analysis, which is described in the methods part and based on the method proposed by Boettger et al. (2007). The other two samples followed the BABAB method to extract the cellulose and dissolve contamination, according to the method of Němec et al. (2010). These differences in preparation leading to varying results were also found by Seiler et al. (2021). Differences between the cellulose-extraction preparation method proposed by Němec et al. (2010) and the Acid-Base-Acid (ABA) method (Hajdas 2008) were found. The latter method led to results showing lower $F^{14}C$ values in the two years prior to the eruption. Seiler et al. (2021) concluded that these lower $F^{14}C$ values could be due to pre-eruptive CO_2 being released into the atmosphere and injected into the soil. This fossil, ^{14}C -dead, CO_2 (Seiler et al. 2021), has been identified to be a potential reason for the lower values observed in the year following the eruption in this work. It is supported by the assumption that volcanic activity is closely linked to local, elevated CO_2 concentrations (Bogue et al. 2023). However, it is not known how the fossil CO_2 was stored in the rings after the eruption, leading to this lower $F^{14}C$ value. Due to the absence of data for the year 2003, it is not possible to see whether fossil CO_2 was already taken up by the trees in 2003. Additionally, the decline in $F^{14}C$ is less pronounced compared to the one observed by Seiler et al. (2021). Nonetheless, stress influences the trees' carbon uptake also during the recovery as shown by Rehschuh et al. (2022). Complex processes in the tree during the recovery period (Rehschuh et al. 2022) could have led to volcanic CO_2 being stored in the ring following the eruption and the missing ring. The higher $F^{14}C$ values in the A3b sample in 2003 and 2004 are difficult to explain and further analysis could be done for a better understanding. Possible explanations can be found in the complicated fractionation processes of the isotopes while entering the plants (Stenström et al. 2011). Further, the stress on the tree during the years following the eruption (Rehschuh et al. 2022) and the differences in the treatments of the samples, which were also found by Seiler et al. (2021), could have led to these results. Nonetheless, no signal was found before the 2002/2003 eruption, that could explain an uptake of fossil CO_2 in the pre-eruptive stage and help to explain the elevated NDVI signal observed during those years.

4.5 LA-ICP-MS

Chemical analyses of tree rings must be interpreted with caution, as elements tend to be mobile inside the tree. The mobility of these elements is closely linked to their size and charge. (Hevia et al. 2018). Tree-species-specific physiological responses, as well as the age of individual trees, have been identified as significant factors that influence elemental mobility within the tree. The differences lie in the availability of the elements in the soil, distinct uptake mechanisms, and complex mobility patterns in the xylem (Dobrzańska et al. 2021). Amais et al. (2021) reveal that plants can take up metals Al, Fe, Mn, Pb, and Zn from particulate matter. Further, Scharnweber et al. (2016) identified the trace metal Al and the nutrients Ca, Mn, and K being suitable for dendrochemical analyses in pine trees. They emphasize that results should be viewed as tendencies, rather than hard facts.

4.5.1 Point measurements

The point measurement results revealed several elemental peaks found in the samples. Figure 3.14 and figure 3.15 illustrate the clearest peaks recorded. In this work, the most intense peaks were recorded for the elements Ca, K, Mn, Mg, Zn, S and, Cu. These peaks are presumably related to Mt. Etna's volcanic activity, as Calabrese et al. (2011) describe that S belongs to the most abundant anions, and K, Ca, and Mg, to the most common metals in volcanic aerosols on Mt. Etna. Additionally, Cu and Zn are also linked to volcanic activity on Mt. Etna, such as degassing (Calabrese et al. 2011). Giammanco et al. (1998) identified the groundwaters of Mt. Etna enriched in Mn among other elements. In addition, Dobrzańska et al. (2021) found that Mn seems to be rather stably embedded within rings and is not easily transferred between ring boundaries.
This thesis' peaks in point measurements all appear in the year 2003, showing a reaction of the trees after the volcanic eruption in 2003. This is consistent with results from Bertin et al. (2021) who found increased levels of Zn and Cu after eruptions. Unlu et al. (2009) also found increased Cu, Zn, and Cu element to ^{13}C ratios during and after a volcanic eruption. Yet, Watt et al. (2007) found no systematic correlation of volcanic eruption and cation levels in tree cores of *P. nigra* on Mt. Etna. No element revealed a clear pre-eruptive peak that would indicate an increased uptake of the nutrients during the observed elevated NDVI period. Furthermore, not all recorded elements with peaks are classified as nutrients for trees. Parzych & Sobisz (2012) describe the elements K, Ca, and Mg among essential nutrients and Zn, Cu, and Mn in small amounts contributing to normal growth patterns in *P. nigra*. Furthermore, elevated phosphorus levels, which act as fertilizers, were not present, contrary to propositions by Seiler (2017c).

4.5.2 Line measurements

The line measurements in figures (3.16- 3.19) have peaks in the elements Pb, Cu, Mn, S, Al, and Fe for the individual trees. Furthermore, a peak in K was found but not shown. These elements have been mentioned in different literature, linking them to volcanic activity (Unlu et al. 2009) (Calabrese et al. 2011) (Bertin et al. 2021) and acting as nutrients in *P. nigra* (Parzych & Sobisz 2012). Still, the line measurements are only connected approximately to the ring-width pictures. Therefore, only rough estimates of periods can be described for elemental peaks. Additionally, only line measurements of individual trees, rather than pooled mean lines can be presented, given that growing patterns are tree-specific (Binda et al. 2021).

The tree sample A3d exhibits peaks in Pb and Cu (figure 3.16, page 42), which are dispersed in volatile aerosols in volcanic plumes (Calabrese et al. 2011). These elements showed elevated concentrations in trees near pollution sites in pine trees (Shcherbenko et al. 2008), showing that the trees of Piano Provenzana likely absorbed substantial quantities during and after the eruption. Especially Cu shows a clear peak at the end of the growing season in 2002, which corresponds temporally to the first unrest before the eruption (Spilliaert et al. 2006). As the higher concentrations of Mn in figure 3.17 on page 43 in the years before the eruption could not be reproduced in the second measurement and because they were only slightly elevated, they are not given a special meaning in this work. Yet, the point measurements also revealed a peak after the eruption, and (Dobrzańska et al. 2021) described Mn as not easily translocated across ring borders. Furthermore, Giammanco et al. (1998) observed elevated concentrations of this nutrient in the groundwaters of Mt. Etna. Further analyses and reproducible measurements could indicate a possible involvement of Mn or increased water availability before and during the eruption of the sampled trees. The three peaks for the A5b sample (figure 3.18, page 43) are located later in the wood, possibly in the year 2005. However, as this tree does not show in the years 2003 and 2004, translocating processes in the living tree (Scharnweber et al. 2016) could be the reason for the delayed signal. The last tree-ring sample, C7b, that shows rising concentrations of elements is presented in figure 3.19 on page 44. In this plot, it is demonstrated that the control trees also have peaks around the time of the eruption. However, these peaks were only observed in the line measurements. The strongest peaks were found in Al and Fe. These metals are among the most abundant elements found in plume emissions on Mt. Etna. The atmospheric transport of the plume leads to these elements being deposited in the surroundings of Mt.Etna (Calabrese et al. 2011). The delayed signal in the trees could be explained by the postponed uptake from deposited metals in the soil. That's because the timing of the environmental influence and the signal in the tree rings are determined by factors like the depth and chemistry of the soil, as well as the depth and structure of the root system (Binda et al. 2021).

4.6 Stem-water stable isotopes

As the stable isotope values between the sites mainly differed in the δ^{18}O values, primarily these values are the primary focus of this discussion. Despite this, all values are situated beneath all five MWLs. These results can be caused by ^{2}H fractionation during CVD. This influence is pronounced when small amounts of water (<600 μL) are extracted (Diao et al. 2022). Chen et al. (2020) also propose a cautious interpretation when extracting water with CVD from plant material.

Overall, the mean water content of the samples doesn't differ much between the sampling sites, and the trees from the sampling site close to the eruption show more depleted δ^{18}O values, as presented in figure 3.19 on page 44 and table 3.4 on page 46. For a comparison to existing data, meteoric δ^{18}O values of Piano Provenzana from the International Atomic Energy Agency (IAEA) Water Isotope System for Electronic Retrieval (WISER) online database for the sampling period may were retrieved. However, only limited data from 1997 to 2000 was available. Further, only the years 1998 and 1999 had values for May, in which this thesis' sampling was done. The data showed values of -7.2 and -5.5 for the years 1998 and 1999, respectively. Compared to the values from this work, they fit in nicely, highlighting no special hydrological conditions being present during this field trip. However, differences between the sites could indicate that trees take up water from different water sources.

One potential explanation is that soil conditions differ between the two sites, leading to diverse results in stem-water δ^{18}O. In chapter two of Candela et al. (2024), they describe that the high permeability of volcanic products leads to a high infiltration percentage of meteoric precipitation into the soil and an impermeable sedimentary basement. Further, the short residence times of the soil water, the chemical characteristics due to volcanic activity, and the cracking due to lava are characteristic. This lithological variability has the potential to influence local water availability and the groundwater table (Candela et al. 2024). Liotta et al. (2013) also highlight the high variability of the isotopic composition in Sicily and Mt. Etna. More depleted δ^{18}O values are attributed to higher altitude regions (Liotta et al. 2013). Table 5.1 on page 66 shows that the trees of the sampling are located at an average altitude which is 44 meters higher. The slightly higher altitude could lead to a more depleted δ^{18}O signal (Liotta et al. 2013). However, Candela et al. (2024) describe a good mixing of water from different altitudes due to the high fracture permeability of rocks on Mt. Etna. This suggests a different reason for the unequal δ^{18}O signal between the sampling sites.

Another possibility is a difference in root depth which could influence the trees' water uptake. Deep root systems can access groundwater tables further in the ground (Maeght et al. 2013). The isotopic signatures of this groundwater can vary due to the mixing of waters from different altitudinal and temporal origins, as compared to more shallow soil water (Liotta et al. 2013). Von Freyberg et al. (2020) also emphasize that soil water might be isotopically more depleted in δ^{18}O in greater depths, where the evaporative fractionation is not a factor anymore. However, variations resulting from the downward transport of evaporatively influenced water and groundwater tables cause the isotopic signature to decrease nonlinearly. With soil water usually being more negative in greater depths, trees from the sampling site might take up their water from greater depths than the control group trees (Von Freyberg et al. 2020). Greater root depth is assumed to play a key role in water uptake and therefore makes the groundwater more accessible for the sampling group trees (Maeght et al. 2013). As groundwater can be chemically changed during seismic activity (Skelton et al. (2014), the trees near Piano Provenzana might have taken up chemically different groundwater from greater depths, during the years prior to the 2002/2003 eruption. Giammanco et al. (1998) showed increased nutrient levels in groundwaters in active volcanic areas on Mt.Etna, possibly making them more available for deep root trees reaching into the groundwater. However, discrepancies in stem-water isotopes have been observed, though the sample size being limited. Further studies and increased sampling sizes are needed to give conclusive evidence of the trees' root depth and possible water sources. As von Freyberg et al. (2020) note, intensive sampling can be required to fully understand root water uptake in plant systems.

Chapter 5

Conclusion

The objective of this study is to analyze the potential factors that contributed to the elevated NDVI signal in 2001 and 2002 in trees prior to the 2002/2003 eruption on Mt.Etna near Piano Provenzana. The findings indicate that the growth of trees in proximity to the eruptive fissure may not be closely related to climatic conditions. This connotes that these trees are influenced by different environmental factors. In order to investigate the potential causes of the elevated NDVI signal, observed in 2001 and 2002, three research questions were formulated, and several hypotheses were suggested.

The first research question was: *"Do stable isotope measurements and radiocarbon analysis reveal that the trees took up fossil CO_2 before the 2002/2003 eruption?"*. A comprehensive review of the extant literature indicates that an increase in the availability of CO_2 from volcanic degassing, could result in a decrease of ^{14}C. This decline would suggest the uptake of fossil CO_2, while variations in stable carbon isotopes would indicate a shift in the CO_2 source. Radiocarbon analysis conducted in this thesis did not exhibit decreased ^{14}C values prior to the eruption in the sampling trees, which would suggest an increased uptake of volcanic CO_2. However, lower values were observed in the year 2004, possibly showing the influence of volcanic CO_2 during and after the eruption. However, it is plausible that the signal was influenced by the complicated fractioning processes occurring within the plants. The stable carbon isotope analysis revealed no obvious switch in CO_2 before the eruption. Nevertheless, lower $\delta^{13}C$ values were found in the period surrounding the eruption, possibly hinting to volcanic-related switches in the carbon source of the trees. A single sample exhibited lower CO_2 in 2002, potentially attributable to a minimal switch in CO_2 supply or demand, due to a change in stomatal conductivity, or a small influence of deep-origine CO_2.

The second research question posed was as follows: *"Are trace elements found in the wood an explanation for increased nutrient availability in the years with the elevated NDVI signal?"*. Literature found higher concentrations of nutrient trace elements before eruptions leading to faster-growing trees. LA-ICP-MS analysis revealed no clear peaks of nutrient trace elements in the tree rings before the eruption. Consequently, it is concluded that there was no increased nutrient availability before the 2002/2003 eruption. Nevertheless, peaks were found in different rings during and after the eruption, indicating higher availability of these nutrients due to the eruption. Yet, these peaks were not constantly observed in the same year, thereby underlying the complexity of the elemental uptake by trees and their root system.

The third research question is as follows: *"Is there evidence that the trees took up water from a different source in 2001/2002?"*. The question was addressed by conducting stable isotope measurements in the tree cellulose and stem-water samples. Several studies have indicated that there is a possibility of a shift in $\delta^{18}O$ in the groundwater during seismic unrest and lower $\delta^{18}O$ values can indicate more humid conditions. $\delta^{18}O$ analysis of the tree cellulose revealed no clear signal before the eruption, which would indicate a switch of the water source before the eruption. Smaller signals were found during and after the eruption, suggesting the influence of the eruption on the water uptake of the trees. Volcanic degassing could have led to more humid conditions or changes in the underground to volcanic water intruding into the groundwater. The stem-water analysis revealed discrepancies in the isotopic composition between the two sampling sites. It can be an indication that the trees near the eruptive fissure take up chemically different water compared to the trees in the control group. However, if trees took up seismically altered water prior to the eruption remains to be determined.

The findings of this thesis underscore the complexity of interpreting environmental shifts through tree rings. This work demonstrates that the tree's reaction plays a major role in the possibilities for the analysis. The absence of rings, for instance, resulted in challenges during interpretation, as the majority of the derived chronologies were not continuous. While this research offers some insights, further studies could refine its conclusions. More precise meteorological data would facilitate a more accurate interpretation of climate conditions at the time of the eruption, thereby enabling a more precise assessment of environmental impacts. Furthermore, the analysis of tree disks could potentially provide more profound insights into post-eruption growth recovery and long-term ecological responses. Future research should focus on a more thorough examination of radiocarbon preparation methods, as this work found differences in the results between the cellulose preparation methods. It must be added that the eruption destroyed the original trees that showed the elevated NDVI signal. Consequently, only assumptions through the proxy trees can be made.

To conclude, the findings of this study demonstrated that various processes influenced the growth of the trees in proximity to the eruptive fissure. Despite the absence of definitive evidence for factors that led to the elevated NDVI signal in the trees prior to the volcanic eruption, indicators concerning the impact of an eruption on trees in their physiology, isotopic composition, and stored trace elements were presented.

References

Aiuppa, A., Moretti, R., Federico, C., Giudice, G., Gurrieri, S., Liuzzo, M., Papale, P., Shinohara, H. & Valenza, M. (2007). Forecasting Etna eruptions by real-time observation of volcanic gas composition. *Geology, 35*(12), 1115-1118.

Aiuppa, A., G. Giudice, S. Gurrieri, M. Liuzzo, M. Burton, T. Caltabiano, A. J. S. McGonigle, G. Salerno, H. Shinohara, and M. Valenza (2008). Total volatile flux from Mount Etna, *Geophys. Res. Lett., 35.*

Amais, R. S., Moreau, P. S., Francischini, D. S., Magnusson, R., Locosselli, G. M., Godoy-Veiga, M., Ceccantini, G., Ortega Rodriguez, D. R., Tomazello-Filho, M. & Arruda, M. A. (2021). Trace elements distribution in tropical tree rings through high-resolution imaging using LA-ICP-MS analysis. *Journal of Trace Elements in Medicine and Biology, 68*, 126872.

Angelopoulos, K., Dichio, B., & Xiloyannis, C. (1996). Inhibition of photosynthesis in olive trees (Olea europaea L.) during water stress and rewatering. *Journal of experimental botany, 47*(8), 1093-1100.

Aschale, T. M., Cancelliere, A., Palazzolo, N., Buonacera, G., & Peres, D. J. (2024). Analysis of the spatiotemporal trends of standardized drought indices in sicily using ERA5-Land Reanalysis Data (1950–2023). *Water, 16*(18), 2593.

Begley, I. S., & Scrimgeour, C. M. (1997). High-precision δ^2H and δ^{18}O measurement for water and volatile organic compounds by continuous-flow pyrolysis isotope ratio mass spectrometry. *Analytical Chemistry, 69*(8), 1530-1535.

Bernabei, M. (2018). Historical and cultural framing of a medieval wooden artwork through dendrochronology. *International Journal of Conservation Science, 9*(2).

Bertin, L. J., Christie, D. A., Sheppard, P. R., Muñoz, A. A., Lara, A., & Alvarez, C. (2021). Chemical signals in tree rings from northern patagonia as indicators of calbuco volcano eruptions since the 16th century. *Forests, 12*(10), 1305.

Bhuyan, U., Zang, C., & Menzel, A. (2017). Different responses of multispecies tree ring growth to various drought indices across Europe. *Dendrochronologia, 44*, 1-8.

Binda, G., Di Iorio, A., & Monticelli, D. (2021). The what, how, why, and when of dendrochemistry:(paleo) environmental information from the chemical analysis of tree rings. *Science of the Total Environment, 758*, 143672.

Boettger, T., Haupt, M., Knöller, K., Weise, S. M., Waterhouse, J. S., Rinne, K. T., Loader, N. J., Sonninen, E., Jungner, H., Masson-Delmotte, V., Stievenard, M., Guillemin, M.,

Pierre, M., Pazdur, A., Leuenberger, M., Filot, M., Saurer, M., Reynolds, C. E., Helle, G., & Schleser, G. H. (2007). Wood cellulose preparation methods and mass spectrometric analyses of δ^{13}C, δ^{18}O, and nonexchangeable δ^{2}H values in cellulose, sugar, and starch: an interlaboratory comparison. *Analytical Chemistry, 79*(12), 4603-4612.

Bogue, R. R., Douglas, P. M., Fisher, J. B., & Stix, J. (2023). Volcanic diffuse volatile emissions tracked by plant responses detectable from space. Geochemistry, Geophysics, *Geosystems, 24*(11), e2023GC010938.

Calabrese, S., Aiuppa, A., Allard, P., Bagnato, E., Bellomo, S., Brusca, L., D'Alessandro, W. & Parello, F. (2011). Atmospheric sources and sinks of volcanogenic elements in a basaltic volcano (Etna, Italy). *Geochimica et Cosmochimica Acta, 75*(23), 7401-7425.

Calabrese, S., D'alessandro, W., Bellomo, S., Brusca, L., Martin, R. S., Saiano, F., & Parello, F. (2015). Characterization of the Etna volcanic emissions through an active biomonitoring technique (moss-bags): Part 1–Major and trace element composition. *Chemosphere, 119*, 1447-1455.

Candela, E. G., Pecoraino, G., Morici, S., & La Pica, L. (2024). Drinking Water in Sicily.

Cercatillo, S., Friedrich, M., Kromer, B., Paleček, D., & Talamo, S. (2021). Exploring different methods of cellulose extraction for 14 C dating. *New Journal of Chemistry, 45*(20), 8936-8941.

Chen, Y., Helliker, B. R., Tang, X., Li, F., Zhou, Y., & Song, X. (2020). Stem water cryogenic extraction biases estimation in deuterium isotope composition of plant source water. *Proceedings of the National Academy of Sciences, 117*(52), 33345-33350.

Clocchiatti, R., Condomines, M., Guénot, N., & Tanguy, J. C. (2004). Magma changes at Mount Etna: the 2001 and 2002–2003 eruptions. *Earth and Planetary Science Letters, 226*(3-4), 397-414.

Cook, E. R., & Kairiukstis, L. A. (Eds.). (2013). Methods of dendrochronology: applications in the environmental sciences. *Springer Science & Business Media*.

Diao, H., Schuler, P., Goldsmith, G. R., Siegwolf, R. T., Saurer, M., & Lehmann, M. M. (2022). On uncertainties in plant water isotopic composition following extraction by cryogenic vacuum distillation. *Hydrology and Earth System Sciences, 26*(22), 5835-5847.

Dobrzańska, J., Lochyński, P., Kalbarczyk, R., & Ziemiańska, M. (2021). Challenges in the Application of dendrochemistry in research on historical environmental pollution in an old copper mining area. *Forests, 12*(11), 1505.

Durre, I., Menne, M.J., & Vose, R.S. (2008). Strategies for evaluating quality assurance procedures. *Journal of Applied Meteorology and Climatology, 47*(6), 1785-1791.

Eckstein, D., & Bauch, J. (1969). Beitrag zur Rationalisierung eines dendrochronologischen Verfahrens und zur Analyse seiner Aussagesicherheit. *Forstwissenschaftliches Centralblatt, 88*, 230-250.

Fourel, F., Martineau, F., Lécuyer, C., Kupka, H. J., Lange, L., Ojeimi, C., & Seed, M.

(2011). $^{18}O/^{16}O$ ratio measurements of inorganic and organic materials by elemental analysis–pyrolysis–isotope ratio mass spectrometry continuous-flow techniques. *Rapid Communications in Mass Spectrometry, 25*(19), 2691-2696.

Gärtner, H., & Nievergelt, D. (2010). The core-microtome: a new tool for surface preparation on cores and time series analysis of varying cell parameters. *Dendrochronologia, 28*(2), 85-92.

Gärtner, H., & Heinrich, S. I. (2013). Glacial Landforms, Tree Rings. Dendrogeomorphology. *Encyclopedia of Quaternary Science, 2*, 91-103.

Gauthier, T. D. (2001). Detecting trends using Spearman's rank correlation coefficient. *Environmental forensics, 2*(4), 359-362.

Giammanco, S., Ottaviani, M., Valenza, M., Veschetti, E., Principio, E., Giammanco, G., & Pignato, S. (1998). Major and trace elements geochemistry in the ground waters of a volcanic area: Mount Etna (Sicily, Italy). *Water Research, 32*(1), 19-30.

Giammanco, S., Krajnc, B., Kotnik, J., & Ogrinc, N. (2017). Temporal analysis of $\delta^{13}C$ CO_2 and CO_2 efflux in soil gas emissions at Mt. Etna: A new tool for volcano monitoring. *Annals of Geophysics, 60*(6), S0665-S0665.

Hajdas, I. (2008). Radiocarbon dating and its applications in Quaternary studies. *E&G Quaternary Science Journal, 57*(1/2), 2-24.

Hatvani, I. G., Smati, A. E., Erdélyi, D., Szatmári, G., Vreča, P., & Kern, Z. (2023). Modeling the spatial distribution of the meteoric water line of modern precipitation across the broader Mediterranean region. *Journal of Hydrology, 617*, 128925.

Hevia, A., Sánchez-Salguero, R., Camarero, J. J., Buras, A., Sangüesa-Barreda, G., Galván, J. D., & Gutiérrez, E. (2018). Towards a better understanding of long-term wood-chemistry variations in old-growth forests: A case study on ancient Pinus uncinata trees from the Pyrenees. *Science of the Total Environment, 625*, 220-232.

Houlié, N., Komorowski, J. C., De Michele, M., Kasereka, M., & Ciraba, H. (2006). Early detection of eruptive dykes revealed by normalized difference vegetation index (NDVI) on Mt. Etna and Mt. Nyiragongo. *Earth and Planetary Science Letters, 246*(3-4), 231-240.

Islam, M., Rahman, M., & Bräuning, A. (2019). Impact of extreme drought on tree-ring width and vessel anatomical features of Chukrasia tabularis. *Dendrochronologia, 53*, 63-72.

Lagios, E., Sakkas, V., Novali, F., Bellotti, F., Ferretti, A., Vlachou, K., & Dietrich, V. (2013). SqueeSAR^{TM} and GPS ground deformation monitoring of Santorini Volcano (1992–2012): Tectonic implications. *Tectonophysics, 594*, 38-59.

Lawrimore, J. H., Menne, M. J., Gleason, B. E., Williams, C. N., Wuertz, D. B., Vose, R. S., and Rennie, J. (2011). An overview of the Global Historical Climatology Network monthly mean temperature data set, version 3, J. *Geophys. Res., 116*, D19121, doi:10.1029/2011JD016187.

Liotta, M., Grassa, F., D'Alessandro, W., Favara, R., Candela, E. G., Pisciotta, A., & Scaletta, C. (2013). Isotopic composition of precipitation and groundwater in Sicily, Italy. *Applied*

Geochemistry, 34, 199-206.

Loader, N. J., McCarroll, D., Barker, S., Jalkanen, R., & Grudd, H. (2017). Inter-annual carbon isotope analysis of tree-rings by laser ablation. *Chemical Geology, 466*, 323-326.

Ly, A., Marsman, M., & Wagenmakers, E. J. (2018). Analytic posteriors for Pearson's correlation coefficient. *Statistica Neerlandica, 72*(1), 4-13.

Maeght, J. L., Rewald, B., & Pierret, A. (2013). How to study deep roots—and why it matters. *Frontiers in plant science, 4*, 299.

Marchese, E. P., & Grillo, M. (2000). Primary succession on lava flows on Mt. Etna. *Acta Phytogeographica Suecica, 85*, 61-70.

Maxwell, R. S., & Larsson, L. A. (2021). Measuring tree-ring widths using the CooRecorder software application. *Dendrochronologia, 67*, 125841.

McAdam, S. A. (2023). What stops stomata reopening after a drought?. *Tree Physiology, 43*(6), 879-882.

McIntyre, C. P., Wacker, L., Haghipour, N., Blattmann, T. M., Fahrni, S., Usman, M., Eglinton, T. I. & Synal, H. A. (2017). Online 13C and ^{14}C gas measurements by EA-IRMS–AMS at ETH Zürich. *Radiocarbon, 59*(3), 893-903.

Němec, M., Wacker, L., Hajdas, I., & Gäggeler, H. (2010). Alternative methods for cellulose preparation for AMS measurement. *Radiocarbon, 52*(3), 1358-1370.

Parello, F., D'Alessandro, W., Aiuppa, A., Federico, C., (2001) Geochemical mapping of Etna's aquifers. Publication No 2190 of the National Group for Defense against Hydrogeological Disasters. *Officine Grafiche Riunite, Palermo.*

Parzych, A., & Sobisz, Z. (2012). The macro-and microelemental content of Pinus sylvestris L. and Pinus nigra JF Arn. needles in Cladonio-Pinetum habitat of the Słowiński National Park.

Paton, C., Hellstrom, J., Paul, B., Woodhead, J., & Hergt, J. (2011). Iolite: Freeware for the visualisation and processing of mass spectrometric data. *Journal of Analytical Atomic Spectrometry, 26*(12), 2508-2518.

Pennisi, M., Leeman, W. P., Tonarini, S., Pennisi, A., & Nabelek, P. (2000). Boron, Sr, O, and H isotope geochemistry of groundwaters from Mt. Etna (Sicily)—hydrologic implications. *Geochimica et Cosmochimica Acta, 64*(6), 961-974.

Perone, A., Cocozza, C., Cherubini, P., Bachmann, O., Guillong, M., Lasserre, B., Marchetti, M. & Tognetti, R. (2018). Oak tree-rings record spatial-temporal pollution trends from different sources in Terni (Central Italy). *Environmental Pollution, 233*, 278-289.

Prasad, G. R., Culp, R., & Cherkinsky, A. (2019). δ13C correction to AMS data: Values derived from AMS vs IRMS values. *Nuclear Instruments and Methods in Physics Research Section B: Beam Interactions with Materials and Atoms, 455*, 244-249.

Ramsperger, U., De Maria, D., Gautschi, P., Maxeiner, S., Müller, A. M., Synal, H. A., & Wacker, L. (2024). LEA—A Novel Low Energy Accelerator for ^{14}C Dating. *Radiocarbon, 66*(5), 1280-1288.

Rehschuh, R., Rehschuh, S., Gast, A., Jakab, A. L., Lehmann, M. M., Saurer, M., Gessler, A. & Ruehr, N. K. (2022). Tree allocation dynamics beyond heat and hot drought stress reveal changes in carbon storage, belowground translocation and growth. *New Phytologist, 233*(2), 687-704.

Reimer, P. J., Brown, T. A., & Reimer, R. W. (2004). Discussion: reporting and calibration of post-bomb ^{14}C data. *Radiocarbon, 46*(3), 1299-1304.

Scharnweber, T., Hevia, A., Buras, A., van der Maaten, E., & Wilmking, M. (2016). Common trends in elements? Within-and between-tree variations of wood-chemistry measured by X-ray fluorescence—a dendrochemical study. *Science of the Total Environment, 566*, 1245-1253.

Schweingruber, F. H. (1996). Tree rings and environment: Dendroecology. Ed. By S. Swiss Federal Institute WSL, Birmensdorf (pp. 609).

Sader, S. A., & Winne, J. C. (1992). RGB-NDVI colour composites for visualizing forest change dynamics. *International journal of remote sensing, 13*(16), 3055-3067.

Seiler, R., Houlié, N., & Cherubini, P. (2017a). Tree-ring width reveals the preparation of the 1974 Mt. Etna eruption. *Scientific Reports, 7*(1).

Seiler, R., Kirchner, J. W., Krusic, P. J., Tognetti, R., Houlié, N., Andronico, D., Cullotta, S., Egli, M., D'Arrigo, R. & Cherubini, P. (2017 b). Insensitivity of tree-ring growth to temperature and precipitation sharpens the puzzle of enhanced pre-eruption NDVI on Mt. Etna (Italy). *PloS one, 12*(1).

Seiler, R. (2017c). Tree growth rings as early indicators of volcanic activity on Mt. Etna (Italy) (Doctoral dissertation, University of Zurich).

Seiler, R., Hajdas, I., Saurer, M., Houlié, N., D'Arrigo, R., Kirchner, J. W., & Cherubini, P. (2021). Tree-ring stable isotopes and radiocarbon reveal pre-and post-eruption effects of volcanic processes on trees on Mt. Etna (Sicily, Italy). *Ecohydrology, 14*(8).

Shcherbenko, T. A., Koptsik, G. N., Groenenberg, B. J., Lukina, N. V., & Livantsova, S. Y. (2008). Uptake of nutrients and heavy metals by pine trees under atmospheric pollution. *Moscow University Soil Science Bulletin, 63*, 51-59.

Shen, Y., Takata, K., Kudo, K., Muraoka, H., Saitoh, T. M., Hirano, Y., & Yasue, K. (2022). Effects of climate on the tree ring density and weight of Betula ermanii in a cool temperate forest in central Japan. *Trees, 36*(5), 1597-1605.

Skelton, A., Andrén, M., Kristmannsdóttir, H., Stockmann, G., Mörth, C. M., Sveinbjörnsdóttir, Á., Jónsson, S., Sturkell, E., Guðrúnardóttir, H.R.,Hjartarson, H.,Siegmund, H. & Kockum, I. (2014). Changes in groundwater chemistry before two consecutive earthquakes in Iceland. *Nature Geoscience, 7*(10), 752-756.

Spilliaert, N., Allard, P., Métrich, N., & Sobolev, A. V. (2006). Melt inclusion record of the conditions of ascent, degassing, and extrusion of volatile-rich alkali basalt during the powerful 2002 flank eruption of Mount Etna (Italy). *Journal of Geophysical Research: Solid Earth, 111*.

Stenström, K., Skog, G., Georgiadou, E., Genberg, J., & Mellström, A. (2011). A guide to radiocarbon units and calculations. Thomas, S. C., & Martin, A. R. (2012). Carbon content of tree tissues: a synthesis. *Forests, 3*(2), 332-352.

Tirivarombo, S. O. D. E., Osupile, D., & Eliasson, P. (2018). Drought monitoring and analysis: standardised precipitation evapotranspiration index (SPEI) and standardised precipitation index (SPI). *Physics and Chemistry of the Earth, Parts a/b/c, 106*, 1-10.

Tognetti, R., Lombardi, F., Lasserre, B., Battipaglia, G., Saurer, M., Cherubini, P., & Marchetti, M. (2012). Tree-ring responses in Araucaria araucana to two major eruptions of Lonquimay Volcano (Chile). *Trees, 26*, 1805-1819.

Trouet, V., Coppin, P., & Beeckman, H. (2006). Annual growth ring patterns in Brachystegia spiciformis reveal influence of precipitation on tree growth 1. *Biotropica: The Journal of Biology and Conservation, 38*(3), 375-382.

Unlu, K., Pearson, C., Hauck, D. K., & Kuniholm, P. I. (2009). Dating volcanic eruptions with tree-ring chemistry. *IEEE Potentials, 28*(5), 36-44.

Varrica, D., A. Aiuppa, and G. Dongarrà. (2000). Volcanic and anthropogenic contribution to heavy metal content in lichens from Mt. Etna and Vulcano island (Sicily).*Environmental Pollution 108.2*: 153-162.

Versace, S., Bräuning, A., Cherubini, P., Di Febbraro, M., Häusser, M., Lombardi, F., Marchetti, M., Marziliano, P.A., Salbitano, F., Szymczak, S. & Tognetti, R. (2022). New evidence for population-specific responses to drought events from tree ring chronologies of Pinus nigra ssp. laricio across the entire distribution range. *Agricultural and Forest Meteorology, 323*, 109076.

Vicente-Serrano, S. M., Camarero, J. J., & Azorin-Molina, C. (2014). Diverse responses of forest growth to drought time-scales in the Northern Hemisphere. *Global Ecology and Biogeography, 23*(9), 1019-1030.

von Freyberg, J., Allen, S. T., Grossiord, C., & Dawson, T. E. (2020). Plant and root-zone water isotopes are difficult to measure, explain, and predict: Some practical recommendations for determining plant water sources. *Methods in Ecology and Evolution, 11*(11), 1352-1367.

Watt, S. F., Pyle, D. M., Mather, T. A., Day, J. A., & Aiuppa, A. (2007). The use of tree-rings and foliage as an archive of volcanogenic cation deposition. *Environmental Pollution, 148*(1), 48-61.

WSL. Skippy. URL:"https://www.wsl.ch/en/services-produkte/skippy/ " (Access: 30.01.25).

Zhao, J., Cao, Y., & Wang, X. (2018). The physical significance of the synthetic running correlation coefficient and its applications in oceanic and atmospheric studies. *Journal of Ocean University of China, 17*, 451-460.

Zuecco, G., Amin, A., Frentress, J., Engel, M., Marchina, C., Anfodillo, T., Borga, M., Carraro, V., Scandellari, F., Tagliavini, M., Zantonelli, D., Comiti, F., & Penna, D. (2022). A comparative study of plant water extraction methods for isotopic analyses: Scholander-type pressure chamber vs. cryogenic vacuum distillation. *Hydrology and Earth System Sciences Discussions, 2020*, 1-23.

Appendix

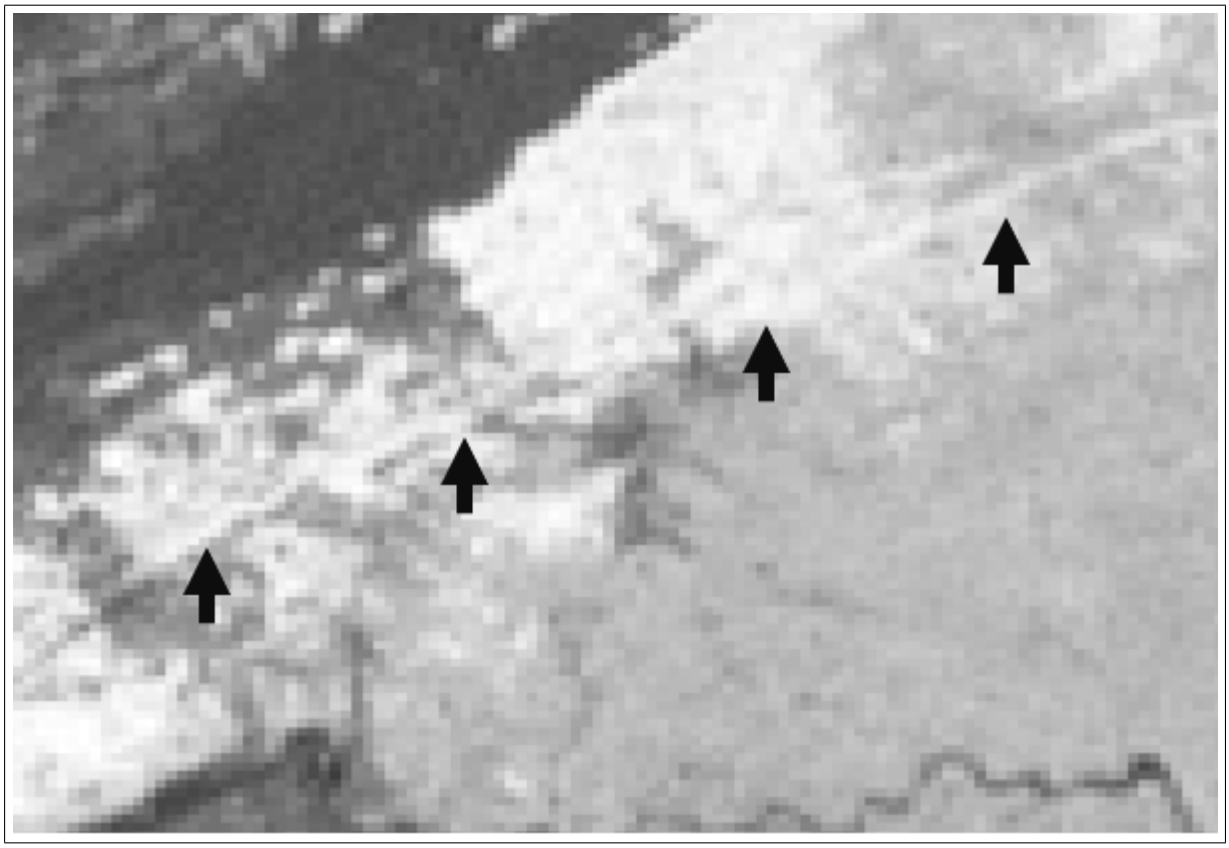

Figure 5.1 NDVI picture from Piano Provenzana in 2002 made with ArcGIS Pro with the band images from MADAS. (zoomed-in)

Table 5.1 Table with the tree ID, location, tree species, altitude, distance to the lava flow, number of samples taken from all the sampled trees.

Tree ID	Location	Tree Species	Altitude [m.a.s.l.]	Distance to Lava flow [m]	Samples No.	Remarks
A1	37.80829, 15.04898	Pinus Nigra J.F. Arnold	1739	15-20	a,b,c,d	
A2	37.80827, 15.04888	Pinus Nigra J.F. Arnold	1741	15-20	a,b,c,d	
A3	37.80822, 15.04883	Pinus Nigra J.F. Arnold	1743	5	a,b,c,d	
A4	37.80814, 15.04874	Pinus Nigra J.F. Arnold	1744	4	a,b,c,d	
A5	37.80808, 15.04865	Pinus Nigra J.F. Arnold	1748	5	a,b,c,d	
A6	37.80805, 15.04860	Pinus Nigra J.F. Arnold	1749	15	a,b,c,d	
A7	37.80795, 15.04862	Pinus Nigra J.F. Arnold	1757	20-25	a,b,c,d	
Fag1	37.80803, 15.04859	Fagus sylvatica L.	1756	-	1	
Fag2	37.80800, 15.04852	Fagus sylvatica L.	1758	-	2	
Fag3	37.80801, 15.04847	Fagus sylvatica L.	1761	-	3	
Fag4	37.80799, 15.04851	Fagus sylvatica L.	1760	-	4	
Fag5	37.80798, 15.04850	Fagus sylvatica L.	1760	-	5	
Tot1	37.80849, 15.04948	-	1733	0	a,b	on top of lavaflow
Tot2	37.80853, 15.04954	-	1733	0	a,b	on top of lavaflow
Tot3	37.80842, 15.04963	-	1728	0	a,b	on top of lavaflow
C1	37.77909, 15.05220	Pinus Nigra J.F. Arnold	1660 (1700)	-	a,b,c,d	() for google altitude
C2	37.77917, 15.05182	Pinus Nigra J.F. Arnold	1645 (1700)	-	a,b,c,d	() for google altitude
C3	37.77892, 15.05163	Pinus Nigra J.F. Arnold	1663 (1705)	-	a,b,c,d	() for google altitude
C4	37.77931, 15.05159	Pinus Nigra J.F. Arnold	1677 (1700)	-	a,b,c,d	() for google altitude
C5	37.77937, 15.05105	Pinus Nigra J.F. Arnold	1690 (1710)	-	a,b,c,d	() for google altitude
C6	37.77914, 15.05072	Pinus Nigra J.F. Arnold	1699	-	a,b,c,d	
C7	37.77934, 15.05049	Pinus Nigra J.F. Arnold	1699	-	a,b,c,d	
FC1	37.77980, 15.05219	Fagus sylvatica L.	1681	-	1	
FC2	37.77980, 15.05219	Fagus sylvatica L.	1681	-	1	
FI1	37.79613, 15.03735	Fagus sylvatica L.	1799	-	1	
FI2	37.79614, 15.03738	Fagus sylvatica L.	1801	-	a,b	
FI3	37.79589, 15.03722	Fagus sylvatica L.	1801	-	3	
FI4	37.79556, 15.03703	Fagus sylvatica L.	1799	-	4	
FI5	37.79616, 15.03739	Fagus sylvatica L.	1800	-	5	
RSI1	37.803972, 15.038778	Pinus Nigra J.F. Arnold	1870	1	a,b	

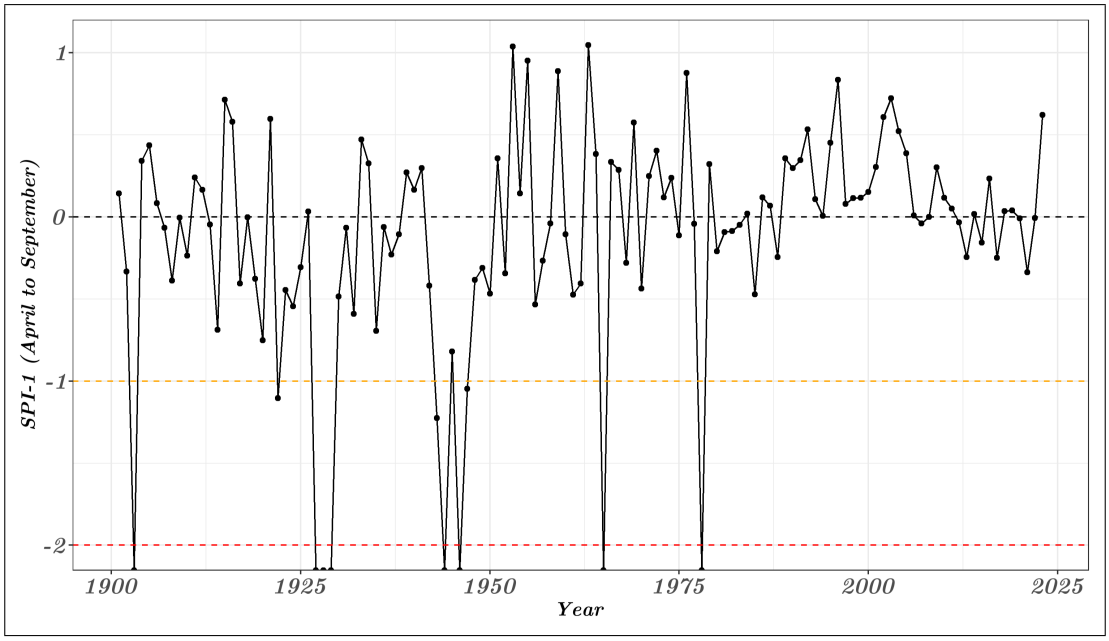

(a) SPI1 of the whole period (1901-2023)

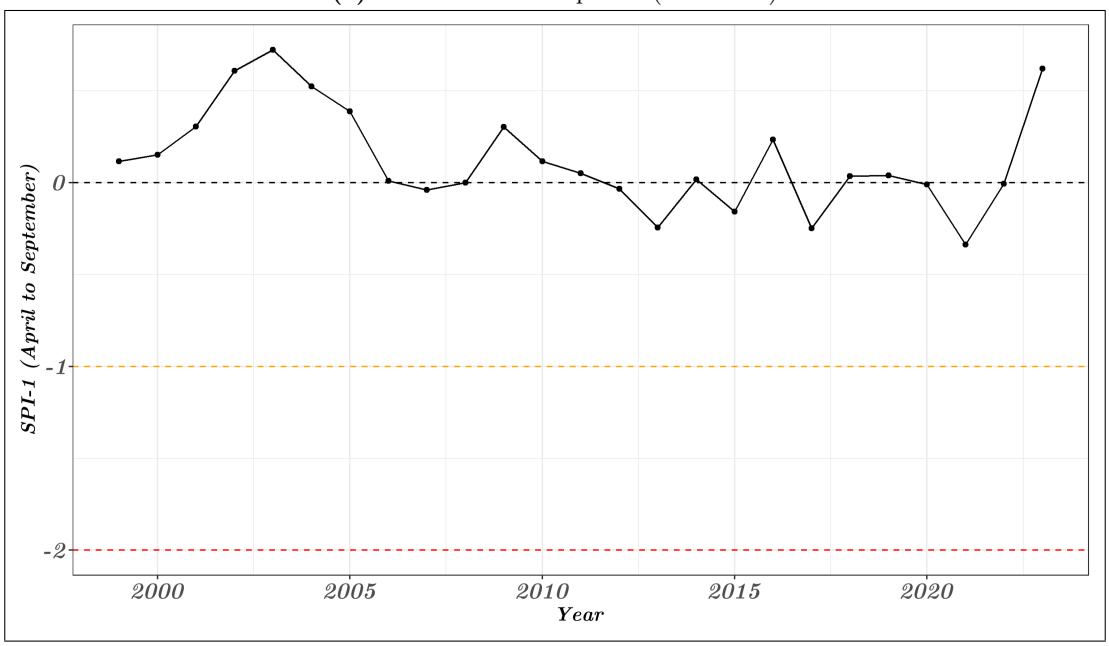

(b) SPI1 of the period (1999-2023)

Figure 5.2 SPI1 plotted against the years 1901 to 2023 for the study area on Mt.Etna.

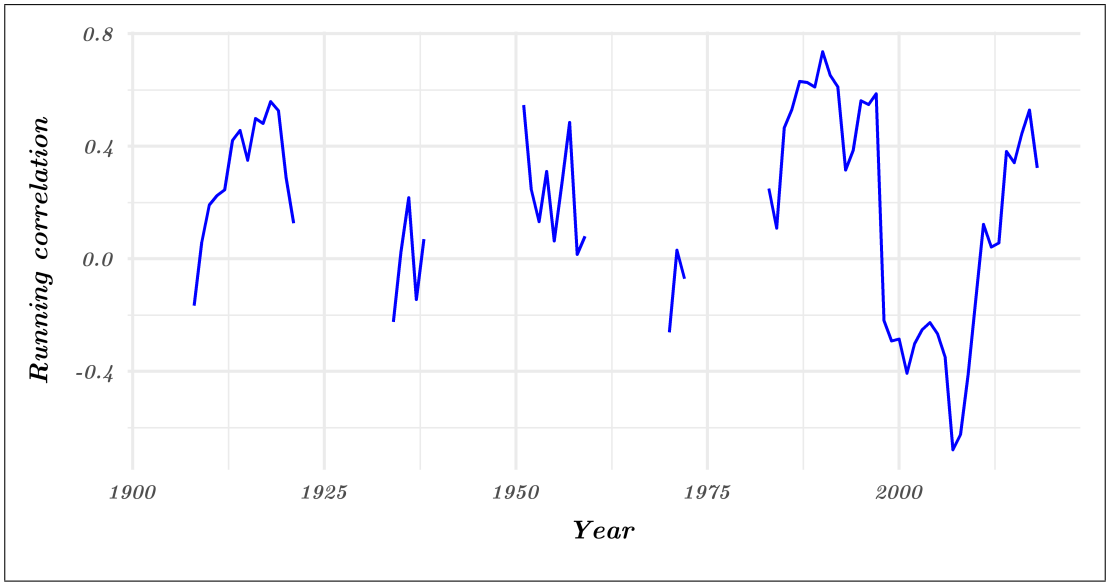

(a) Running correlation of the whole period (1901-2023)

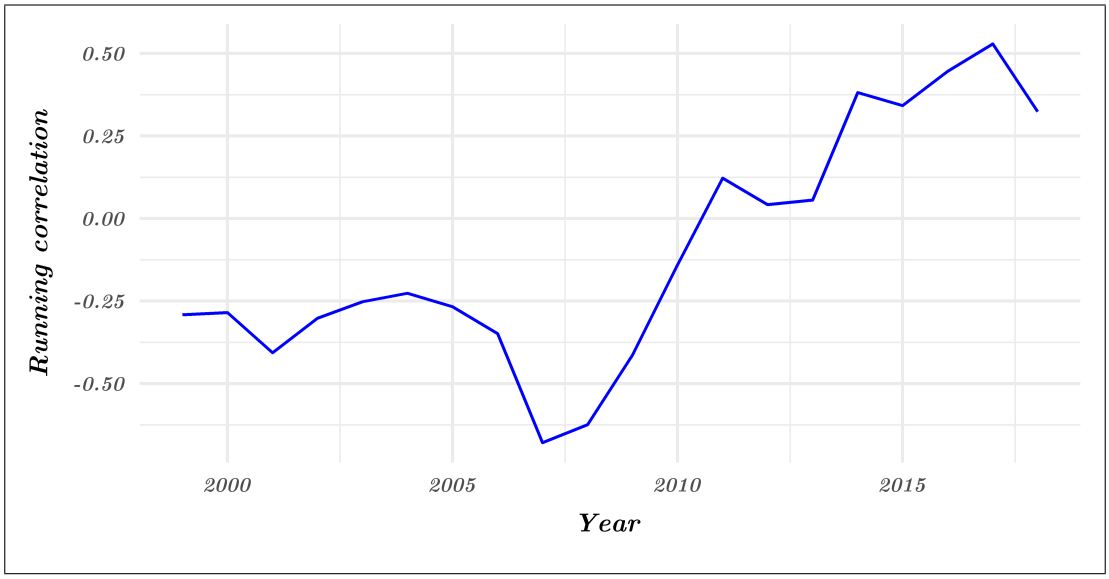

(b) Running correlation of the period (1999-2023)

Figure 5.3 Running correlation values of the detrended tree ring chronology vs. SPI1 for the years 1901 to 2023 and 1999 to 2023.

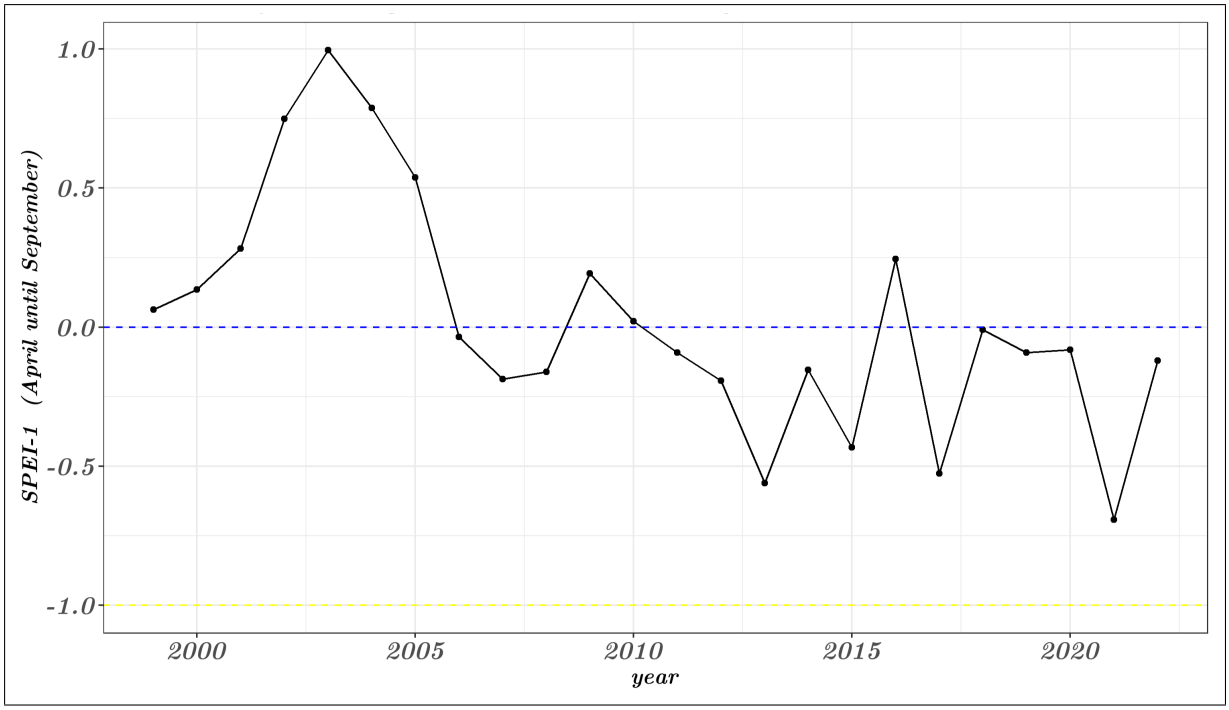

Figure 5.4 SPEI1 plotted against the years 1999 to 2022 for the study area on Mt.Etna.

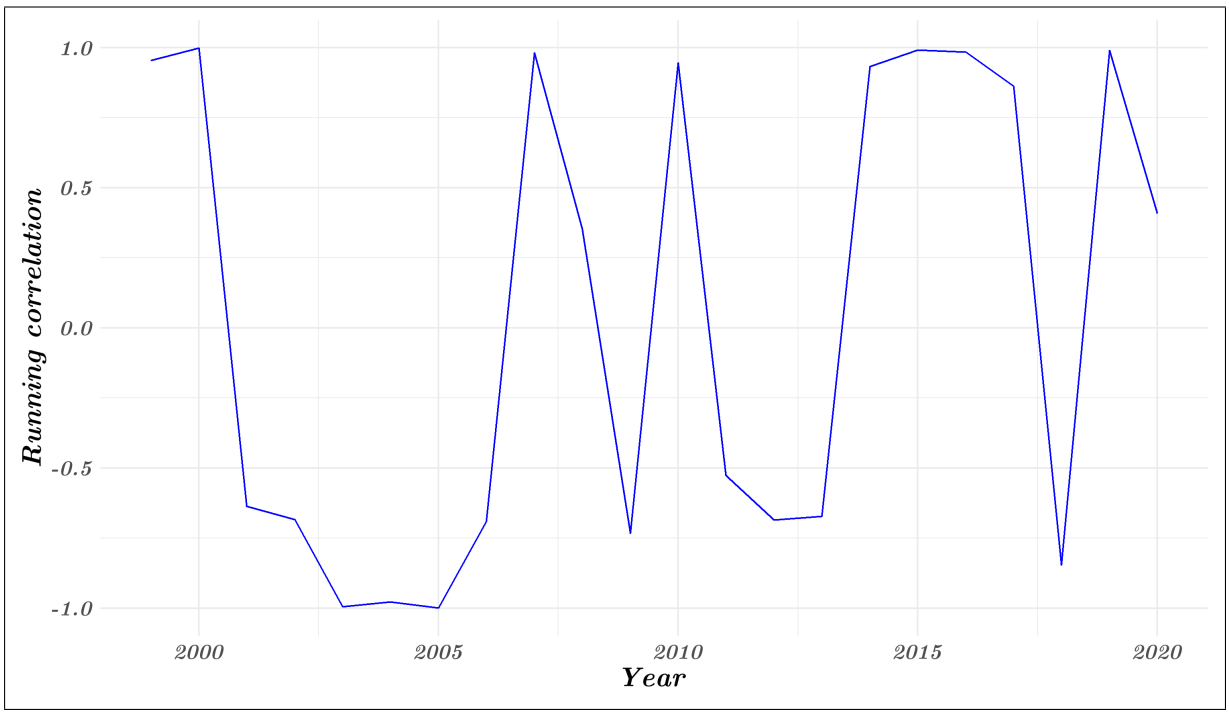

Figure 5.5 Running correlation values of the detrended tree ring chronology vs. SPEI1 for the years 1999 to 2020.

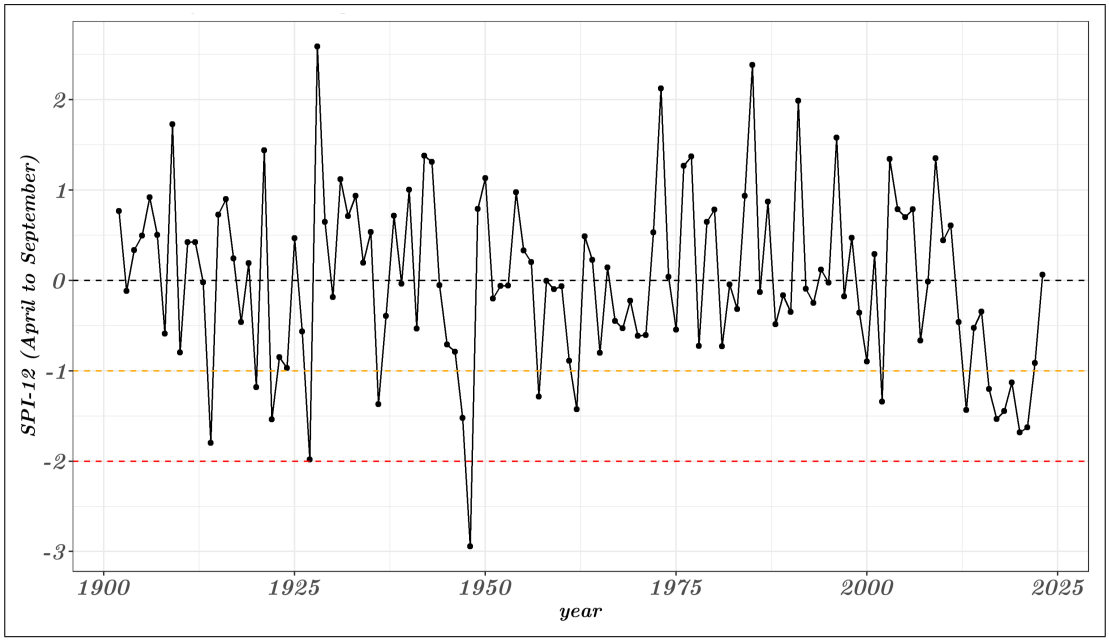

(a) SPI12 of the whole period (1901-2023)

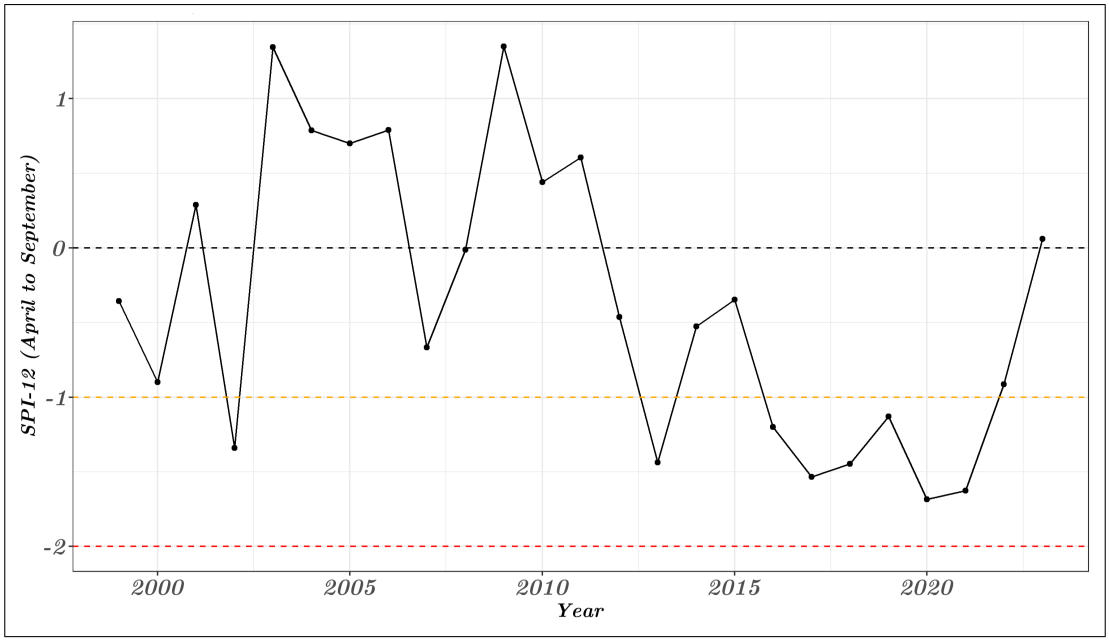

(b) SPI12 of the period (1999-2023)

Figure 5.6 SPI12 plotted against the years 1901 to 2023 for the study area on Mt.Etna.

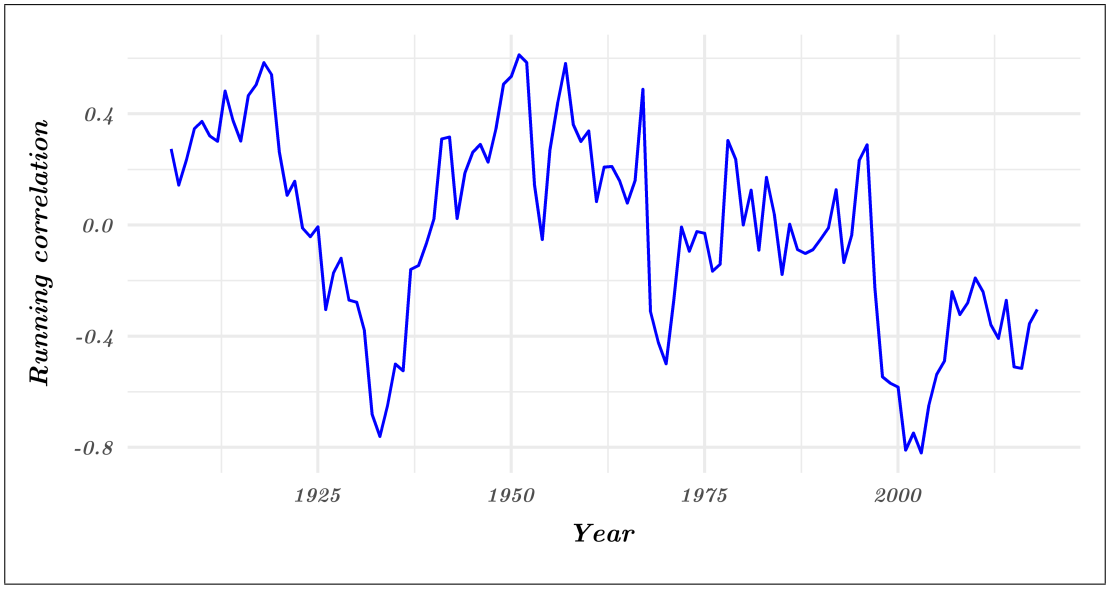

(a) Running correlation of the whole period (1901-2023)

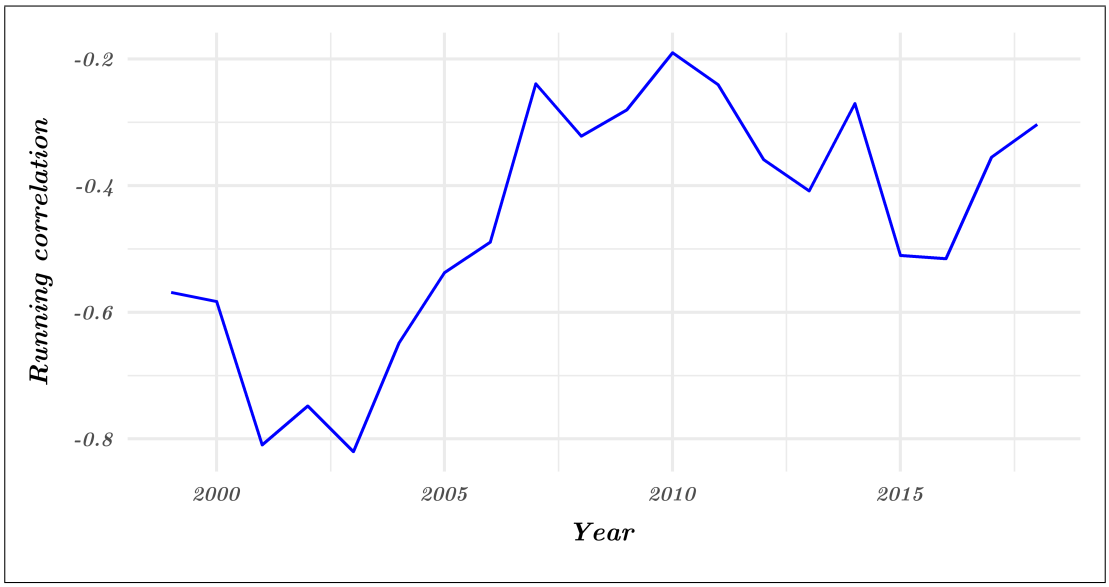

(b) Running correlation of the period (1999-2023)

Figure 5.7 Running correlation values of the detrended tree ring chronology vs. SPI12 for the years 1901 to 2023 and 1999 to 2023.

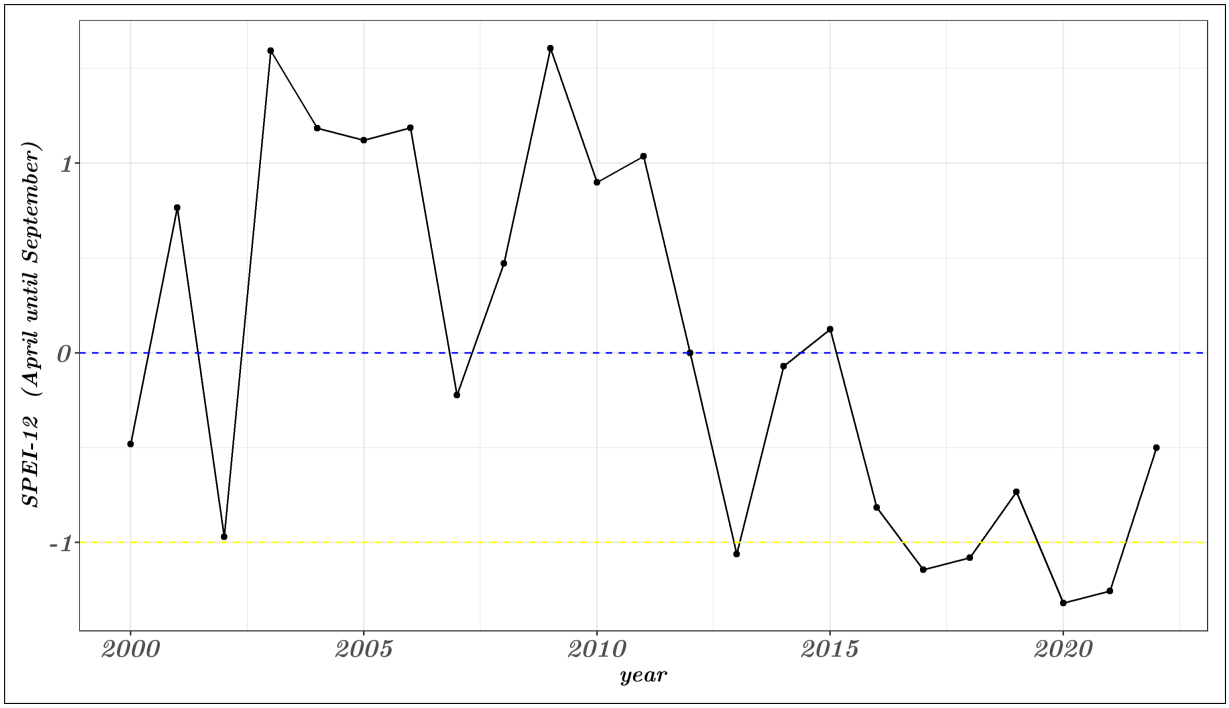

Figure 5.8 SPEI12 plotted against the years 1999 to 2022 for the study area on Mt.Etna.

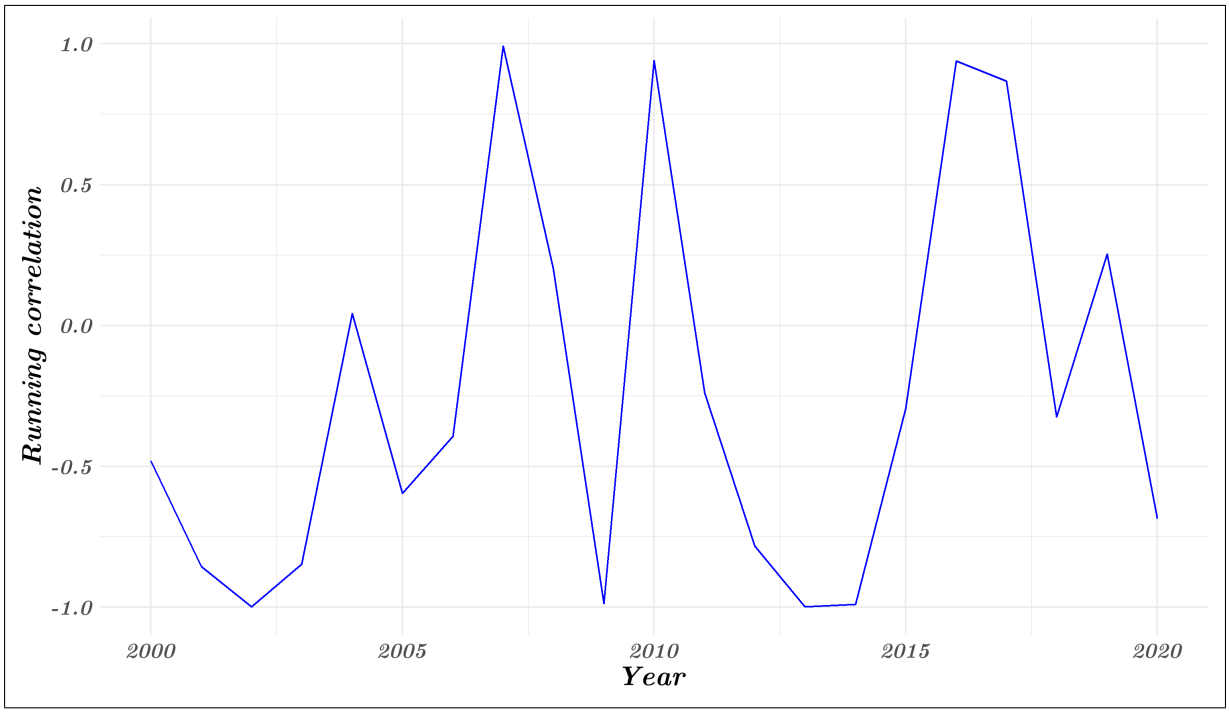

Figure 5.9 Running correlation values of the detrended tree ring chronology vs. SPEI12 for the years 1999 to 2020.

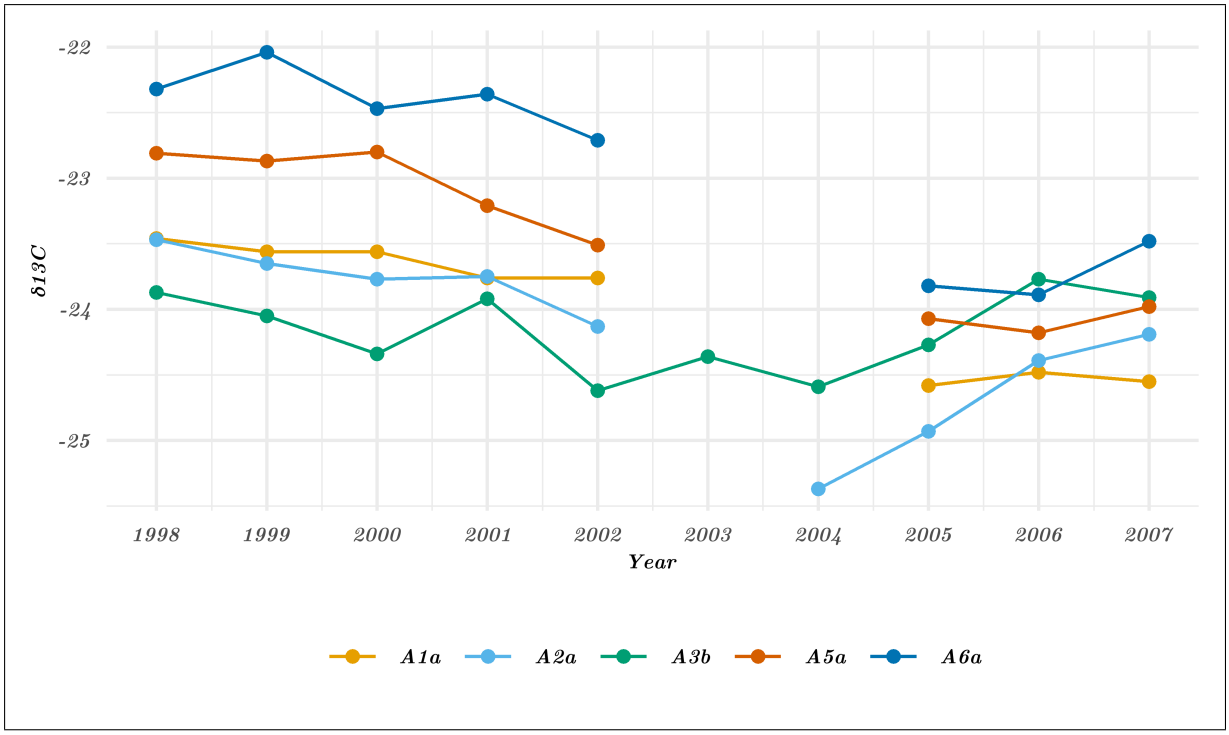

Figure 5.10 δ^{13}C values of the measured sampling site trees plotted against the year.

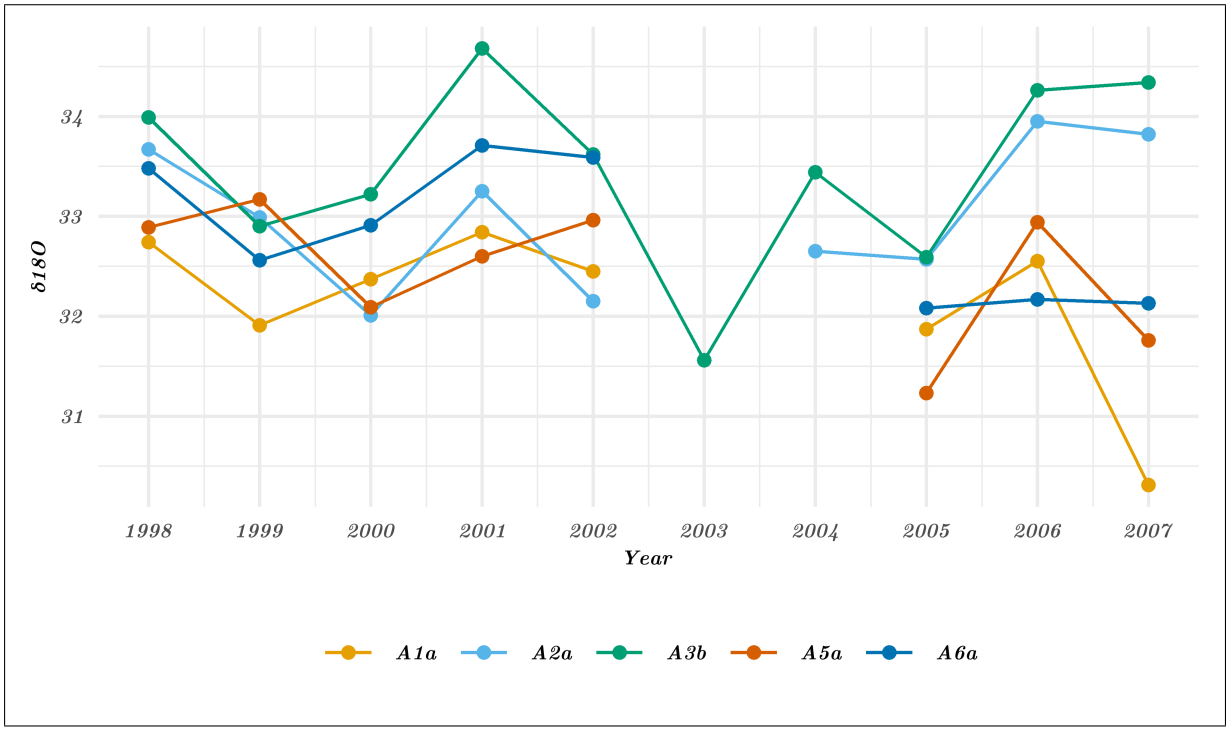

Figure 5.11 δ^{18}O values of the measured sampling site trees plotted against the year.

Declaration of Authorship

Personal declaration: I hereby declare that the submitted thesis is the result of my own, independent work. All external sources are explicitly acknowledged in the thesis.

Valentino Känzig: 

Place, date: *Brüttisellen, 24.4.2025*